REAL-TIME IMPLEMENTATION OF NONLINEAR OPTICAL DATA PROCESSING FUNCTIONS

Yuri Owechko and Bernard Soffer

Hughes Research Laboratories
3011 Malibu Canyon Road
Malibu, California 90265

November 1990

Final Report
Contract F49620-88-C-0063
March 1988 through June 1990

Sponsored by:

Air Force Office of Scientific Research
Bolling AFB
Washington, D.C. 20332-6448

DISCLAIMER NOTICE

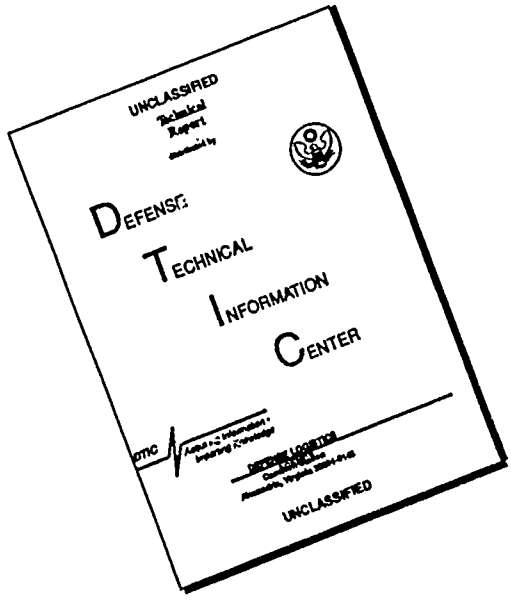

THIS DOCUMENT IS BEST QUALITY AVAILABLE. THE COPY FURNISHED TO DTIC CONTAINED A SIGNIFICANT NUMBER OF PAGES WHICH DO NOT REPRODUCE LEGIBLY.

UNCLASSIFIED

SECURITY CLASSIFICATION OF THIS PAGE

REPORT DOCUMENTATION PAGE

Form Approved OMB No. 0704-0188

1a. REPORT SECURITY CLASSIFICATION: UNCLASSIFIED

1b. RESTRICTIVE MARKINGS:

2a. SECURITY CLASSIFICATION AUTHORITY:

2b. DECLASSIFICATION / DOWNGRADING SCHEDULE:

3. DISTRIBUTION / AVAILABILITY OF REPORT: Approved for public release; distribution unlimited.

4 PERFORMING ORGANIZATION REPORT NUMBER(S):

5. MONITORING ORGANIZATION REPORT NUMBER(S):

6a. NAME OF PERFORMING ORGANIZATION: Hughes Research Laboratories

6b. OFFICE SYMBOL (If applicable):

7a. NAME OF MONITORING ORGANIZATION: Air Force Office of Scientific Research

6c. ADDRESS (City, State, and ZIP Code): 3011 Malibu Canyon Road, Malibu, CA 90245

7b. ADDRESS (City, State, and ZIP Code): Bolling AFB, Washington, D.C. 20332-6448

8a NAME OF FUNDING / SPONSORING ORGANIZATION: Air Force Office of Scientific Research

8b. OFFICE SYMBOL (If applicable): NE

9. PROCUREMENT INSTRUMENT IDENTIFICATION NUMBER: F49620-88-C-0063

8c. ADDRESS (City, State, and ZIP Code): Same as 7b

10. SOURCE OF FUNDING NUMBERS

PROGRAM ELEMENT NO.	PROJECT NO.	TASK NO.	WORK UNIT ACCESSION NO
61102F	2305	B1	

11. TITLE (Include Security Classification): REAL-TIME IMPLEMENTATION OF NONLINEAR OPTICAL DATA PROCESSING FUNCTIONS

12. PERSONAL AUTHOR(S): Yuri Owechko and Bernard Soffer

13a. TYPE OF REPORT	13b. TIME COVERED	14. DATE OF REPORT (Year, Month, Day)	15. PAGE COUNT
Final	FROM 3/88 TO 6/90	90 NOV 30	109

16. SUPPLEMENTARY NOTATION:

17. COSATI CODES			18. SUBJECT TERMS (Continue on reverse if necessary and identify by block number)
FIELD	GROUP	SUB-GROUP	neural networks, optical neural networks, optical processing

19. ABSTRACT (Continue on reverse if necessary and identify by block number)

In this final report for work performed in the period March 1988 to June 1990 we describe our efforts toward optical implementations of neural network models. The parallelism of optics will allow the hardware implementation of very large numbers of neurons with high throughputs. Under this effort we have begun development of SPONN (Stimulated Photorefractive Optical Neural Network), a hybrid optoelectronic system for programmable, adaptive, and fully parallel direct physical implementations of neural network models which is based on self-pumped photorefractive phase conjugate mirrors.

UNCLASSIFIED

20. DISTRIBUTION / AVAILABILITY OF ABSTRACT: ☒ UNCLASSIFIED / UNLIMITED ☐ SAME AS RPT. ☐ DTIC USERS

21. ABSTRACT SECURITY CLASSIFICATION: UNCLASSIFIED

22a. NAME OF RESPONSIBLE INDIVIDUAL: Dr. Alan Craig

22b. TELEPHONE (Include Area Code): 202-767-4931

22c. OFFICE SYMBOL: NE

DD Form 1473, JUN 86 — Previous editions are obsolete

SECURITY CLASSIFICATION OF THIS PAGE

UNCLASSIFIED

TABLE OF CONTENTS

LIST OF FIGURES

LIST OF FIGURES

SECTION 1

INTRODUCTION

Neural network models are highly parallel alternatives to conventional methods of computation for solving such ill-structured problems as pattern recognition or robotic control. Their architecture resembles that of biological nervous systems, which solve such problems so efficiently. Sophisticated neural network models and training procedures have evolved, since the pioneering work of the 1940s. Even so, neural network models have not yet convincingly demonstrated their superiority over the algorithm-oriented approaches of artificial intelligence or classical statistical techniques. Widespread application of neural network technology depends on advances in both theoretical understanding and the development of computing platforms explicitly designed for the parallel implementation of such models. Those areas of research naturally interact and complement each other. For example, scaleup and convergence issues can be studied both theoretically and by actual operation of neural networks.

In the 1988-1989 contract period, we addressed the need for hardware realizations of neural networks by implementing a hybrid optoelectronic architecture. The massive parallelism of neural network models that makes them run very inefficiently on serial machines also allows them to be implemented very efficiently on parallel optical machines. The potential speedup factors are high.

Our approach is a direct analog realization of neural network models in which a physical node is dedicated to representing each "neuron," or processing element. By not having to multiplex neurons among physical nodes and by simultaneously updating all weights between two layers, using optics, we achieve very large throughputs with large numbers of relatively slow processors, as in biological nervous systems. The stimulated photorefractive optical neural network (SPONN), developed under this contract in 1988-1989, is a fine-grained optoelectronic architecture characterized by massive parallelism and much greater connectivity than is possible in electronic approaches.

SPONN is capable of implementing neural network models comprising 10^5 neurons with 10^{10} interconnections. SPONN's optical architecture is inherently suited to the mapping of multilayer neural network models; moreover, it is easily programmable. Its weight updating rate is independent of the number of neurons. In contrast, most electronic approaches must deal with data routing and contention problems arising from the limited connectivity of electronic structures, and therefore depend strongly on the number of neurons and their interconnections.

In SPONN, neurons are implemented as pixels on a two-dimensional spatial light modulator (SLM) and interconnection weights are established holographically as gratings in photorefractive crystals. A unique feature is our use of a continuum of spatially and angularly distributed gratings

SECTION 1
INTRODUCTION

Neural network models are highly parallel alternatives to conventional methods of computation for solving such ill-structured problems as pattern recognition or robotic control. Their architecture resembles that of biological nervous systems, which solve such problems so efficiently. Sophisticated neural network models and training procedures have evolved, since the pioneering work of the 1940s. Even so, neural network models have not yet convincingly demonstrated their superiority over the algorithm-oriented approaches of artificial intelligence or classical statistical techniques. Widespread application of neural network technology depends on advances in both theoretical understanding and the development of computing platforms explicitly designed for the parallel implementation of such models. Those areas of research naturally interact and complement each other. For example, scaleup and convergence issues can be studied both theoretically and by actual operation of neural networks.

In the 1988-1989 contract period, we addressed the need for hardware realizations of neural networks by implementing a hybrid optoelectronic architecture. The massive parallelism of neural network models that makes them run very inefficiently on serial machines also allows them to be implemented very efficiently on parallel optical machines. The potential speedup factors are high.

Our approach is a direct analog realization of neural network models in which a physical node is dedicated to representing each "neuron," or processing element. By not having to multiplex neurons among physical nodes and by simultaneously updating all weights between two layers, using optics, we achieve very large throughputs with large numbers of relatively slow processors, as in biological nervous systems. The stimulated photorefractive optical neural network (SPONN), developed under this contract in 1988-1989, is a fine-grained optoelectronic architecture characterized by massive parallelism and much greater connectivity than is possible in electronic approaches.

SPONN is capable of implementing neural network models comprising 10^5 neurons with 10^{10} interconnections. SPONN's optical architecture is inherently suited to the mapping of multilayer neural network models; moreover, it is easily programmable. Its weight updating rate is independent of the number of neurons. In contrast, most electronic approaches must deal with data routing and contention problems arising from the limited connectivity of electronic structures, and therefore depend strongly on the number of neurons and their interconnections.

In SPONN, neurons are implemented as pixels on a two-dimensional spatial light modulator (SLM) and interconnection weights are established holographically as gratings in photorefractive crystals. A unique feature is our use of a continuum of spatially and angularly distributed gratings

to represent each weight, rather than the single grating employed by prior holographic optical neural networks. Multiple gratings eliminate the ambiguous readout of gratings and the crosstalk that results from the angular degeneracy of the Bragg condition for diffraction from a volume grating. Our new technique eliminates the need for subsampling the input/output planes and therefore permits full utilization of the SLM space-bandwidth product for representing neurons, unlike other holographic approaches. We can implement multilayer neural network models using a single photorefractive crystal and SLM, which produces a compact modular system.

The continuum of gratings is generated by focusing the input plane into a self-pumped or mutually-pumped phase-conjugate mirror (PCM). Stimulated photorefractive processes in the PCM cause each pixel in the input plane to form connections with all other pixels via distributed volume gratings. Moreover, the gratings arrange themselves to redistribute the incident light into a phase-conjugate output wavefront that is a time-reversed version of the input light. Such self-organization yields a fully parallel and massively interconnected physical system that is an ideal implementation medium for neural network models. The distributed gratings in the PCM both store the weights and route the optical beams.

An important feature of SPONN is its hybridization of optics and electronics. It combines the large storage capacity, parallelism, and connectivity of optical structures with the easy programmability and controllable nonlinearity of electronic structures. A video frame grabber in conjunction with the host computer carries out the nonlinear neuron activation functions with minimal computational overhead. We can implement multilayer neural networks by spatially segregating the input and output planes. Unlike all-optical neural networks, SPONN can be easily and reproducibly controlled.

SECTION 2

VOLUME HOLOGRAM IMPLEMENTATIONS OF NEURAL NETWORKS

Volume holograms offer two features required by neural networks: enormous storage capacity and fully parallel processing of the stored interconnection weight values. In such an optical neural network, neurons are represented by pixels on two-dimensional SLMs. Pixel brightness corresponds to the activation level of the neuron. When the SLM is placed in the back focal plane of a lens and coherent readout is used, the light emitted by the pixels is converted to coherent beams that illuminate a real-time holographic medium.

In this report, we represent each light beam by a momentum or k vector. (The direction of the k vector corresponds to the direction of propagation; its magnitude is the inverse of the optical wavelength in the holographic medium.) Interconnection weights between neurons are established when a pair of light beams interfere in the holographic medium, producing a volume sinusoidal light-intensity pattern that interacts with the medium. The photorefractive effect is a suitable physical mechanism for converting the light-intensity pattern into a semipermanent deformation of the optical properties of the material, thus recording the weight values.

In the photorefractive effect, incident light excites carriers (electrons, holes) from traps into the conduction or valence band. The carriers are then transported by diffusion and drift until they fall into empty traps, thereby creating an internal space-charge field that in turn modulates the birefingence of the material through the electro-optic effect.[1] Because of the long dark-decay times of some photorefractive materials, the resultant phase gratings can be stored with a time constant of many hours.[2] (Storage for longer periods is also possible using various hologram-fixing methods, discussed below in subsection 3.7.)

When one of the original two beams subsequently addresses the grating, the other beam is reconstructed with a diffraction efficiency that represents the interconnection weight value between the two neurons. In general, reading out the grating partially erases it unless the readout beam is much weaker than the original writing light or the crystal is fixed by means of special techniques. Such light sensitivity allows us to implement learning in our photorefractive optical neural network, since we can selectively decrease as well as increase the weights. Photorefractive materials and their application in optical data processing is an active area of research at HRL.

The physical mechanism that allows large numbers of gratings to be stored in a photorefractive crystal is described by the Bragg condition for constructive scattering off a volume grating: a beam will be reconstructed only if its angle of incidence is approximately equal to that of

the original writing beam. The angular selectivity for reconstruction can be derived from coupled mode theory.[3] It is given by

$$\Delta\theta = \frac{\lambda}{nT_z \sin(\phi)}$$

where λ is the optical wavelength, n is the index of refraction of the photorefractive crystal, T_z is the hologram thickness, and ϕ is the mean angle between the reference and object beamlets. The angular selectivity is greater for thicker crystals. Phase matching arguments permit the Bragg condition to be described geometrically as a vector sum: $K_j + K_g = K_i$, where K_j and K_i are the wave vectors of the incident and diffracted beams, respectively, and K_g is the grating wave vector. Figure 1 illustrates a holographic interconnection between two optical neurons, with Figure 1(a) showing how holographic gratings form an outer-product or Hebbian interconnection matrix and Figure 1(b) describing the Bragg condition geometrically.

A geometric construction for the theoretical maximum storage capacity of a volume hologram can be drawn in k space, as shown in Figure 2. If the first writing beam varies over solid angle θ_o whereas the second writing beam varies over angle θ_r, then the vector difference between the two beams (the grating wave vector K_g) will trace out a three-dimensional region in k space. The volume of the region depends on such geometric factors as the focal lengths of the optics and the spacing of the neurons on the SLMs.

The grating wave vector K_g has an uncertainty volume associated with it because of the lens aperture, the finite physical size of the hologram, and the nonzero size of the SLM pixels. Dividing the accessible volume of k space by the value of the uncertainty volume yields the maximum theoretical number of resolvable gratings or weights that can be stored in the photorefractive crystal. For a 1-cm^3 crystal, the theoretical upper limit is 10^{10} weights, assuming currently available SLM resolution and reasonable optics. That number of weights is sufficient to form a fully interconnected network of 10^5 neurons. Partially interconnected networks with more neurons can also be accommodated. Moreover, the entire neural network can be read out or updated in parallel without the time-multiplexing, data-contention, or bottleneck problems common in electronic implementations. The great storage capacity is a direct result of the three-dimensional nature of optical holographic storage.[4]

the original writing beam. The angular selectivity for reconstruction can be derived from coupled mode theory.[3] It is given by

$$\Delta\theta = \frac{\lambda}{nT_z \sin(\phi)}$$

where λ is the optical wavelength, n is the index of refraction of the photorefractive crystal, T_z is the hologram thickness, and ϕ is the mean angle between the reference and object beamlets. The angular selectivity is greater for thicker crystals. Phase matching arguments permit the Bragg condition to be described geometrically as a vector sum: $K_j + K_g = K_i$, where K_j and K_i are the wave vectors of the incident and diffracted beams, respectively, and K_g is the grating wave vector. Figure 1 illustrates a holographic interconnection between two optical neurons, with Figure 1(a) showing how holographic gratings form an outer-product or Hebbian interconnection matrix and Figure 1(b) describing the Bragg condition geometrically.

A geometric construction for the theoretical maximum storage capacity of a volume hologram can be drawn in k space, as shown in Figure 2. If the first writing beam varies over solid angle θ_o whereas the second writing beam varies over angle θ_r, then the vector difference between the two beams (the grating wave vector K_g) will trace out a three-dimensional region in k space. The volume of the region depends on such geometric factors as the focal lengths of the optics and the spacing of the neurons on the SLMs.

The grating wave vector K_g has an uncertainty volume associated with it because of the lens aperture, the finite physical size of the hologram, and the nonzero size of the SLM pixels. Dividing the accessible volume of k space by the value of the uncertainty volume yields the maximum theoretical number of resolvable gratings or weights that can be stored in the photorefractive crystal. For a 1-cm^3 crystal, the theoretical upper limit is 10^{10} weights, assuming currently available SLM resolution and reasonable optics. That number of weights is sufficient to form a fully interconnected network of 10^5 neurons. Partially interconnected networks with more neurons can also be accommodated. Moreover, the entire neural network can be read out or updated in parallel without the time-multiplexing, data-contention, or bottleneck problems common in electronic implementations. The great storage capacity is a direct result of the three-dimensional nature of optical holographic storage.[4]

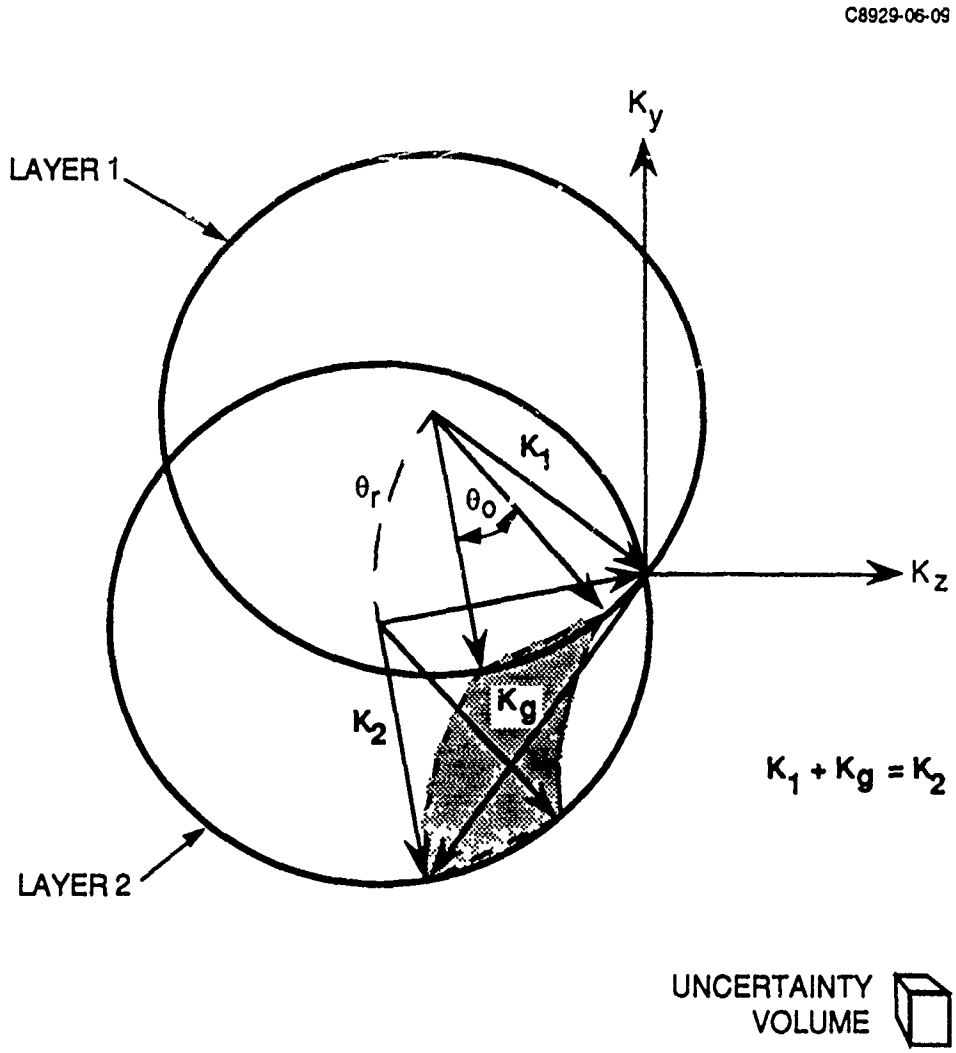

Figure 2. Region of k space used for information storage in optical neural network based on volume hologram.

The challenge is to devise practical neural network systems able to approach the theoretical limit. Perhaps the most important obstacle is the degenerate nature of the Bragg condition, which states that the angle of incidence of a light beam relative to a volume grating must match that of the original writing beam in order for its associated beam to be reconstructed. However, that condition is satisfied by a set of beams whose k vectors form a cone normal to the grating, as shown by Figure 3. Therefore, a large set of beams other than the original beam can constructively scatter off the grating, forming erroneous reconstructions and crosstalk. Two methods for avoiding the problem have been suggested in the literature: subsampling of the SLMs and spatial multiplexing of holograms. However, both methods are problematic.

In the subsampling method, neurons are arranged in special nonredundant patterns on the SLMs, and output planes are sampled only at certain locations. Thus, though false reconstructions still occur, they do not contribute to the output. The special patterns can consist of fractal grids[5] or a combination of one- and two-dimensional sampling.[6] If the SLMs are capable of displaying NxN neurons, then this method can implement a total of $N^{3/2}$ neurons and N^3 weights. The storage capacities of both the crystal and the SLMs thus have the same functional dependence on dimensional scaling (ignoring limiting effects due to nonzero SLM pixel size).

However, the subsampling method does not allow the SLM space-bandwidth product to be fully utilized for representing neurons. That is a major drawback. As discussed above, the storage capacity of a 1-cm^3 crystal should be sufficient to store the interconnections for an NxN array of neurons where N = 500, which matches the capabilities of current SLMs such as the HRL liquid crystal light valve (LCLV). Unfortunately, because of the subsampling, only $N^{3/2}$ neurons can be implemented even though the SLM is capable of displaying N^2 neurons. Since N = 500, the neuron and weight storage capacity/throughput are reduced by factors of 22 and 500, respectively, from the theoretical maximums for current SLMs. The light efficiency is also low because some of the light is diffracted to dead areas due to the Bragg ambiguity.

The spatial multiplexing method avoids the Bragg ambiguity problem by physically dividing the crystal into separate volumes for each weight. However, such divisions effectively reduce the storage capacity to the low level of a two-dimensional hologram.

Figure 4 shows the general architecture of a subsampling photorefractive optical neural network. Pixels in the object and reference planes represent individual neurons. The neurons are optically interconnected by coherent light beams diffracted from volume phase gratings, which are stored in a photorefractive crystal and which control the strength and phase of the interconnection weights. The object and reference planes are physically located on the output faces of CRT-addressed LCLVs that modulate incident, collimated coherent light beams, resulting in the reflection of diverging beamlets of light from each neuron. The amplitude of each beamlet is

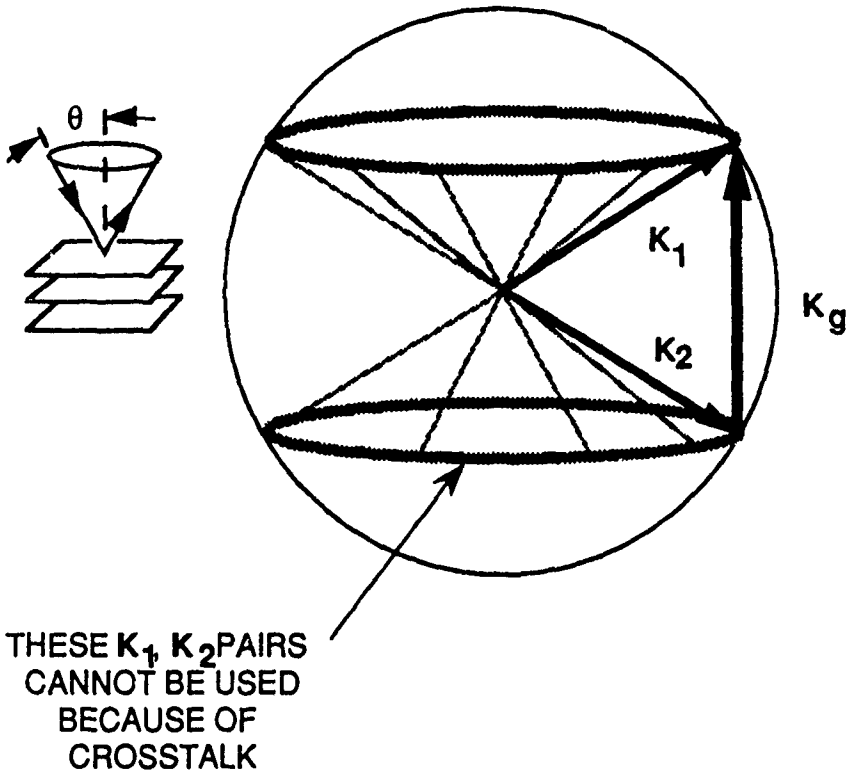

Figure 3. Geometric construction of Bragg ambiguity in single-grating-per-weight storage. Many wave-vector pairs can read out each grating, but this architecture restricts the arrangement of neurons on the SLM.

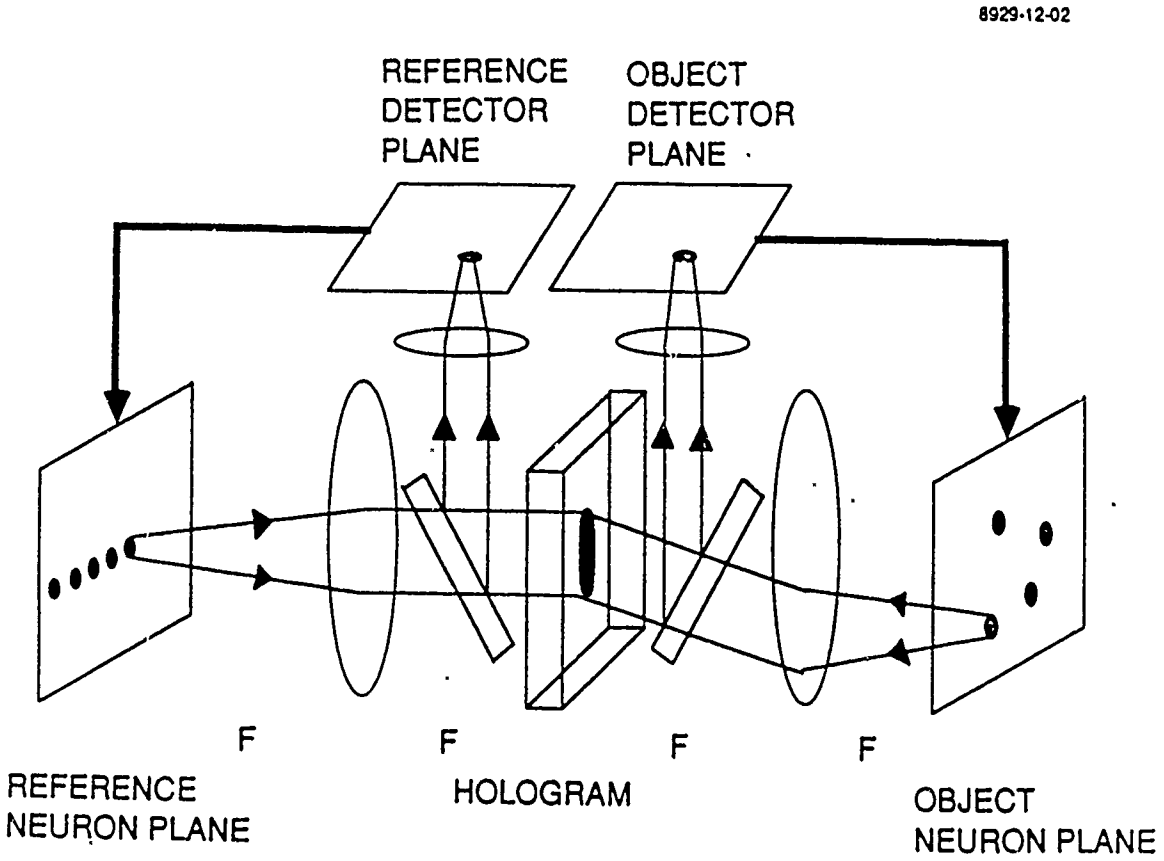

Figure 4. Photorefractive optical neural network produced by subsampling method.

controlled by the activation level of the neuron. The object and reference beamlets are collimated by two lenses of focal length F. The collimated object and reference beamlets are incident on the photorefractive crystal, where they interfere to form volume gratings and thus determine the interconnection weights. Such holographic gratings form an outer-product or Hebbian interconnection matrix [see Figure 1(a)] between the object and reference planes. Positive, negative, or complex contributions to the interconnection weights can be implemented using two exposure stages, with different phases of the LCLV readout light.

During readout, light from a particular neuron is diffracted from a photorefractive grating, sampled by a beam splitter, and focused onto a detector plane, which can be a charge-coupled device (CCD) or vidicon video camera. The object/reference detector planes are then optically or electronically mapped onto the object/reference neuron planes.

Reflection holograms would be formed, as in Figure 4. That result is usually undesirable because the diffracted light from the reference plane would not propagate in the desired direction to reconstruct the object plane. However, an additional component, a phase-conjugate mirror, can be introduced to phase-conjugate the light from the reference plane after it passes through the hologram. The reference and object beamlets then form a transmission hologram that in turn produces a real image of the object plane when the hologram is illuminated with light from the reference plane. Using a PCM to allow a single SLM to both expose and read gratings in an optical neural network was first suggested by Wagner and Psaltis.

The projected performance of the subsampled system can be estimated by analyzing the type and amount of light. Three quantities of interest can be defined: N, the total number of neurons; N_{conn}, the total number of interconnections; and R, the interconnection updating rate. N is simply given by the LCLV active area divided by the square of the neuron separation:

$$N = \frac{\pi(D/2)^2}{(\Delta x)^2}$$

where D is the diameter of the LCLV active area and Δx is the neuron separation, which is determined by the angular selectivity of the volume hologram, $\Delta\theta$, and the focal length F:

$$\Delta x = 2F\Delta\theta$$

where the expression for $\Delta\theta$ was given previously. Combining the above expressions results in

controlled by the activation level of the neuron. The object and reference beamlets are collimated by two lenses of focal length F. The collimated object and reference beamlets are incident on the photorefractive crystal, where they interfere to form volume gratings and thus determine the interconnection weights. Such holographic gratings form an outer-product or Hebbian interconnection matrix [see Figure 1(a)] between the object and reference planes. Positive, negative, or complex contributions to the interconnection weights can be implemented using two exposure stages, with different phases of the LCLV readout light.

During readout, light from a particular neuron is diffracted from a photorefractive grating, sampled by a beam splitter, and focused onto a detector plane, which can be a charge-coupled device (CCD) or vidicon video camera. The object/reference detector planes are then optically or electronically mapped onto the object/reference neuron planes.

Reflection holograms would be formed, as in Figure 4. That result is usually undesirable because the diffracted light from the reference plane would not propagate in the desired direction to reconstruct the object plane. However, an additional component, a phase-conjugate mirror, can be introduced to phase-conjugate the light from the reference plane after it passes through the hologram. The reference and object beamlets then form a transmission hologram that in turn produces a real image of the object plane when the hologram is illuminated with light from the reference plane. Using a PCM to allow a single SLM to both expose and read gratings in an optical neural network was first suggested by Wagner and Psaltis.

The projected performance of the subsampled system can be estimated by analyzing the type and amount of light. Three quantities of interest can be defined: N, the total number of neurons; N_{conn}, the total number of interconnections; and R, the interconnection updating rate. N is simply given by the LCLV active area divided by the square of the neuron separation:

$$N = \frac{\pi(D/2)^2}{(\Delta x)^2}$$

where D is the diameter of the LCLV active area and Δx is the neuron separation, which is determined by the angular selectivity of the volume hologram, $\Delta\theta$, and the focal length F:

$$\Delta x = 2F\Delta\theta$$

where the expression for $\Delta\theta$ was given previously. Combining the above expressions results in

Substituting all of the above expressions into $R = N_{conn}/\tau_E$ results in a final expression that contains only the independent parameters of the system:

$$R_{conn} = \frac{8.7\text{x}10^{-4} d_{neuron}^4}{\lambda^5 W_{1\%} I_{det}} \left(\frac{DnT_z \sin(\phi)}{F}\right)^3 \left(\frac{I_{inc}}{F_{det}}\right)^2$$

Assume the following reasonable values for the independent parameters:

λ	514 nm
n	2.5
T_z	5 mm
ϕ	45 deg
D	50 mm
d_{neuron}	30 μm
I_{inc}	5 mW/cm^2
I_{det}	0.1 mW/cm^2
W(1%)	6 mJ/cm^2
F	500 mm
F_{det}	275 mm

Those assumptions yield $N = 1.7\text{x}10^5$ neurons, $N_{conn} = 7\text{x}10^7$ interconnections, and $R = 1\text{x}10^7$ interconnections processed per second ($\tau_E = 8$ s). This is the weight updating rate. Readout of the neural net would occur at video rates, e.g. the corresponding readout rate would be $7\text{x}10^7$ interconnections divided by 30 ms, or $2\text{x}10^9$ interconnections per second. Though the exposure time τ_E is relatively long, the massive parallelism resulting from the optical interconnections results in a very high processing rate comparing favorably with that of electronic implementations.

The assumed values for the independent parameters are based on the current state of the art for LCLVs and commercially available detectors without cooling or image intensification. The value of $W_{1\%} = 6$ mJ/cm^2 is a best-case measured value for $BaTiO_3$ with an applied electric field of 10 kV/cm.[5] The assumed values are impressive compared with the corresponding values of electronic implementations, but they are limited by the subsampling of the SLM input plane. Improved storage and throughput values would result if the need for subsampling to avoid crosstalk could be avoided.

SECTION 3

STIMULATED PHOTOREFRACTIVE OPTICAL NEURAL NETWORK

3.1 SPONN CONCEPT

We have begun experimental verification of SPONN, a new and unique alternative method for avoiding the Bragg ambiguity problem. Without sacrificing parallelism, it makes full use of the SLM space-bandwidth product and provides much greater storage capacity than does the subsampling method. The essence of our idea is to store each weight in a set of angularly and spatially multiplexed gratings rather than in a single grating. The rejection of crosstalk may be greatly increased by forcing a light beam to match the Bragg condition at each of a series of spatially and angularly distributed gratings, as shown in Figure 5(b). An undesirable beam on the degenerate cone of one grating (see Figure 3 above) is rejected by the remaining gratings. That rejection allows the neurons to be arranged in arbitrary patterns on the SLM, increasing both storage capacity and throughput as well as offering other benefits such as less stringent alignment requirements and the use of the same crystal for both beam routing and storage of weights. Though we use a larger fraction of the hologram space-bandwidth product to store each weight, the increased storage space is more than offset by the improved utilization of the SLM input plane.

The physical process used to generate multiple-grating weight representation is phase conjugation based on stimulated photorefractive scattering. Specifically, we propose the use of a self- or mutually-pumped photorefractive PCM as both the storage element and the beam router in a programmable optical neural network. Basically, self-pumped phase conjugation starts with an image-bearing optical beam focused into a photorefractive crystal. Light scattered from crystal inhomogeneities will write gratings by interfering with the incident beam. The gratings will in turn scatter more light through a dynamic two-wave mixing interaction in which light energy is transferred from the incident beam to other scattered beams.

If the relevant electro-optical coefficient is large enough and the interaction length long enough, scattered light will be selectively amplified through the stimulated photorefractive gain mechanism, which can be easily observed as beam fanning in crystals of $BaTiO_3$. Through reflections of the fanned light at crystal corners[7] or through photorefractive backscattering[8], the stimulated process arranges gratings in volume distributions, which generate the phase-conjugate or time-reversed image beam propagating backward along its original incident direction.

A mutually pumped PCM operates similarly except that two image beams are focused into the crystal.[9] The light from one beam forms the phase conjugate of the other beam and vice versa, though the two beams may be incoherent with respect to each other. Gratings produced by the

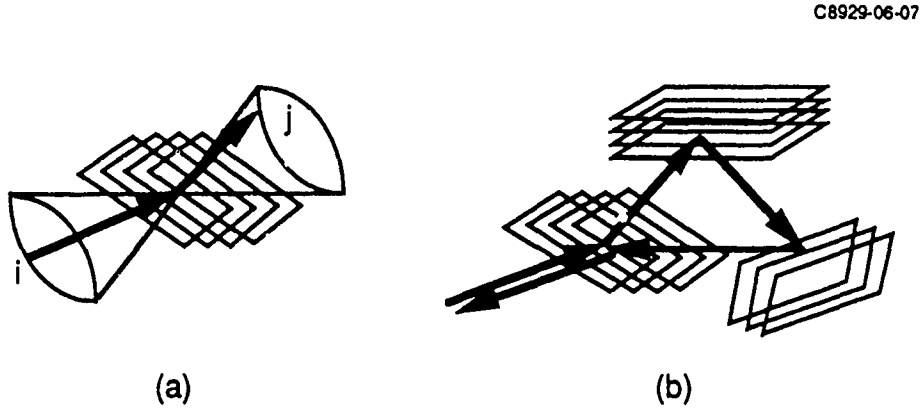

Figure 5. Use of multiple gratings to reduce crosstalk resulting from Bragg ambiguity. (a) Single grating. (b) Multiple gratings.

interference of each beam with its own fanning light arrange themselves so as to form the phase conjugates of the two incident beams. We will refer to self- and mutually-pumped PCMs collectively as stimulated PCMs, or SPCMs.

The key point for our SPONN architecture is that each pixel in the image incident on the crystal forms gratings with, and hence is connected to, many other pixels. The degree of connectivity can be adjusted by varying the position of the crystal relative to the input lens. For example, if the crystal is in the back focal plane of the lens where the Fourier transform of the input image is found, light from each pixel will overlap with light from all other pixels, establishing a very large, fully interconnected physical system suitable for implementing fully interconnected neural network models. On the other hand, if a slightly misfocused version of the input image is incident on the crystal, the pixel connections will be more localized, allowing neighborhood neural network operations such as lateral inhibition to be implemented.

Moreover, the distributed gratings form precisely the continuum of spatially and angularly multiplexed gratings described above as a method for avoiding Bragg ambiguity in optical neural networks. Simultaneously, the gratings produce an output that is the phase conjugate of the input, simplifying the optical design and making the system tolerant of component imperfections and variations. The following subsections will discuss the architecture and operation of the SPONN system as well as some initial experimental results.

3.2 SPONN ARCHITECTURE

SPONN systems using self- and mutually-pumped PCMs are diagramed in Figures 6 and 7, respectively. Neurons are represented by pixels on the HRL-invented LCLV[10] an SLM capable of displaying 10^5 pixels at video frame times (33 ms). In Figure 7, the plane of neurons is divided into sections, L_1, L_2, L_3, L_4, each of which represents a layer in the neural network. Light from the optical neurons is directed into the self-pumped PCM. The conjugate return, consisting of the input summed over the photorefractive weights, is directed by a beam splitter into a video detector such as a CCD camera. The weighted sums are passed through nonlinear neuron-activation functions electronically at video rates in the image processor, a frame grabber with nonlinear lookup tables. The result can be either sent to the host computer as a final calculation or back to the PCM through the LCLV if the network is being iteratively trained.

Incremental weight changes follow an outer-product or Hebbian learning rule. Multilayer neural networks are implemented by devoting separate areas of the LCLV to each layer. Large training sets of exemplar patterns can be accessed by means of optical or magnetic disk image storage technology. For example, commercially available disk technology will allow us to access thousands of 10^5-pixel exemplar patterns for training with random access times of less than 200 ms per pattern.

The readout time of an optical neural network (operative mode) in SPONN is one video frame time (33 ms). The current limiting factors are the respons :ime of the LCLV and our use of commercially available image processing components that are compatible with American video engineering standards. The time required to modify the weights (training mode) depends on the incident light intensity. However, for readily available continuous-wave (CW) argon laser powers of 100 mW, the parallel weight modification time is approximately 100 ms for crystals of commercially available $BaTiO_3$ at room temperature. (Other HRL researchers have successfully reduced the response time of $BaTiO_3$ by two orders of magnitude through heating to 120°C.[11]) A significant advantage of SPONN is that its optical parallelism makes the readout and modification times independent of the neural network size. With room-temperature $BaTiO_3$, the theoretical weight-processing throughput would therefore be 10^{11} interconnections per second for a network of 10^5 neurons.

Phase conjugation enables the weight storage method to compensate for optical distortions and simplify the optical design and alignment. The only critical alignment is between the output and detected images, but that can be performed electronically by the image processor. The use of a single photorefractive crystal is another beneficial feature of SPONN, especially for multilayer neural network models. Since coherent interference in SPCMs occurs between an incident beam

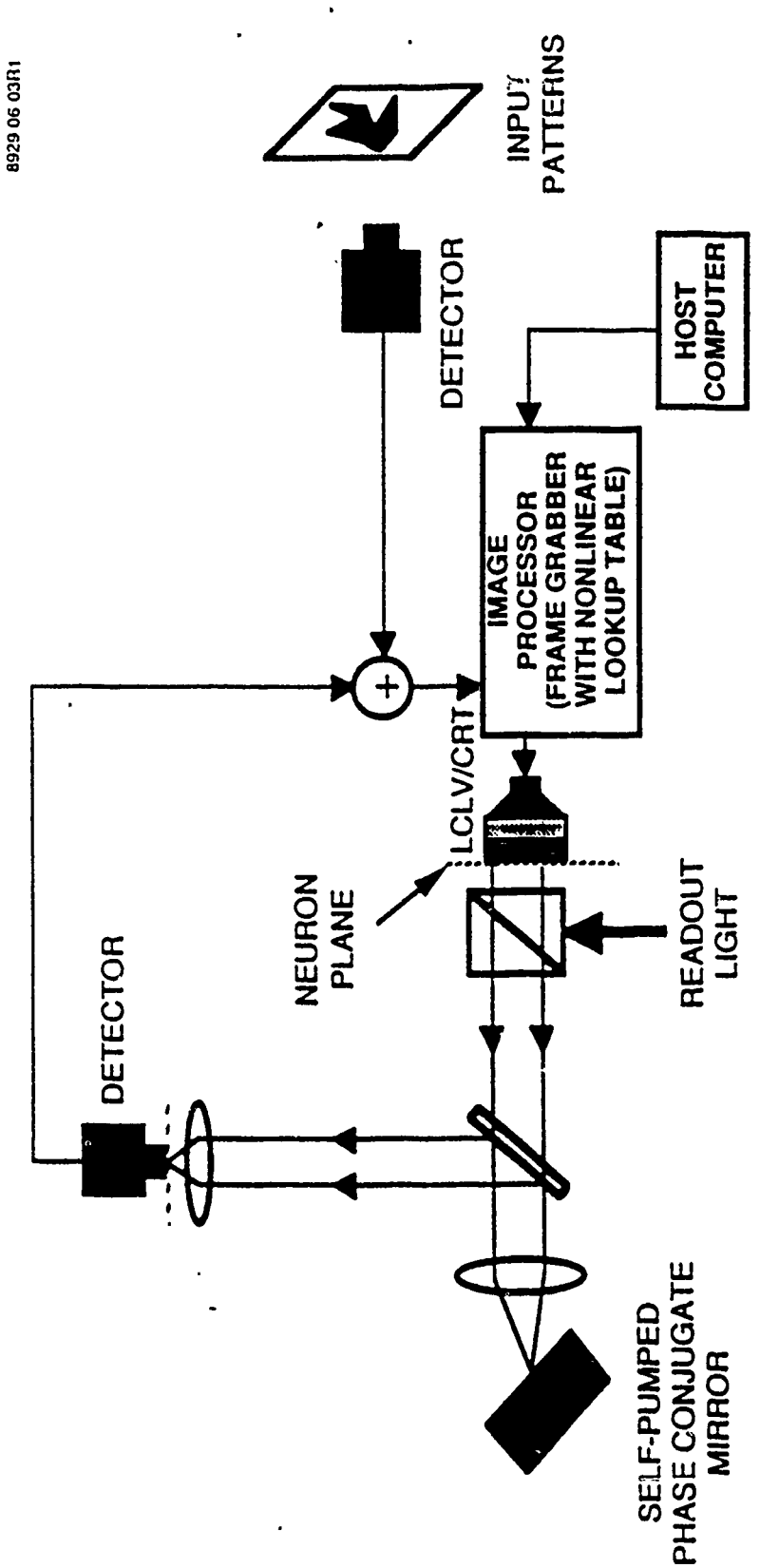

Figure 6. Self-pumped SPONN with electronic thresholding.

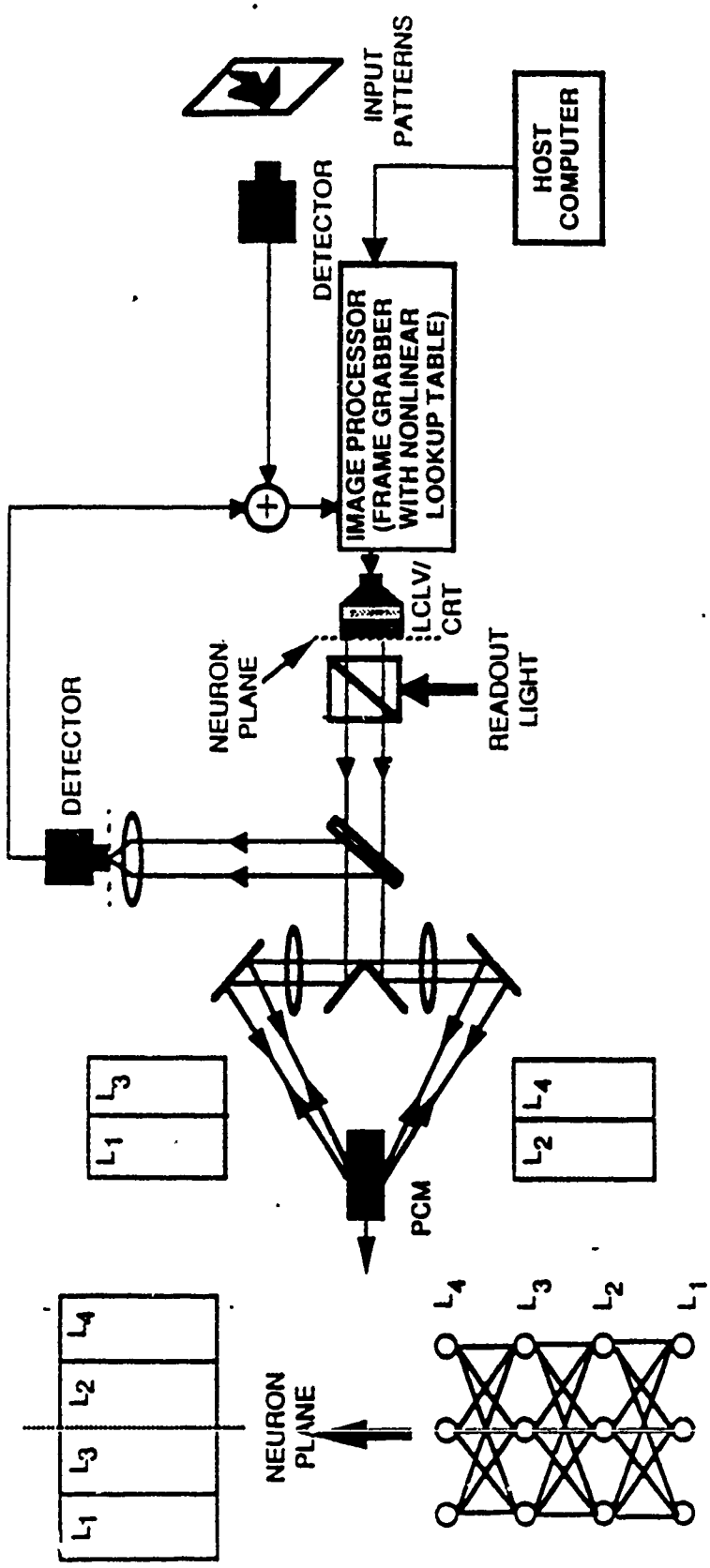

Figure 7. Three-layer SPONN using single mutually pumped PCM.

and light scattered from it, SPONN is less sensitive to vibration than other coherent interferometric optical neural networks in which separate, externally generated beams propagating over large distances must be held stable with respect to each other to within a fraction of a wavelength.

Compact, rugged, laser-diode-pumped solid state lasers with large output powers are becoming commercially available.[12] They could replace the relatively bulky, water-cooled argon laser used in our evaluation experiments. With such a laser, the SPONN system would occupy less than one cubic foot and be able to implement parallel neural networks potentially consisting of up to 10^{10} interconnections. SPONN also lends itself to modularity, as multiple units could be connected to the host computer bus, as shown in Figure 8. Multiple neural networks could then execute simultaneously on the SPONN modules, with cooperative data exchange coordinated by the host computer. Such a system could be readily expanded by simply adding more SPONN modules to the host bus.

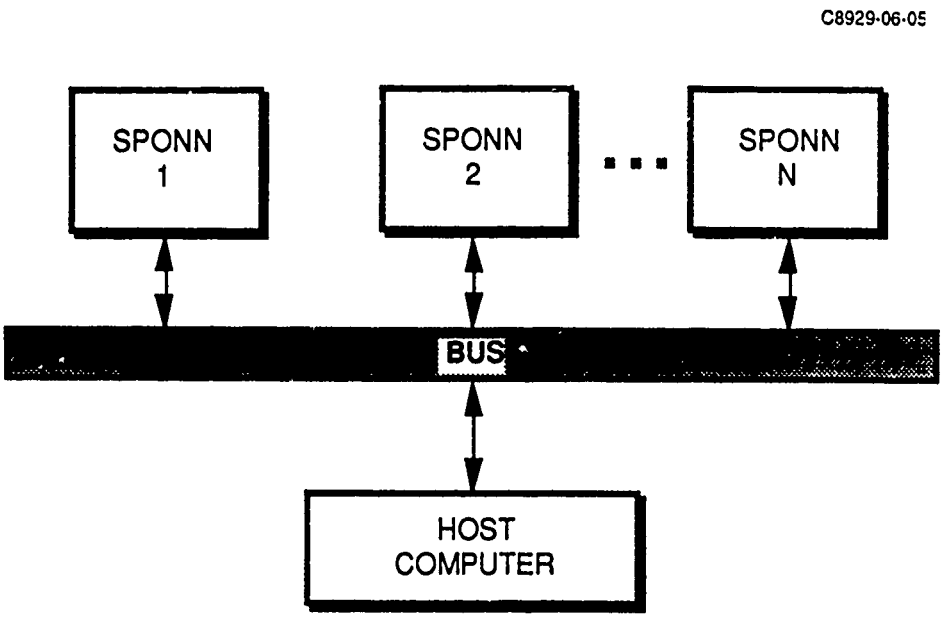

Figure 8. Expandable SPONN architecture for parallel implementation of multiple neural network modules operating cooperatively.

3.3 SPONN WEIGHT MODIFICATION

Learning, i.e., weight modification, in SPONN is accomplished by modifying the interconnection weights between neurons through changing the gratings in the photorefractive material. The material equations of Kukhtarev et al.[13] permit the derivation of a set of coupled differential equations that describe grating formation in photorefractive materials, assuming that two complex optical amplitudes A_p and A_s (of the pump and scattered beams, respectively) interfere coherently to form the space-charge field E:[14]

$$\frac{\partial A_p}{\partial x_p} = -i\frac{1}{2}(k/n_p)\, r_{eff,p} A_s E - \frac{\alpha}{2} A_p$$

$$\frac{\partial A_s}{\partial x_s} = -i\frac{1}{2}(k/n_s)\, r_{eff,s} A_p E^* - \frac{\alpha}{2} A_s$$

$$\frac{\partial E}{\partial t} + \frac{E}{t} = \frac{iE_{sc} A_p A_s^*}{\left[\tau\left(|A_p|^2 + |A_s|^2\right)\right]}$$

where x_p and x_s are coordinates along the directions of propagation of the pump and scattered waves, respectively, n_p and n_s are the refractive indices in those directions, k is the optical wave number, r_{eff} is the effective electro-optical coefficient, α is the optical absorption coefficient, τ is the space-charge field decay rate, and E_{sc} is a function of the material constants and grating wave number. The above equations cannot begin to model the full complexity of SPONN, where a great number of beams scatter and interact with each other in order to form a connection weight.

A more realistic model would require the solution of a very large system of coupled differential equations consisting of a set of equations similar to those above for each grating in the crystal, all coupled together. The boundary conditions would depend on details of crystal geometry and inhomogeneities. Nevertheless, some understanding of the grating dynamics relevant to weight formation can be obtained from the above equations by considering a single isolated grating. For example, the above equations demonstrate that the amplitude diffraction efficiency or connection weight increases with the grating space-charge field E. Also, at initial stages of grating formation ($E \equiv 0$), the rate of formation is proportional to the product of the

writing beam amplitudes. That value corresponds to outer-product or Hebbian learning. The steady-state value of E, obtained by setting the time derivative to zero, is also given by the product of the steady-state pump and scattered beams.

One approach to learning in SPONN is to first initialize the connection pathways by turning on all neurons. That establishes the gratings, which will then be modified during learning. Since the time required to form gratings in a blank crystal is much longer than the grating adjustment time, initialization also improves the learning rate. The gratings are adjusted during outer-product or Hebbian learning in SPONN by forming outer products between error signals and the input signals in the previous layer. The host computer calculates error signals by determining the difference between the actual output of SPONN and the desired output, as discussed in subsection 3.4. Learning is conducted at a rate faster than the photorefractive response time, so the gratings are never in equilibrium with the error signals. Since the photorefractive response time is intensity-dependent, SPONN can be switched from the learning mode to the readout mode simply by reducing the readout light intensity. Alternatively, hologram-fixing techniques can possibly be used for nondestructive readout.

An important advantage of SPONN is its ability to implement bipolar weights that can be selectively increased or decreased. That can be accomplished in several ways. For example, shifting the phase of a neuron on the LCLV in turn shifts the phase of the gratings written by that neuron and selectively erases connections between it and other neurons. Another method is to use two sets of gratings for each weight, one for positive weights and the other for negative weights. The difference between the two weight contributions is calculated electronically by using two SLM pixels per neuron.

3.4 EXPERIMENTAL VERIFICATION OF SPONN CONNECTIVITY

We have experimentally verified SPONN connectivity using the apparatus diagramed in Figure 6. Sample SPONN output demonstrating connectivity is shown in Figure 9 for an arbitrary abstract array of 1024 fully switched on neurons. Readout with a partial version of the training image fills in the central blank area, demonstrating that the outermost neurons have formed connections with the central ones. Another example of connectivity is shown in Figure 10, which presents complete SPONN outputs for complete and partial input images of a resolution chart.

Figure 11 illustrates the elimination of Bragg degeneracy. The steady-state phase-conjugate output for a 1024-neuron input array on the LCLV is shown in the middle photograph. When the entire array was shifted half a period in any direction by moving the data in the image proce: or

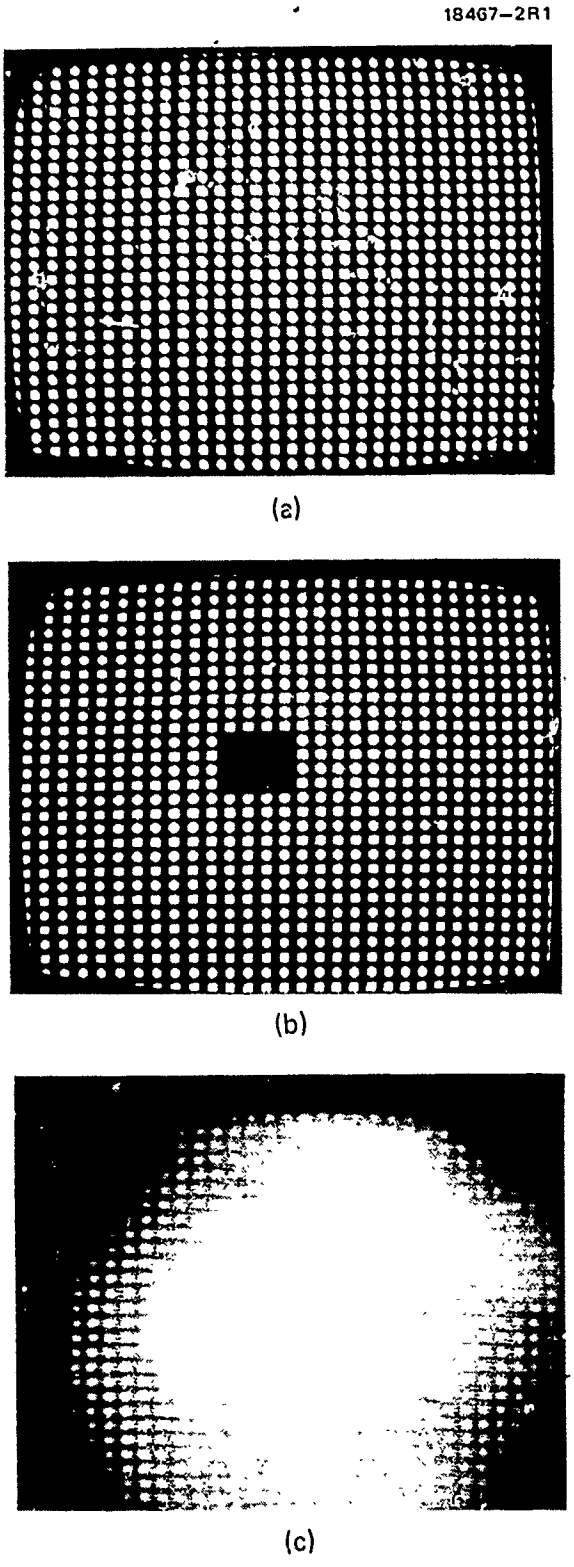

Figure 9. Experimental demonstration of SPONN connectivity. (a) Input training pattern. (b) Partial input. (c) Complete SPONN output.

18494–1

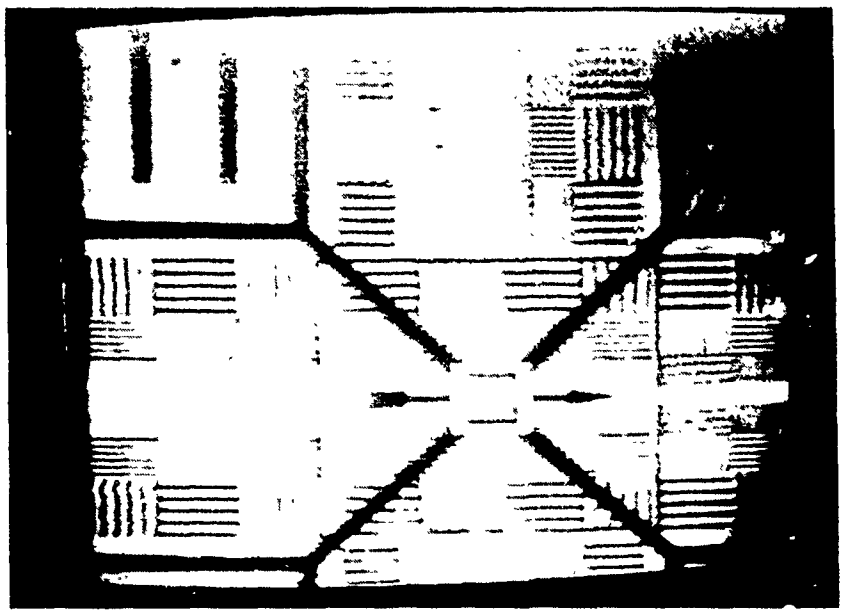

(a)

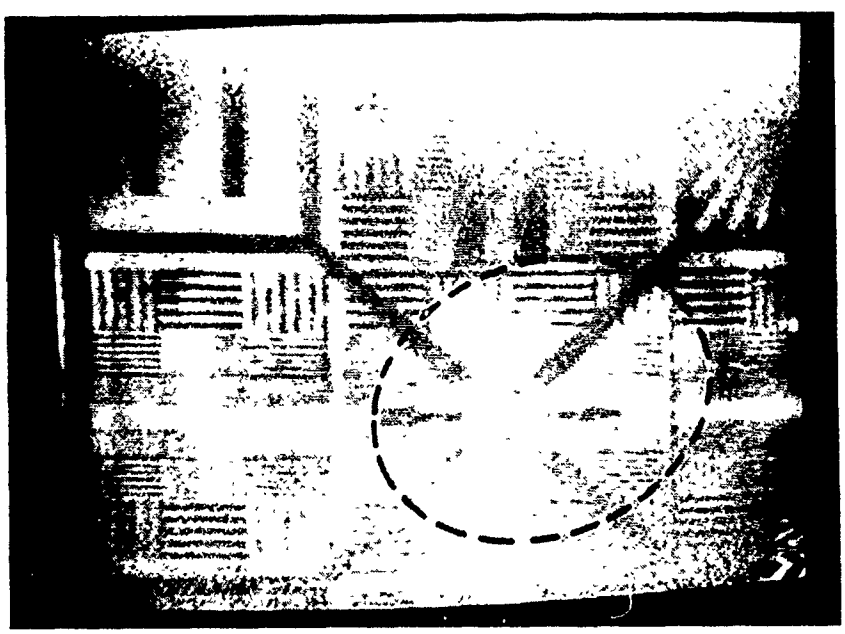

(b)

Figure 10. Experimental demonstration of SPONN connectivity with images of resolution chart. (a) SPONN output for training pattern input. b) SPONN output for partial input: region enclosed by dashed line.

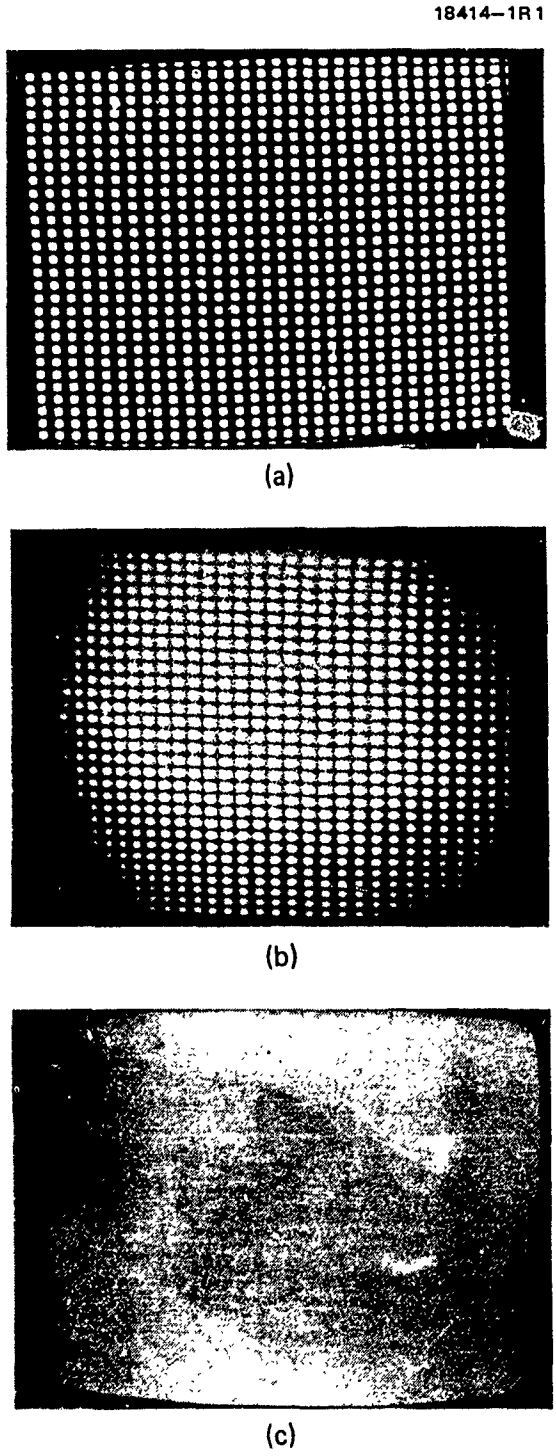

Figure 11. Experimental demonstration of crosstalk reduction in SPONN. (a) Input training pattern. (b) SPONN output for input a. (c) SPONN output for input a shifted by half an array period.

18414–1R1

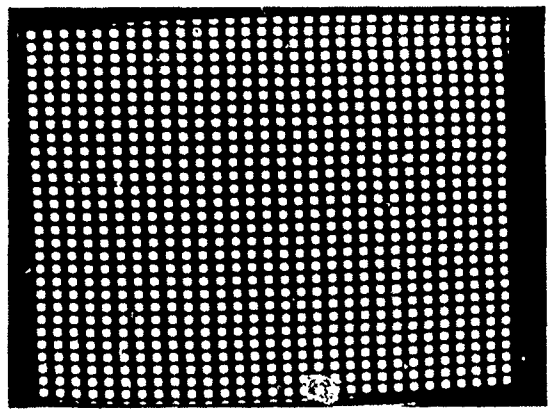

(a)

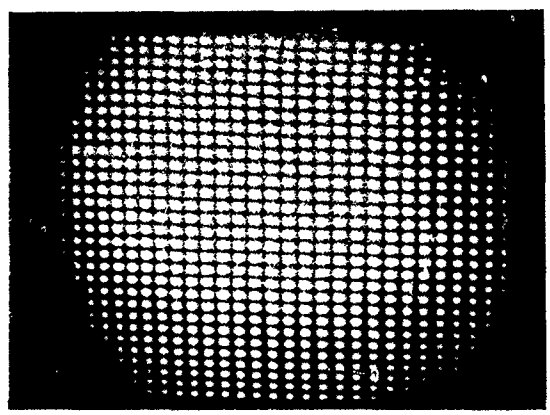

(b)

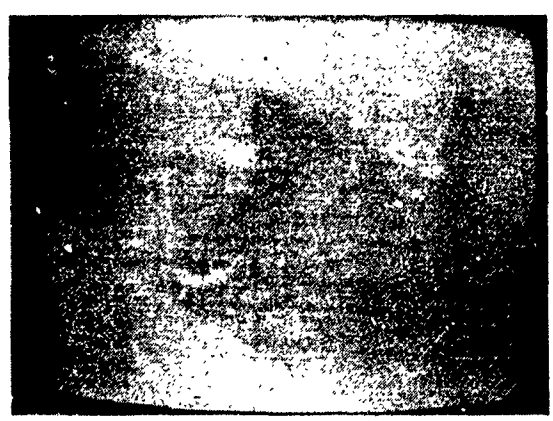

(c)

Figure 11. Experimental demonstration of crosstalk reduction in SPONN. (a) Input training pattern. (b) SPONN output for input a. (c) SPONN output for input a shifted by half an array period.

frame memory, the output disappeared immediately, demonstrating crosstalk suppression without subsampling of the SLM. The output reappeared when the array was shifted a full period.

Figure 12 illustrates selective grating weight erasure by shifting the phase of a single neuron on the LCLV. The phase of the indicated optical neuron was shifted by π without affecting its amplitude by modifying the optical amplitude versus applied voltage transfer curve. This was done by rotating the LCLV relative to the input polarization which resulted in a non-monotonic transfer curve. By adjusting the operating parameters two operating points with the same intensity but phase shifted could be defined. Computer input via the crt which addresses the LCLV was then used to select between the two operating points. A complementary grating in the crystal could then be written which compensated the initial grating, implementing active coherent erasure of weights by in effect adding a weight vector opposite in sign. In this manner bipolar weights can be implemented in a photorefractive crystal. A disadvantage of this approach to implementing bipolar weights is that although it requires only a single LCLV, gray scale operation is not possible since independent control of both phase and amplitude is not possible over a continuous range of values. This problem can be avoided by using a second LCLV operated in phase-only mode and imaging it onto the amplitude/phase LCLV. The phase-only LCLV would then be used to both implement bipolar weights and to compensate for phase distortions in the amplitude/phase LCLV. In this type of coherent representation of bipolar weights it is necessary to measure the phase of the PCM output interferometrically in order to determine the sign of the neuron outputs, which may result in practical difficulties due to stability and alignment requirements. Spatial multiplexing of the positive and negative parts of the weights using strictly positive connections can also be used to represent bipolar weights. This approach has the advantages of requiring only a single LCLV and not requiring coherent detection, but at the expense of using two pixels to represent each neuron rather than one. However, the practical advantages may be worth the trade-off in neuron number.

We have investigated the effects of crystal position relative to the focusing lens on SPONN connectivity. When the entrance face of the crystal is located in the back focal plane of the lens the connectivity is global. As shown in Figure 13, each neuron is connected to almost all of the other neurons in the input plane. This is perhaps not surprising since the region around the Fourier plane contains the largest degree of spatial overlap between beams originating from neurons in the input plane. In our initial experiments we were able to demonstrate a fanout of 256. When the crystal was moved a few mm from the Fourier plane became more localized, with the range of connections greater in the horizontal direction, as illustrated in Figure 14. This was probably due to the character of the light distribution at the entrance face being closer to an image of the input plane rather than the Fourier transform. The spatial overlap between neuron light beams was then more dependent on scattering and fanning in the crystal due to photorefractive two-beam coupling

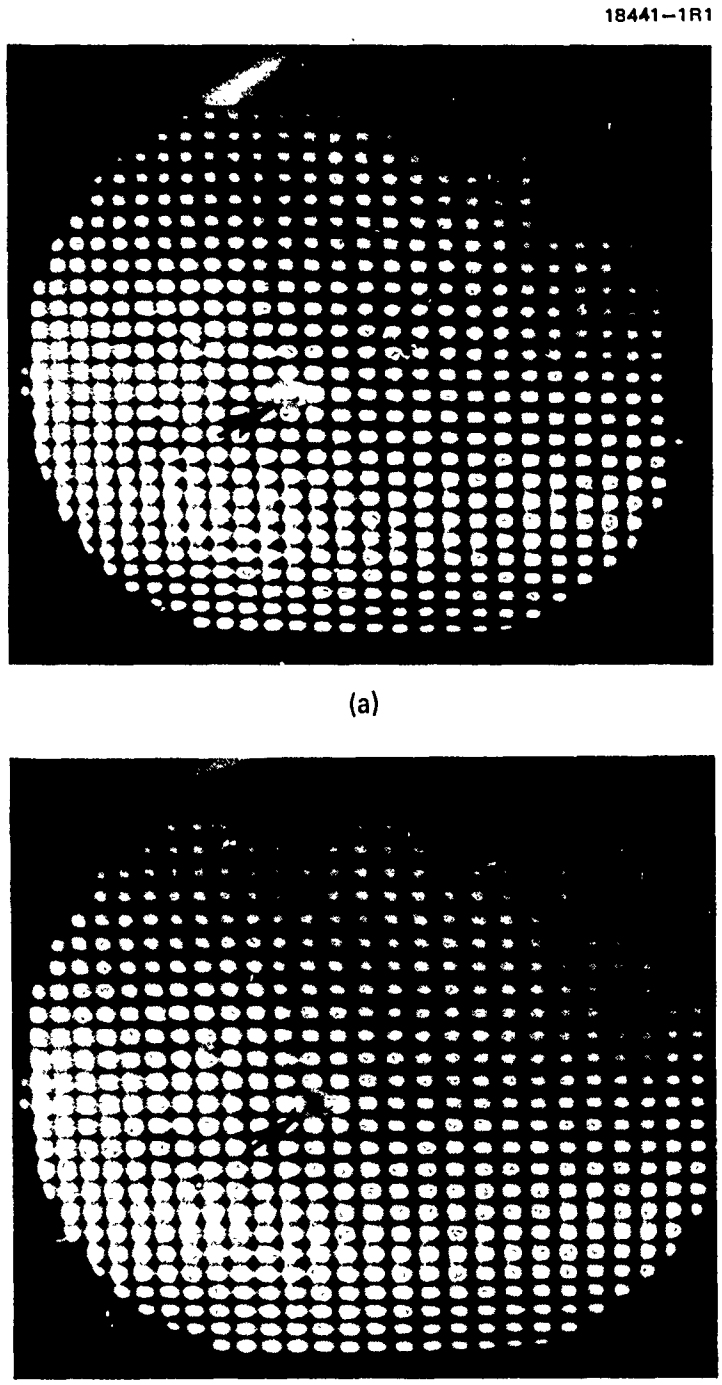

Figure 12. Experimental demonstration of selective grating weight erasure in SPONN by phase-shifting an optical neuron. (a) SPONN output for rectangular array input. (b) SPONN output after phase shifting.

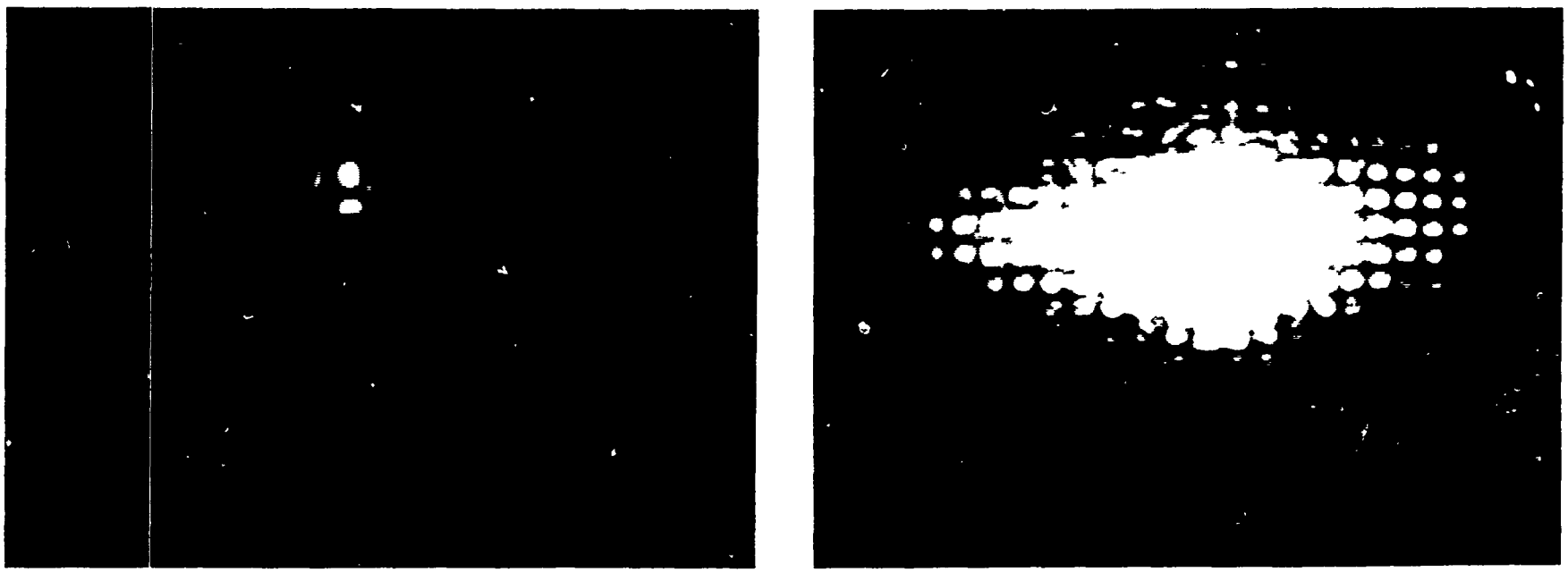

Figure 14. Demonstration of localized connectivity; crystal situated a few mm from Fourier plane of input.

effects, and also Fresnel reflections at the sides of the crystal. Since fanning occurs predominantly in the horizontal direction in $BaTiO_3$ in this geometry, it is not surprising that the connectivity has a larger range in the horizontal direction. The ability to control the range of connectivity by adjusting the position of the crystal will be useful for implementing neural network models with localized connections, such as many early vision models.

A nonfundamental but possibly practical limitation to SPONN connectivity is noise. Potential types and sources of noise include laser temporal noise, backscattered nonconjugate light from the PCM, poor conjugation fidelity, and detector noise. Fixed spatial noise or poor SLM contrast can be partially offset during the learning phase. We believe that the detector signal-to-noise ratio (SNR) may be the practical limitation for neuron fan-in/fan-out. Commercially available cooled CCD or charge-injection device (CID) detectors may be necessary to achieve the full connectivity potential of SPONN.

3.5 MAPPING OF NEURAL NETWORK MODELS

Abstract neural network models must be somehow mapped onto the optical hardware. Figure 15 illustrates the neural network topology for a self-pumped SPONN. Figure 15(a) shows a back-propagation neural network with a single hidden layer. The neuron plane on the SLM is divided into three regions, L_1, L_2, and L_3, which correspond to the input, hidden, and output layers of the neural network, respectively. The neuron activation levels are controlled by the image processor (represented schematically in Figure 6). The grating connection pathways are initialized by setting all neurons in all layers fully on until a steady-state phase-conjugate return is observed on the video detector. Learning can then proceed.

First, as shown in Figure 15(b), an exemplar pattern is created by the image processor in region L_1 while inputs to regions L_2 and L_3 are turned off. The resultant light intensities that arise from L_1 and are detected in region L_2 are then stored in the image processor after electronic thresholding by means of lookup tables. Region L_1 is then switched off, the thresholded output of L_2 is displayed on the SLM, and the resultant output intensity pattern in L_3 is detected, thresholded, and recorded in the image processor. An error pattern is formed electronically using point-by-point subtraction in the image processor. (Because only one operation is required per neuron, that step is not computationally burdensome.) The incremental weight adjustment for each layer in the back-propagation procedure is given by the outer product of the error signal and the input pattern for that layer.[15] As discussed previously, the incremental change in the diffraction efficiency of a photorefractive grating is given by the outer product of the writing beams. Therefore, the gratings in the PCM are adjusted and a single back-propagation pass is completed

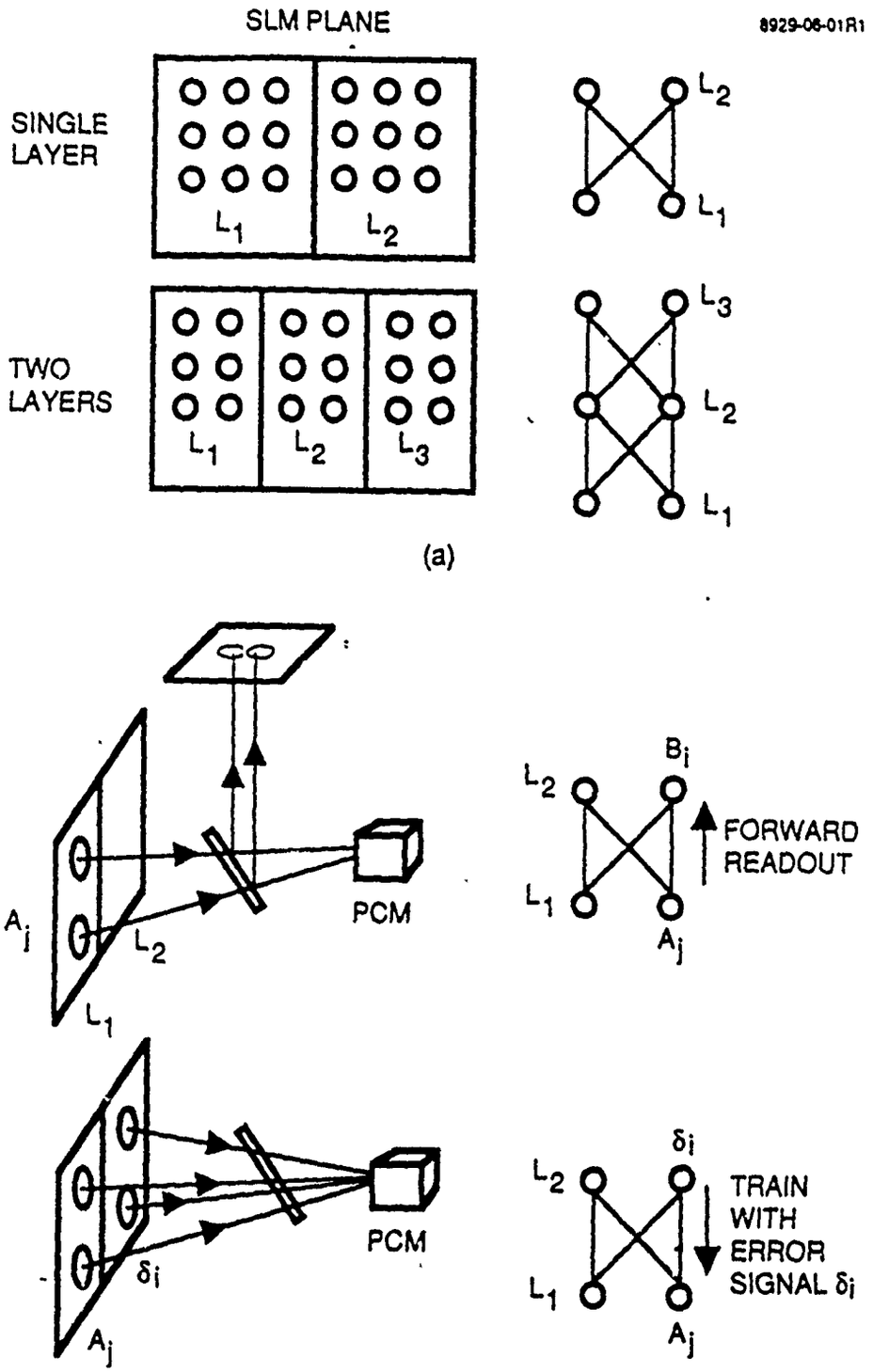

Figure 15. Neural network topology for self-pumped SPONN, with with $\delta_i = B_i - B_i^m$ formed electrically. (a) Example of supervised learning. (b) Neural network model mapped onto optical hardware.

by displaying the error pattern in L_n and the input pattern in L_{n-1}, then sequencing down through the layers. Subsequently, the next exemplar is displayed in L_1 and the procedure repeated. Since learning is a nonequilibrium process, the exemplar integration time must be less than the photorefractive time constant to prevent the "forgetting" of previous exemplar contributions.

Learning networks with localized lateral connections can also be realized by placing the PCM in a slightly misfocused image plane of the SLM rather than in the Fourier plane, as was demonstrated experimentally in the previous section. Such an arrangement would be useful for vision models that use lateral inhibition.

Holographic gratings normally form symmetric connections. Many neural network models, such as the well-known back-propagation model, assume symmetric weights. However, SPONN can also accept asymmetric weights. As shown in Figure 16(a), asymmetric SPONN interconnections in which the forward weight is different from the backward weight can be implemented by spatially shifting the output plane relative to the input plane in the image processor. That produces two separate connections between pairs of neurons, one for the forward direction and one for the backward direction. Such asymmetric weights would be useful for neural network models with dynamic feedback.

Second-order neural networks can also be implemented within the SPONN framework. Higher-order neural networks use weight tensors $w_{ijk}...$ to interconnect products of neuron activation levels $x_jx_k...$ to outputs y_i:

$$y_i = \sum_j \sum_k w_{ijk\ldots} x_j x_k \cdots$$

Such networks are useful because a single layer of such high order neurons can be used to solve problems that are not linearly separable and are therefore much more powerful than first order single layer networks such as the Perceptron. In addition, several types of invariance (such as translation and rotation) can be built into them on an a *priori* basis.[16] A limitation of high-order networks is the large increase in the number of weights as the order is increased. The parallel architecture of SPONN can be used to advantage in implementing a high-order neural network optically. For example, a possible SPONN implementation of a second order neural network is illustrated in Figure 17. The products x_jx_k formed from the neuron input layer activation levels are formed optically by crossing two one-dimensional modulators to form a outer-product of the activation vector **x** with itself. A third one-dimensional SLM is used to modulate input light with the output neuron layer activation vector **y**. The second order weighted connections are formed by

C8929-06-06

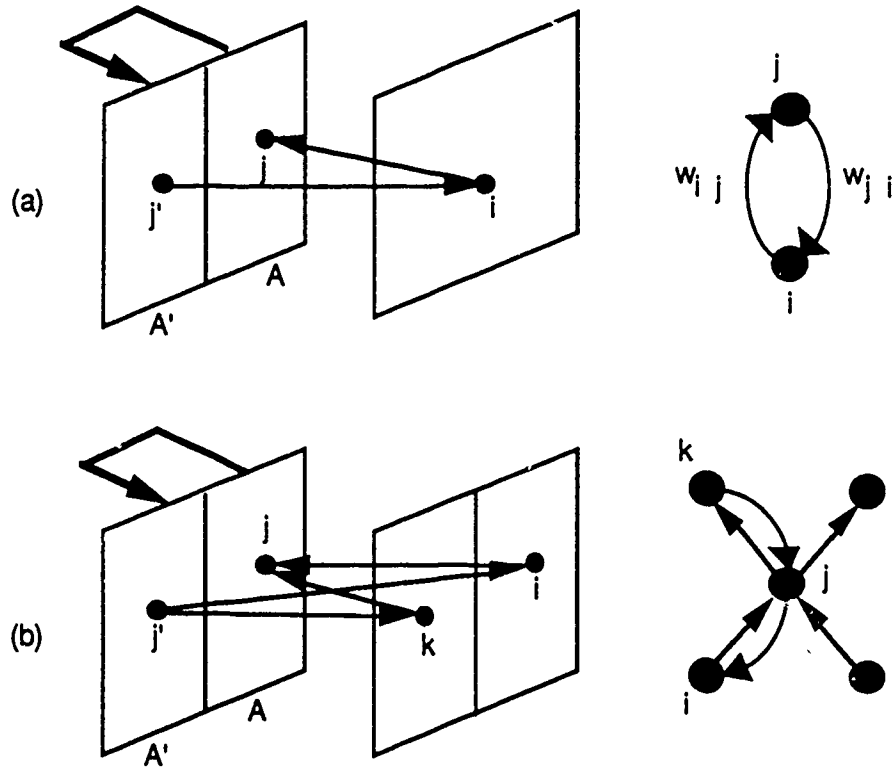

Figure 16. Asymmetric SPONN interconnections. (a) Single layer. (b) Multiple layers.

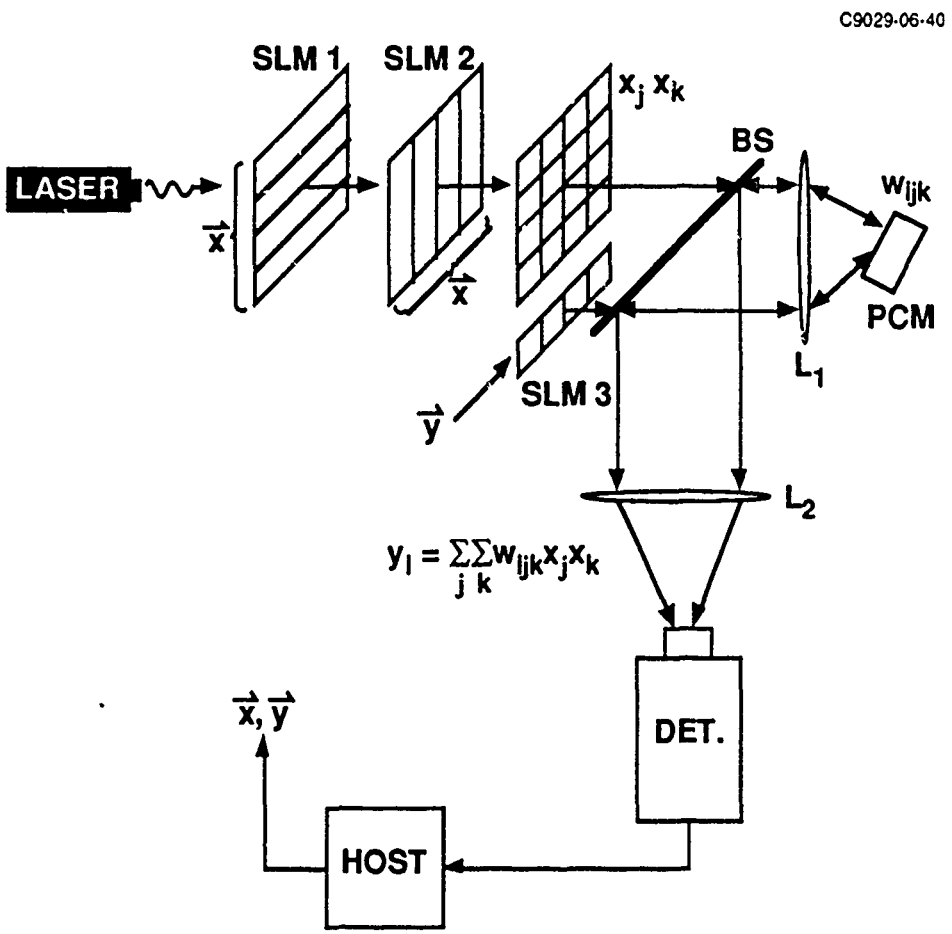

Figure 17. Second order optical interconnects using one-dimensional SLMs in an outer-product configuration.

focusing both the product matrix xTx and y into the PCM and detecting the conjugate signal. Since separate weights are formed between each pair of input pixels, a weight w_{ijk} is formed between each product $x_j x_k$ and each output neuron y_i. In this way a second order weighted tensor sum described by the above equation is formed.

3.6 RESULTS OF PERCEPTRON LEARNING EXPERIMENTS

During the 1988-1990 contract period, we performed experiments implementing the concepts discussed above for optical learning in SPONN. Our first experiment was an attempted implementation of the well-known Perceptron learning algorithm in a self-pumped SPONN, using the apparatus diagramed in Figure 6. The Perceptron learning algorithm is a single-layer neural network consisting of a set of input neurons connected to a single output neuron. It can classify linearly separable input patterns. We chose it for our first attempt at implementation because it is the simplest neural network capable of learning and adaptation. The Perceptron learning algorithm can be summarized as follows:

1. Initialize weights between input and output nodes to random values.

2. Enter pattern A_j^m and store resultant value B_i of output node.

3. Form error signal $\delta_i^m = B_i - B_i^m$ where B_i^m is the desired output.

4. Modify weights according to the outer product of the error signal and the input pattern: $\Delta w_{ij} = \eta \delta_i^m A_j^m$, where η is the adjustable convergence parameter.

5. Increase m by one and return to step 2.

The loop is iterated until the error δ is less than a specified small numerical value ε for all training patterns.

In our SPONN implementation, positive and negative weights were represented with two pixels per node pair, one for the positive part and one for the negative part of the weight. The two pixel values were subtracted electronically to form the bipolar output. The training set of input patterns consisted of the two images shown in Figure 18, a truck and a person. The neuron array size was 64x64. The bright square in the central part of each image represents the desired state of

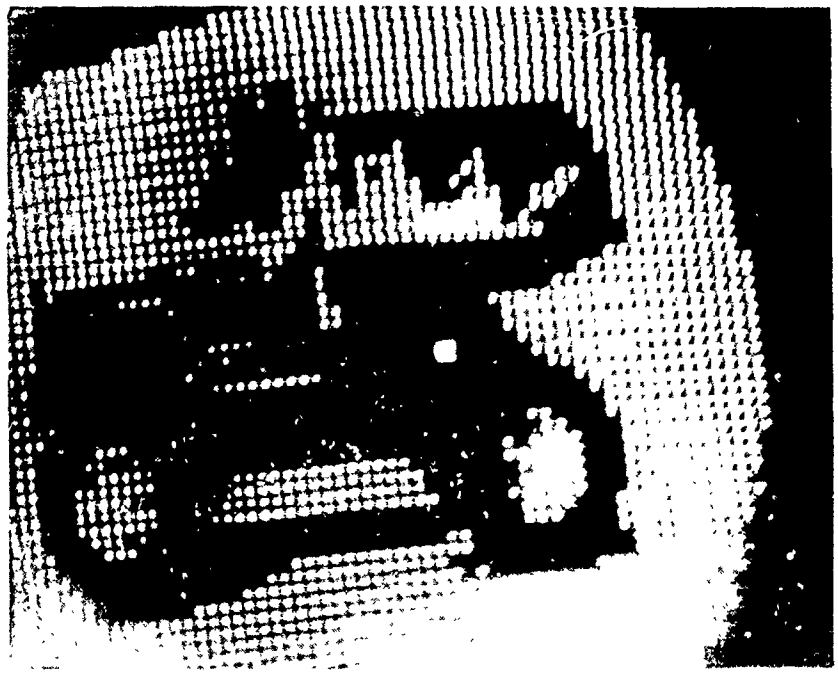

(a)

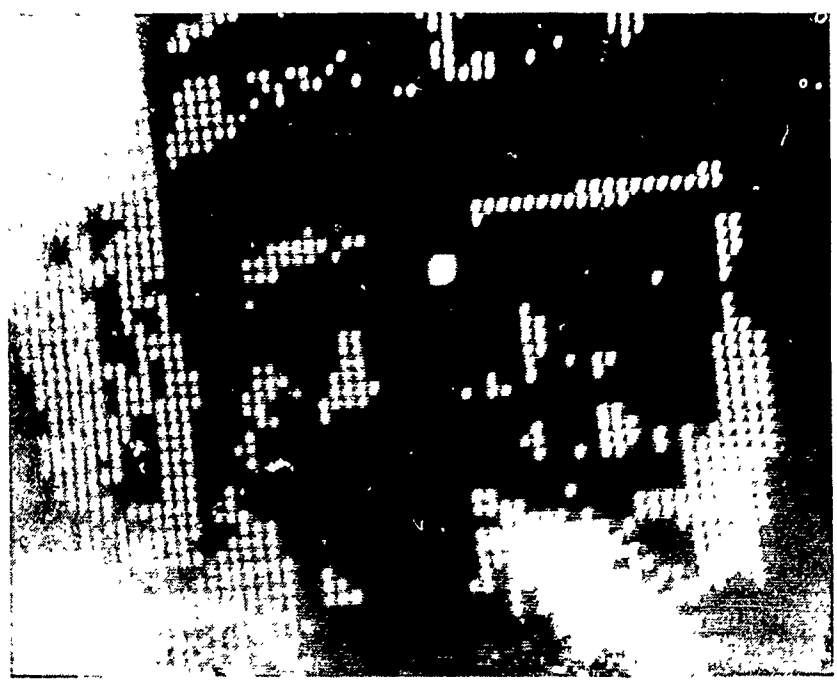

(b)

Figure 18. Input training patterns for Perceptron learning. (a) Input truck image. (b) Input person image.

the output node. As each image was input into the PCM, the output node state was read by the frame grabber and compared with the desired state. An error signal, used in displaying the weights, was then shown on the LCLV along with the input pattern. The frame time was adjusted to be shorter than the photorefractive response time to prevent the photorefractive gratings from being in equilibrium with the input patterns.

The result is evident in Figure 19, which shows the PCM optical output for the two input training patterns; the overlapping output patterns are due to the nonorthogonality of the input patterns. We are currently investigating the reasons for the similarity of the two outputs. Even though the two input patterns have many pixels in common one would expect a greater difference between the output patterns. Figure 20 presents photographs of the scattered-light distributions in the crystal taken from a vantage point above the crystal for the two input training patterns. The photographs indirectly show the general locations of photorefractive gratings. The two light distributions are not identical, indicating that different gratings were formed for the two input patterns.

Plots of the total error versus iteration number showed that, after about 300 iterations, the error decreased to zero for several iterations, after which it would increase and then decrease again. That behavior was, we believe, due to unintended grating decay caused by the destructive readout of the PCM gratings. A zero value for the error signal indicated that a solution had been found for the weights. The weights, however, were subsequently modified by the readout process.

3.7 PERMANENT STORAGE OF WEIGHT VALUES

Conventional hologram-fixing techniques in photorefractive crystals involve heating and/or application of an external electric field in order to transfer photoinduced gratings to space-charge gratings in optically insensitive levels.[17] Initially, a hologram is written using conventional photorefraction. A π-phase-shifted space-charge pattern that compensates for the photorefractive hologram is then induced by heating the crystal until ionic charge can move and cancel the space charge arising from the trapped carriers. Reducing the temperature immobilizes the ions again. The trapped grating charges are then activated by flooding the crystal with light. Under an applied or photovoltaic field, the mobile charges drift and become spatially uniform, leaving only the mirror-image hologram, which cannot be erased with optical radiation alone. The ionic hologram can be erased by reheating the crystal. In some cases, externally applied electric fields can be used in place of or in combination with heating of the crystal to move the ionic charge. Researchers at HRL recently demonstrated hologram fixing in $Bi_{12}TiO_{20}$ using these techniques.[18]

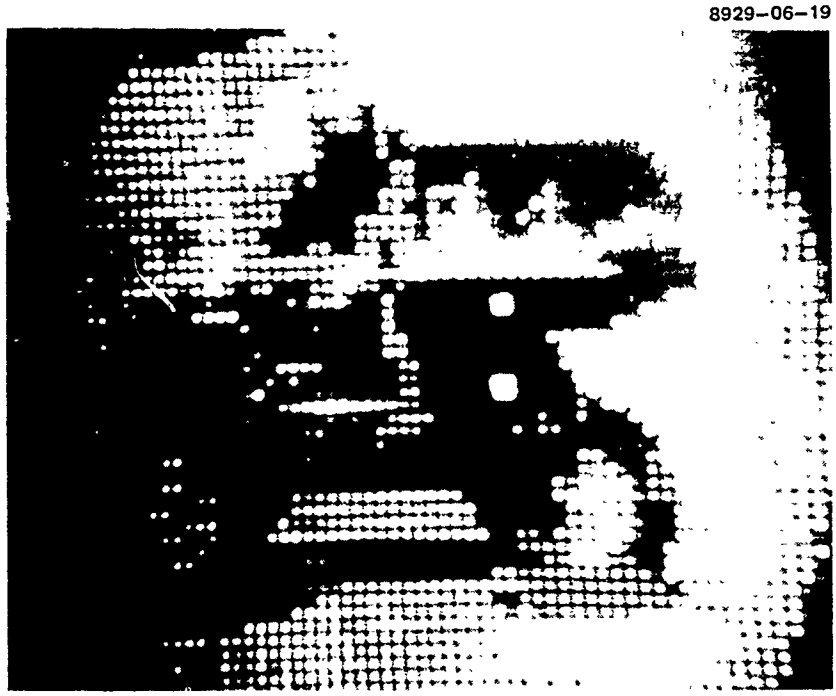

(a)

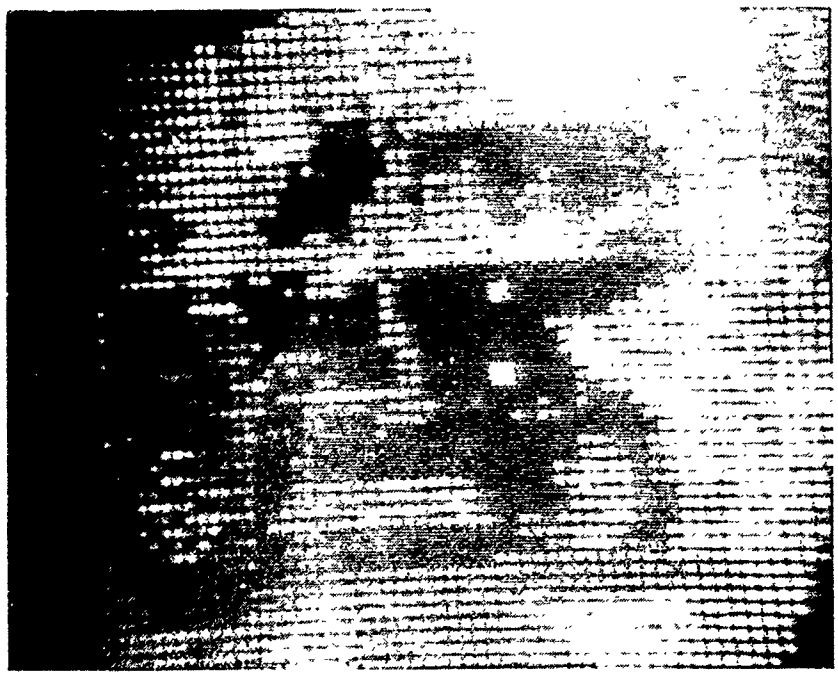

(b)

Figure 19. Output patterns displayed during Perceptron learning. (a) For input truck image. (b) For input person image.

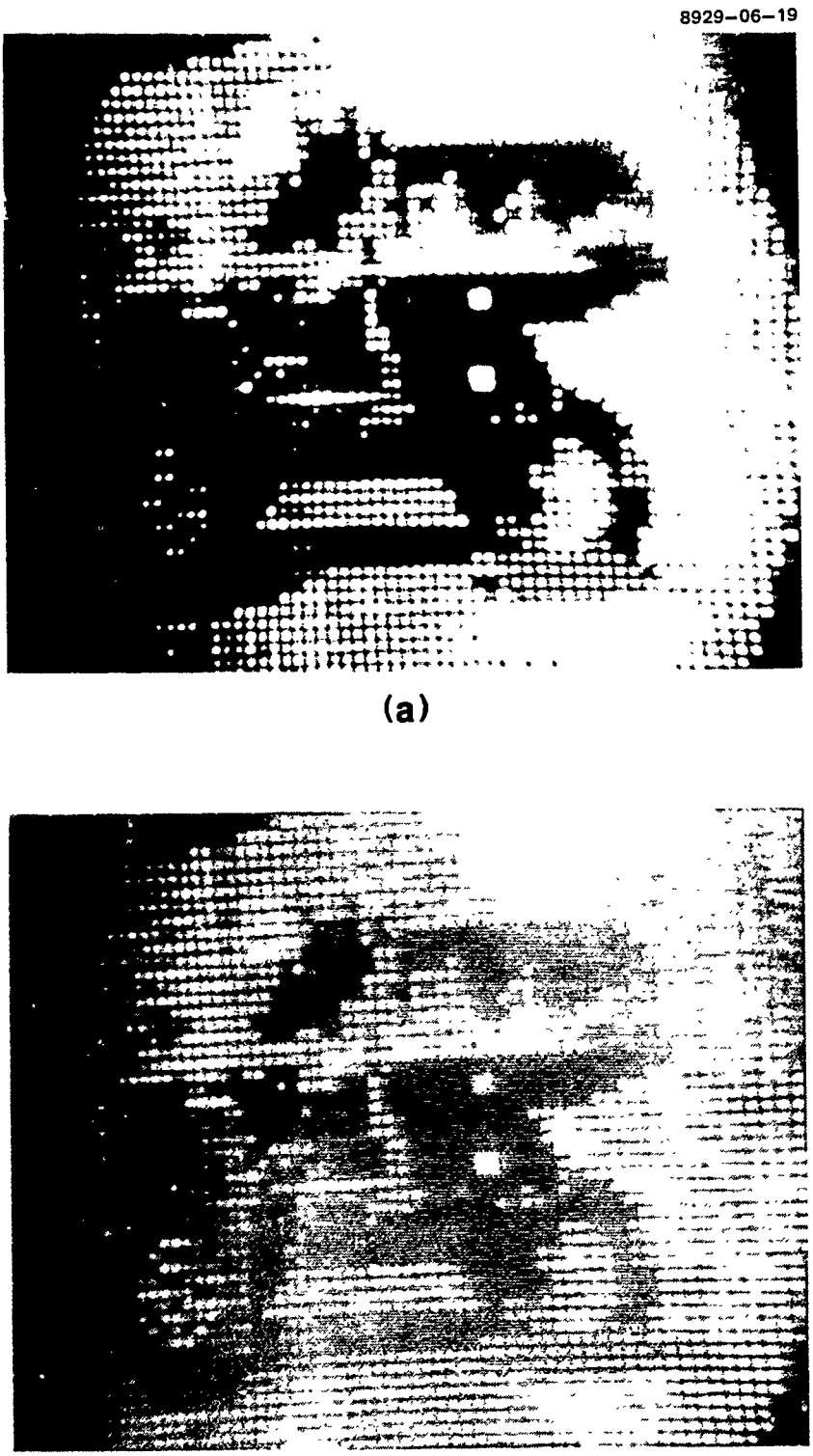

Figure 19. Output patterns displayed during Perceptron learning. (a) For input truck image. (b) For input person image.

In ferroelectric materials with low coercive fields (on the order of 1 kV/cm) such as $BaTiO_3$ and $Sr_{1-x}Ba_xNb_2O_6$ (SBN), an alternative technique has been demonstrated: electrical fixing by domain reversal.[19] (The coercive field is the critical applied electrical field required to reverse the polarization of a ferroelectric crystal.) A spatial pattern of domains can be produced by applying a field just below the coercive value and opposed to the orientation of the existing polarization. If that is done after the hologram is recorded, the domain pattern can mirror the recorded hologram. Holograms fixed using domain reversal cannot be erased optically, but application of a strong poling field will restore the initial blank state in the crystal.

Storage times greater than an hour can be obtained in $BaTiO_3$ without fixing by reducing the readout light intensity. Initial learning experiments would use dynamic refreshing of the weights instead of fixing.

SECTION 4

SUMMARY

In this final report for work performed in the period March 1988 to June 1990 we have described our efforts toward optical implementations of neural network models. Under this effort we have begun development of SPONN (Stimulated Photorefractive Optical Neural Network), a hybrid optoelectronic system for programmable, adaptive, and fully parallel direct physical implementations of neural network models. In SPONN, neurons are implemented as two-dimensional arrays of pixels (10^5 to 10^6 neurons) on a spatial light modulator which are interconnected optically in the third dimension. The nonlinear neuron activation functions are implemented electronically. Individual connection weights are stored optically as a set of angularly and spatially distributed gratings generated by stimulated processes in a photorefractive medium. These dynamic processes also generate the phase conjugate of the input light distribution. This approach greatly reduces crosstalk between neurons due to Bragg degeneracy and permits significant increases in neuron and interconnection storage capacities and throughput over subsampled optical neural network implementations. Potential throughput rates are as high as 10^{11} interconnections per second. Reduced system size and complexity result from the use of a single photorefractive crystal for all optical tasks, including weight storage and beam routing by means of phase conjugation. In addition, the phase conjugation compensates for distortions in the optical components. The architecture is programmable and expandable, and it permits the implementation of both fully and partially interconnected multilayer neural network learning models (e.g., the well known back-propagation model), including laterally connected models. Both globally and locally connected neural network models can be mapped onto the architecture. Higher order neural network models in which connection weights are tensors rather than matrix elements can also be implemented. We have described experimental results on SPONN connectivity, crosstalk suppression, and weight modification using the Perceptron learning algorithm.

REFERENCES

1. G.C. Valley and M.B. Klein, "Optimal properties of photorefractive materials for optical data processing," Opt. Eng. **22**, 704-711 (1983).

2. E. Kratzig, F. Welz, R. Orlowski, V. Doorman, and M. Rosenkranz, "Holographic storage properties of BaTiO3," Solid State Commun. **34**, 817-819 (1980).

3. H. Kogelnik, "Coupled wave theory for thick hologram gratings," Bell Syst. Tech. J. **48**, 2909 (1969).

4. P.J. van Heerden, "A new optical method of storing and retrieving information," Appl. Opt. **2**, 387-392 (1963).

5. D. Psaltis, J. Yu, X.G. Gu, and H. Lee, "Optical neural nets implemented with volume holograms," in Technical Digest of Topical Meeting on Optical Computing (Optical Society of America, Washington, D.C., 1987).

6. Y. Owechko, "Optoelectronic resonator neural networks," Appl. Opt. **26**, 5104-5111 (1987).

7. J. Feinberg, "Self-pumped continuous wave phase conjugation using internal reflection," Opt. Lett. **7**, 486 (1982).

8 J.F. Lam, "Origin of phase conjugate waves in self-pumped photo-mirrors," Appl. Phys. Lett. **46**, 909-911 (1985)

9. S. Weiss, S. Sternklar, and B. Fischer, "Double phase conjugate mirror: Analysis, demonstration, and applications," Opt. Lett. **12**, 114-116 (1987).

10. U. Efron, J. Grinberg, P.O. Braatz, M.J. Little, P.G. Reif, and R.N. Schwartz, "The silicon liquid-crystal light valve," J. Appl. Phys. **57**, 1356-1368 (1985).

11. D. Rytz, M.B. Klein, R.A. Mullen, R.N. Schwartz, G.C. Valley, and B.A. Wechsler, "High-efficiency fast response in photorefractive BaTiO3 at 120oC," Appl. Phys. Lett. **52**, 1759-1761 (1988).

12. G.T. Forrest, "Diode-pumped solid-state laser markets and production expand," Laser Focus/Electro-optics **24**, 57-74 (1988).

13. N.V. Kukhtarev, V. Markov, and S. Odulov, "Transient energy transfer during hologram formation in LiNbO3 in external electric field," Opt. Commun. **23**, 338-343 (1977).

14. G.C. Valley, "Competition between forward- and backward-stimulated photorefractive scattering in BaTiO3," J. Opt. Soc. Am. **B4**, 14-19 (1987).

15. D.E. Rumelhart and J.L. McClelland, eds., Parallel Distributed Processing, Massachusetts Institute of Technology Press, Cambridge, MA, 1986.

16. C. L. Giles and T. Maxwell, "Learning, Invariance, and Generalization in High-Order Neural Networks," Appl. Opt. **26**, 4972, 1987.

17. D.L. Staebler and J.J. Amodei, "Thermally fixed holograms in LiNbO3," Ferroelectrics 3, 107-113 (1972).

18. S.W. McCahon, D. Rytz, G.C. Valley M.B. Klein, and B.A. Wechsler, "Hologram fixing in $Bi_{12}TiO_{20}$ using heating and an AC electric field," submitted to Applied Optics (Dec 1988).

19. F. Micheron and G. Bismuth, "Electrical control of fixation and erasure of holographic patterns in ferroelectric materials," Appl. Phys. Lett. **20**, 79-81 (1972).

Publications

Y. Owechko and B. H. Soffer, "An Optical Interconnection Method for Neural Networks Using Self-Pumped Phase Conjugate Mirrors," submitted to Optics Letters, Nov. 1990.

Y. Owechko, "Nonlinear Holographic Associative Memories," IEEE J. Quan. Electron. 25, 619, March, 1989. (Invited Paper)

Y. Owechko, B. H. Soffer, and G. J. Dunning, "Optoelectronic Neural Networks Based on Holographically Interconnected Image Processors," SPIE Vol. 882, 143 (1988).

Y. Owechko, "Holographic Associative Memories," SPIE Vol. 1150, 164 (1989).

Patent

Y. Owechko, "Self-Pumped Optical Neural Networks," Filed U.S. Patent Application, PD 88450.

Presentations

Y. Owechko, G. J. Dunning, and B. H. Soffer, "Optical Neural Networks Based on Stimulated Photorefractive Effects," 1990 Optical Society of America Annual Meeting, Boston. (Invited Talk)

Y. Owechko, "Photorefractive Optical Neural Networks," 1990 International Topical Meeting on Optical Computing, Kobe, Japan. (Invited Talk)

Y. Owechko, "Self-Pumped Optical Neural Networks," Salt Lake City Topical Meeting on Optical Computing, Feb. 1989.

Y. Owechko and B. H. Soffer, "Programmable Multi-Layer Optical Neural Networks With Asymmetric Interconnection Weights," International Conference on Neural Networks, San Diego, July 1988.

APPENDIX A

Submitted to Optics Letters
(Shortened Version)

An Optical Interconnection Method for Neural Networks Using Self-Pumped Phase Conjugate Mirrors

Y. Owechko and B. H. Soffer

Hughes Research Laboratories
3011 Malibu Canyon Rd
Malibu, CA 90265

Abstract

We describe an optical interconnection method based on self-pumped phase conjugate mirrors in which each connection weight is distributed among many angularly and spatially multiplexed gratings. This approach greatly reduces crosstalk caused by the conical Bragg degeneracy associated with a single grating and permits the entire input plane to be used. Applications to optical neural networks are described.

Optics is often suggested as an alternative to electronic implementations of neural network models because of its inherent parallelism and three-dimensional connectivity. The global connectivity of optics is particularly appealing with regard to the communication requirements of many neural network models in which each processing node or "neuron" receives a weighted sum of the outputs of the neurons in the preceeding layer. Both spatial light modulator (SLM) -based and holographic approaches for storing the weights have been proposed. Holographic approaches based on photorefractive materials are attractive for the implementation of large neural networks because of the large storage capacity[1] and the capability for the adjustment of all inter-layer weights in parallel. To the best of our knowledge, all previous holographic proposals have utilized one photorefractive grating to store each connection weight.

A limitation of the single grating per weight approach is that even if the gratings are formed in a thick medium with high Bragg selectivity, reading beams other than the pair that originally wrote the grating can reconstruct an output beam. For a single grating, all incident K vectors which lie on a cone defined by the Bragg angle will read out the grating. This Bragg degeneracy cone results in crosstalk between neurons which is unacceptable in neural network models. One approach which has been suggested to avoid this problem is to arrange the pixels on the input and output planes in special nonredundant patterns such that unique angles between pairs of writing and reading beams are defined.[2] Extraneous connections are still formed but they are made to areas of the input/output planes which are not allowed to contribute to the final output. Although this approach solves the grating crosstalk problem, it also results in subsampling of the input SLMs and under-utilization of the available SLM space-bandwidth product. Specifically, if the SLM is capable of displaying N^2 neurons with N^4 potential interconnections, then the single grating per weight approach can only implement $N^{3/2}$ neurons and N^3 weights, provided the storage capacity of the photorefractive crystal is not exceeded. [2] The diffraction efficiency is also reduced because

Optics is often suggested as an alternative to electronic implementations of neural network models because of its inherent parallelism and three-dimensional connectivity. The global connectivity of optics is particularly appealing with regard to the communication requirements of many neural network models in which each processing node or "neuron" receives a weighted sum of the outputs of the neurons in the preceeding layer. Both spatial light modulator (SLM) -based and holographic approaches for storing the weights have been proposed. Holographic approaches based on photorefractive materials are attractive for the implementation of large neural networks because of the large storage capacity[1] and the capability for the adjustment of all inter-layer weights in parallel. To the best of our knowledge, all previous holographic proposals have utilized one photorefractive grating to store each connection weight.

A limitation of the single grating per weight approach is that even if the gratings are formed in a thick medium with high Bragg selectivity, reading beams other than the pair that originally wrote the grating can reconstruct an output beam. For a single grating, all incident K vectors which lie on a cone defined by the Bragg angle will read out the grating. This Bragg degeneracy cone results in crosstalk between neurons which is unacceptable in neural network models. One approach which has been suggested to avoid this problem is to arrange the pixels on the input and output planes in special nonredundant patterns such that unique angles between pairs of writing and reading beams are defined.[2] Extraneous connections are still formed but they are made to areas of the input/output planes which are not allowed to contribute to the final output. Although this approach solves the grating crosstalk problem, it also results in subsampling of the input SLMs and under-utilization of the available SLM space-bandwidth product. Specifically, if the SLM is capable of displaying N^2 neurons with N^4 potential interconnections, then the single grating per weight approach can only implement $N^{3/2}$ neurons and N^3 weights, provided the storage capacity of the photorefractive crystal is not exceeded. [2] The diffraction efficiency is also reduced because

where x_p and x_s are coordinates along the directions of propagation of A_p and A_s, n_p and n_s are the refractive indices in those directions, k is the optical wavenumber, r_{eff} is the effective electrooptic coefficient in the direction of propagation, τ is the space-charge field decay rate, α is the absorption coefficient, and $E_{sc}=E_D/(1+E_D/E_q)$ where E_D is the diffusion field and E_q is the limiting space-charge field. It is clear from the above equations that the connection weight between the two amplitudes A_p and A_s increases with the space-charge field E. The growth of E during the formation of the grating is in turn determined by the product $A_pA_s^*$, which matches the Hebbian learning rule common to many neural net models. Moreover, the observed distributions of beams within a self-pumped PCM, which are determined by the high coupling gain of $BaTiO_3$, scattering centers, reflections from crystal faces, and the geometry of the PCM configuration,[4] suggest that light beams from the entire input plane mix in the crystal, resulting in the global interconnection of input pixels by a self-pumped PCM, especially if the PCM is in the Fourier plane of the input spatial light modulator.[5,6] Since a beam from one pixel must diffract from a large set of spatially distributed gratings in order to form the conjugate of a second pixel, the crosstalk should be low according to the arguments presented previously.

We have performed a series of experiments to test these conjectures for the grating selectivity and global connectivity of the SPONN (Stimulated Photorefractive-effect Optical Neural Network) approach. In our first set of experiments, we tested the Bragg selectivity of a self-pumped PCM operating in the internal loop geometry.[7] The $BaTiO_3$ crystal was obtained from Sanders Associates. The laser source was an argon ion laser operating at 514 nm which illuminated a fixed mask with a 9x9 square array of pixels consisting of 1 mm diameter holes. The transmitted light was then focused into the crystal using a 100-mm focal length lens. The crystal was located in the Fourier plane of the mask in order to maximize the overlap between light beams from the pixels. The steady state conjugate return is shown in Fig. 2a. The mask was then translated in a direction transverse to the beam path by half of

the hole period in a time span short compared to the photorefractive response time of 5 sec, which was set by the total power incident into the crystal of 1 mw. The output plane immediately after the translation is shown in Fig. 2b. The lack of any observable signal despite the regular arrangement of pixels in the input plane confirms that very little crosstalk due to the Bragg degeneracy effect is present in SPONN. The signal-to-noise ratio of the CCD video camera was 100:1. Translating the array by another half period so that the original positions of the holes were reproduced resulted in the immediate reconstruction of the conjugate signal, verifying that the gratings had not been erased.

We then replaced the fixed mask with a Hughes Liquid Crystal Light Valve (LCLV) in order to demonstrate global connectivity and associative recall. In this experiment the initial input consisted of a 16x16 array of pixels, each of which was randomly assigned values of 1 or 0. The steady state conjugate output is shown in Fig. 3a. We then switched to an input consisting of a single pixel by translating an opaque mask with a single small aperture in front of the LCLV. (By using an opaque mask rather than simply turning off the other pixels we eliminated extraneous readout of the PCM by background light due to the finite contrast ratio of the LCLV.) The single-pixel input is shown in Fig. 3b and the resultant conjugate output of the entire input pattern is shown in Fig. 3c. Note that weights were formed between the pixel and all of the other active pixels, demonstrating associative recall and global connectivity with a fanout of 1:128. The degree of fanout we could demonstrate was limited by the sensitivity of our CCD camera, not by the PCM. The fact that each pixel occupied 1/1000 of the active area of the LCLV suggests that a fanout of 1:1000 could have been observed if a sufficiently sensitive camera had been available.

Neural network models can be implemented using the multiple-grating per weight approach. The complex reflectance of pixels on the LCLV would represent neuron activation levels. The conjugate return, consisting of the inputs to each neuron summed over the photorefractive weights, is directed by a beam splitter into the CCD camera, the output of which is digitized and thresholded at video rates using lookup tables in an image processor

card in the host computer. In the case of feedforward supervised learning networks such as backpropagation, error signals can be calculated by the host and displayed on the LCLV. As discussed above, weight changes follow a Hebbian or outer-product learning rule. The frame time of the LCLV would be adjusted to be shorter than the photorefractive response time so that the gratings are not in equilibrium with the input light, since learning requires that the output be dependent on the previous exposure history. Bipolar weights and weight changes can be implemented either by coherent detection and erasure or by employing separate positive and negative weights. The bipolar outputs can be formed electronically by subtracting the contributions of the two sets of weights. Muti-layer neural networks can be programmed in the same system by spatially multiplexing the layers on the LCLV and sequencing through adjacent layers.

In summary, we have discussed SPONN, a method for holographically interconnecting optical neurons which distributes each connection weight among a set of angularly and spatially multiplexed gratings generated in self- and mutually-pumped phase conjugate mirrors. We have presented experimental evidence of the reduced crosstalk, optimum SLM space-bandwidth product utilization, and global connectivity of SPONN, and discussed an architecture for implementation of multi-layered feedforward neural networks.

This work was supported in part by the Air Force Office of Scientific Research and the Defense Advanced Research Projects Agency. We would like to thank C. Deanda for skillful technical assistance and G. Valley and G. Dunning for helpful discussions.

Figure Captions

Figure 1-A. Ewald sphere momentum-space diagram for Bragg matching to two gratings in series. Only a single input/output wavevector pair can lie on the two Bragg cones and satisfy the Bragg conditions at both gratings simultaneously.

Figure 2-A. Demonstration of elimination of Bragg degeneracy and crosstalk suppression. (a) Steady state conjugate output. (b) Zero output observed after input array was shifted by half a period. The conjugate returned immediately after the input array was shifted by another half period.

Figure 3-A Demonstration of 1:128 fanout, global connectivity, and associative recall. (a) Steady-state conjugate output for a 16x16 random binary pattern input. (b) Partial input consisting of a single pixel. This represents only 1/1000 of the active area of the LCLV. (c) Corresponding PCM output immediately after input was switched to that shown in (b).

[1] K. Blotekjaer, Appl. Opt. Vol. 18, 57-67 (1979).

[2] D. Psaltis, X. G. Gu, and D. Brady, SPIE Vol. 963, 468-474, 1988.

[3] N. V. Kukhtarev, V. Markov, and S. Odulov, Opt. Comm. **23**, 338-343 (1977).

[4] A. V. Nowak, T. R. Moore, and R. A. Fisher, J. Opt. Soc. Am. B, Vol. 5, No. 9, 1864-1878, (1988).

[5] Y. Owechko, in Proceedings of Topical Meeting on Optical Computing, (Optical Society of America, Salt Lake City, Feb. 1989), p. 44-47.

[6] Y. Owechko, in Conference Record of 1990 International Topical Meeting on Optical Computing, (Japan Society of Applied Physics, Kobe, Japan, 1990), p.142-146.

[7] J. Feinberg, Opt. Lett. **7**, 486-488, (1982).

9029-06-16

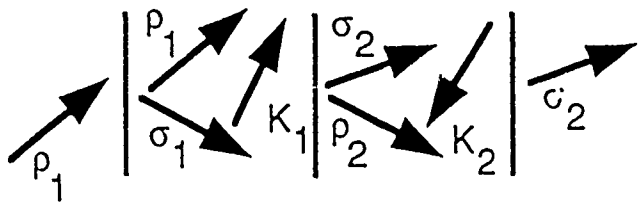

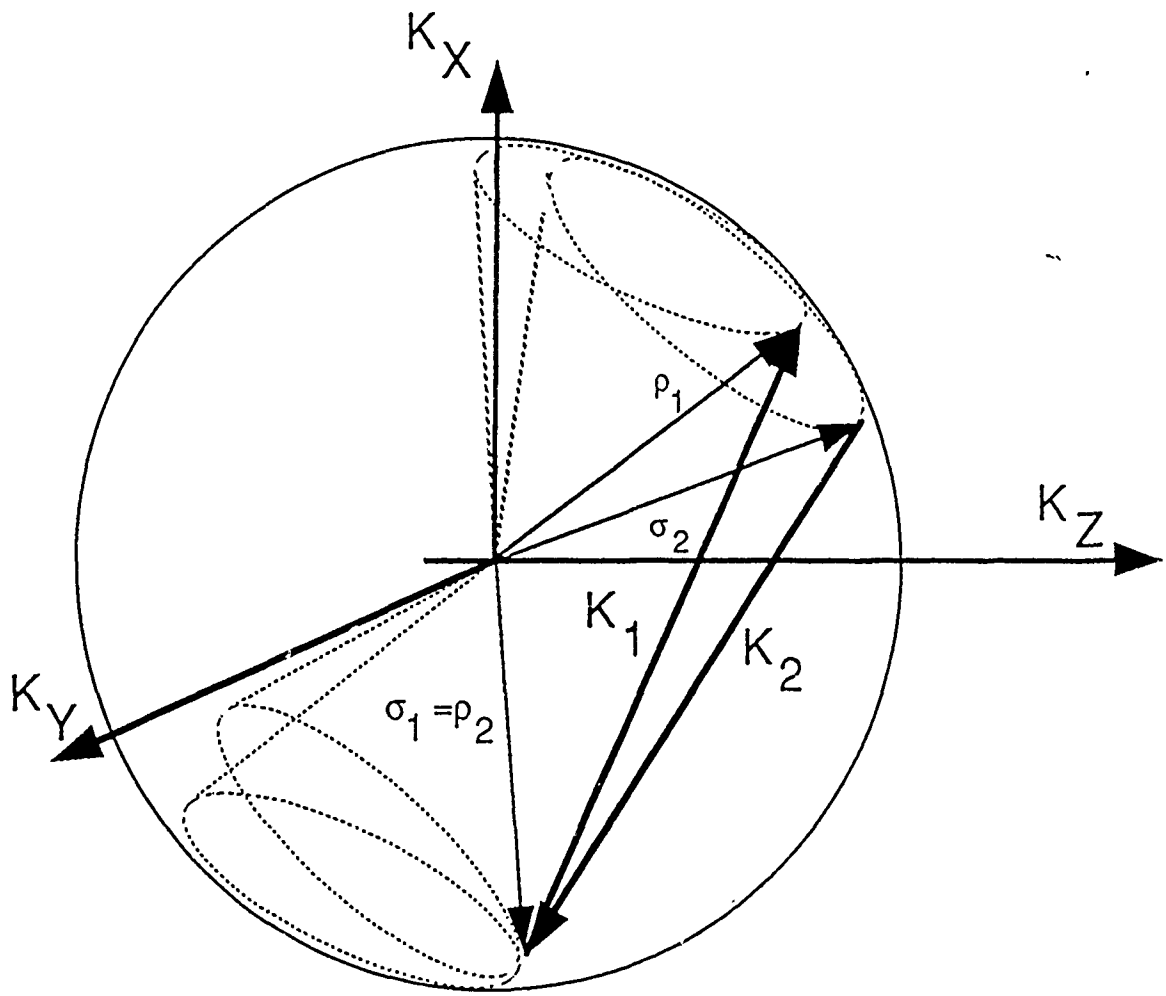

Figure A-1

9029-06-03

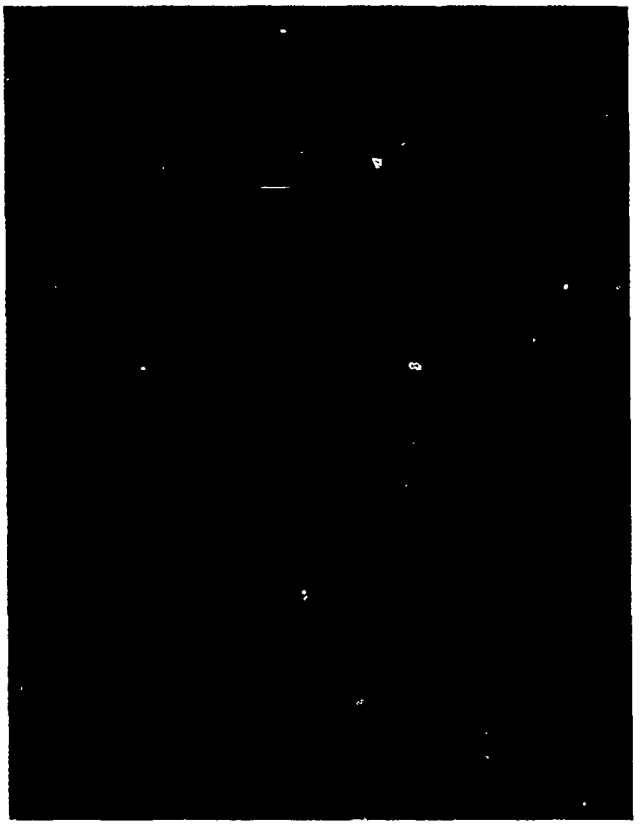

(b)

Figure A-2

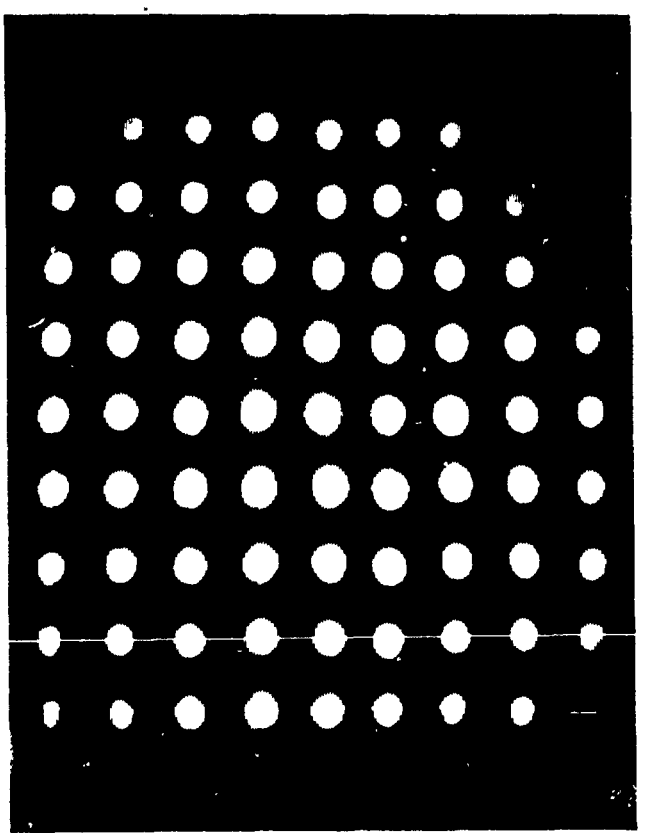

(a)

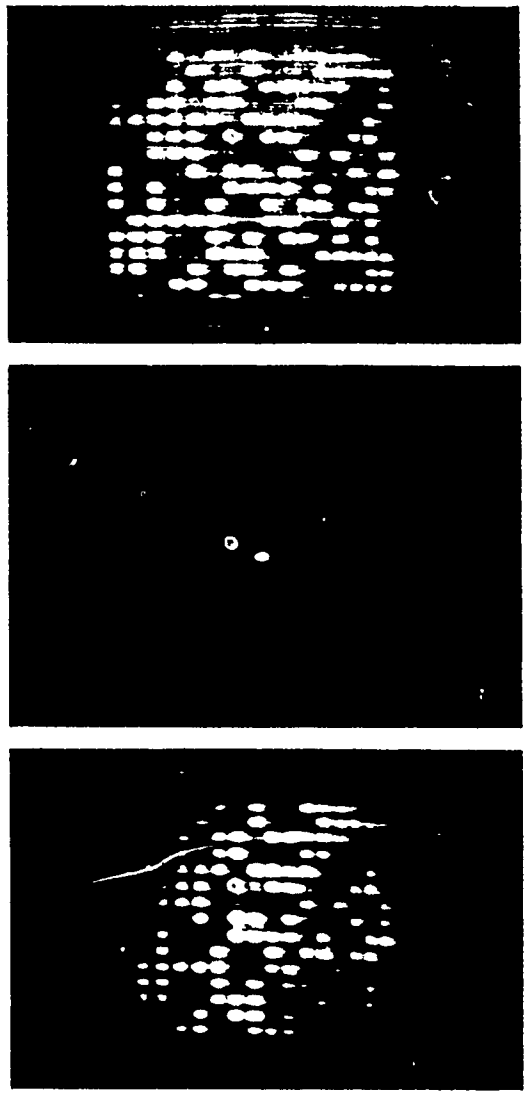

Figure A-3

APPENDIX B

Nonlinear Holographic Associative Memories

Yuri Owechko

Reprinted from
IEEE JOURNAL OF QUANTUM ELECTRONICS
Vol. 25, No. 3, March 1989

APPENDIX B

Nonlinear Holographic Associative Memories

Yuri Owechko

Reprinted from
IEEE JOURNAL OF QUANTUM ELECTRONICS
Vol. 25, No. 3, March 1989

met by conventional computer architectures which use a small number of processing units, bus-oriented architectures, and address-based random access memory.

A more suitable memory approach for neural network models is associative memory. Associative memories have long been a subject of active research in both optical and electronic computing. As described above, this type of memory is fundamentally different from conventional random access memory in that no separate address exists for each stored entity. Instead, the datum itself acts as a pointer to either itself (homoassociation) or to other stored data (heteroassociation). Data can flow through the system, exciting chains of associations until a decision is reached in a global and parallel manner. Associative memories also have error correction properties in that a complete undistorted set of data can be retrieved using a distorted or partial version of input data. Error correction, which stabilizes the flow of decision making through the neural network, is implemented using nonlinearities and feedback. Many associative memory mathematical models have been published and simulated on serial electronic computers [1]. However, it is inefficient to map such highly-parallel and fine-grained models onto single-processor serial computers. Ideally, the architecture of a neural network computer should reflect the highly parallel, associative, fine-grained, and nonlinear analog nature of the neural network models. In particular, it would be advantageous to devote a processing unit to each neuron rather than multiplex neurons among processing units. One approach to achieving such an architecture is to use analog optical methods for parallel communication between a large number of processing units represented by planes of pixels.

The good match between the parallelism and interconnectivity of optics and the requirements of associative memory paradigms has not gone unnoticed over the years. Gabor, the inventor of holography, appreciated its associative properties [9]. Some of the early experiments in holographic associations were performed by Collier and Pennington. These efforts, in which a hologram was formed from two object wavefronts, were termed "ghost image holography." When the hologram was subsequently illuminated with part of wavefront A, a complete version of wavefront B was reconstructed. These holographic associative memories suffered from distortions, poor signal-to-noise ratio (SNR), and low storage capacity. Later, page-oriented holographic memories were developed which used mechanical or acoustooptic deflection of reference beams to read out one of many spatially-separated subholograms. The selection of a particular stored page for readout was based on the correlation of the input wavefront with the stored wavefronts.

The results of recent research in neural network models has inspired workers in optics to add gain, nonlinear feedback, and competition to holography and create a new class of optical associative memory. NHAM (nonlinear holographic associative memory). Phase conjugation is often used to implement these features of associative memory. The performance of NHAM-type associative memories is potentially superior to linear correlator approaches because, in addition to increased storage capacity and discrimination, the nonlinearities in NHAM allow it to make decisions and choose between a set of competing possibilities on the basis of ambiguous inputs. Most importantly, its conceptual basis can be expanded to include optical implementations of neural network models.

In Section II, after briefly describing linear holographic associative memories, I will discuss some of the theoretical aspects of a generic NHAM. In particular, I will describe the relationship of NHAM to certain higher order correlation neural network models. Well-known examples of first-order correlation neural network models are the outer-product models of Anderson [10], Kohonen [5], and Hopfield [11]. Grossberg's formulations [12] also contain outer-product terms. Outer-product models are in fact forms of the well-known Hebbian model of synaptic learning. Higher order correlation models are generalizations of outer-product models in which the coupling matrix between neurons is a tensor. Section III is devoted to descriptions of some representative experimental implementations of NHAM's.

In any review paper it is necessary to limit the topic of discussion. In keeping with the theme of this special issue, I will limit myself to nonlinear optical holographic implementations of associative memory using phase conjugation or optical retroreflection. I will not discuss matrix-vector multiplier optical implementations of associative memory [13], nor will I discuss more general optical neural network architectures capable of supervised or unsupervised learning. Optical neural networks based on matrix-vector multiplication use spatial light modulators as two-dimensional masks to store the interconnection weights between arrays of discrete emitters and detectors. Multilayer optical neural network architectures [14] based on storing weights as holographic gratings in photorefractive crystals have been proposed which are capable of implementing such neural network paradigms as backward propagation and simulated annealing. For more information on these subjects the reader should consult the references. Finally, I wish to apologize in advance to any workers whose relevant work has inadvertently not been included here.

II. Optical Associative Memories

In this section I will discuss some theoretical issues related to storage capacity which are common to various NHAM implementations. However, it will be instructive first to briefly discuss earlier work in linear holographic associative memories in order to establish basic principles. These principles will provide a framework for the discussion of nonlinear holographic associative memories which incorporate feedback and gain using phase conjugate resonator configurations.

A. Linear Holographic Associative Memories

1) Ghost Image Holography and Page-Oriented Holographic Memories. The associative properties of holog-

raphy have been recognized ever since the invention of holography by Gabor [15]. Van Heerden [16] predicted in 1963 that a hologram would produce a "ghost image" of a stored image upon illumination of the hologram with a fragment of the original image. This was subsequently confirmed by Stroke *et al.* [17]. These early ghost image experiments were characterized by poor image quality and signal-to-noise ratio (SNR). The invention of off-axis holography by Leith and Upatnieks [18] greatly improved the SNR by angularly separating the desired signal term from the undesired noise due to self-interference among scattered waves from the original image. Pennington and Collier [19] demonstrated ghost image reconstructions using this off-axis approach.

Ghost image holography can be mathematically described as follows. Consider two complex wave amplitudes $a(x, y)$ and $b(x, y)$ in a first plane (x, y). The two wavefronts are allowed to propagate over a distance L to a second plane (u, v) where a photosensitive holographic plate is located. Assuming the transmission of the developed plate is linearly proportional to the incident light intensity and diffraction within the hologram can be neglected (thin hologram approximation), the amplitude transmission of the plate will be proportional to

$$T(u, v) = \left|A(u, v) + B(u, v)\right|^2 = |A|^2 + |B|^2 + \bar{B}A + B\bar{A} \qquad (1)$$

where $A(u, v)$ and $B(u, v)$ are the Fresnel-Kirchhoff transforms of $a(x, y)$ and $b(x, y)$, respectively:

$$A(u, v) = e^{\pi i(u^2+v^2)/\lambda L} \iint a'(x, y) \cdot e^{-2\pi i(xu+yv)/\lambda L}\, dx\, dy$$

where

$$a'(x, y) = a(x, y)e^{\pi i(x^2+y^2)/\lambda L}.$$

When the hologram is subsequently illuminated with wavefront A, the resultant output $A(u, v)\, T(u, v)$ will consist of several terms:

$$A(u, v)\, T(u, v) = |A|^2 A + |B|^2 A + AA\bar{B} + BA\bar{A}. \qquad (2)$$

The first two terms represent on-axis noise terms. The third term is an off-axis "twin wave" which is not of interest. The last term (which is angularly separated from the other terms assuming $a(x, y)$ and $b(x, y)$ were spatially separated in the (x, y) plane) represents the basis for holographic associative memory. The analysis will be simplified without loss of generality if we assume the spherical phase terms in $a'(x, y)$ and $b'(x, y)$ are canceled using lenses so that $a'(x, y) = a(x, y)$. This corresponds to forming Fourier rather than Fresnel holograms. If we Fourier transform the output of the hologram with a lens and consider only the last term in (2), the result is

$$\text{output} = \text{FT}\left\{BA\bar{A}\right\} = b * (a \odot a) \qquad (3)$$

where $*$ and $\odot$ denote convolution and correlation, respectively. The origin of the associative ghost image is now clear. The input image $a(x, y)$, is correlated with itself and then convolved with the associated image $b(x, y)$. If the autocorrelation of $a(x, y)$ is sharply peaked, the convolution of $a(x, y)$ with $b(x, y)$ results in an output closely resembling $b(x, y)$. Thus upon input of $a(x, y)$ the wavefront $b(x, y)$ is reconstructed, forming a heteroassociation. Since fragments of $a(x, y)$ also form sharp correlation peaks when correlated with $a(x, y)$, a complete version of $b(x, y)$ is still formed when a partial version of $a(x, y)$ addresses the hologram, although the reconstruction is of reduced resolution. Leith and Upatnieks demonstrated the marked improvement in image reconstruction quality possible by using diffuse illumination. This has the effect of increasing the spatial frequency content of $a(x, y)$ and thereby sharpening its autocorrelation, which improves the resolution of $b(x, y)$.

Vander Lugt [20] introduced the use of off-axis holography for matched filter recognition of objects by letting $b(x, y)$ be a delta function so that $B(u, v)$ is a tilted plane wave. If a lens is now placed behind the hologram the correlation of the input image with the stored image appears in the back focal plane. If the input image matches the stored image a bright spot appears in the back focal plane or correlation plane. Moreover, the location of this spot corresponds directly to the location of the matching image in the input plane.

The Vander Lugt linear optical correlator has found many applications in pattern recognition, signal processing, and optical associative memories. One of the earliest applications of the optical correlator for optical associative memories was in the page-oriented holographic associative memory (HAM) [21] for digital computers. In this application memory data were stored in a large number of spatially-multiplexed holograms. During recording different data planes or "pages" were recorded in each hologram sequentially by shifting a plane wave reference from hologram to hologram. In the readout phase the light from the input data page illuminated the entire set of holograms. An associative search of all of the stored data could be performed simultaneously. A detector matrix determined the location of the resultant correlation peak which determined the location of the hologram containing the matching data. This information was used to shift a readout reference to the proper hologram for readout of the associated data. The system could also be used for heteroassociation by shifting the readout beam to a hologram different from the matching one. Associations could be made by processing the correlation plane with lookup tables.

Such page-oriented associative holographic memories are capable of large storage capacities but are limited in

some respects. In particular, the systems are not shift invariant. They work best if the matching patterns always appear in the same position. In addition, they handle multiple associations serially because of the mechanical scanning of the readout beam. This lookup table approach makes page-oriented HAM's unsuitable for implementations of neural network model-inspired associative memories. In response to the need for highly-parallel architectures for neural network models, a new class of HAM's has been developed recently which is also based on the optical correlator. These new devices also perform associations using correlation as a measure of similarity. However, unlike page-oriented HAM's, these nonlinear holographic associative memories (NHAM's) use nonlinear gain and feedback provided by phase conjugation to implement competition between stored memories. This competition is used to perform associations with error correction and improved SNR on multiple inputs in parallel.

B. Nonlinear Holographic Associative Memories

1) General Description. Both ghost image holography and Vander Lugt (matched filter) correlators are forms of optical associative memories in that they return one image when addressed with another. Ghost image holography, however, suffers from poor storage capacity and SNR due to distortions arising from the correlation-convolution operations described in the previous section. Spatial multiplexing cannot be used to improve the SNR if all stored images or "objects" are to be recalled in the same position, which results in the superposition of cross-correlation noise in the output plane. This superposition further reduces the SNR and the storage capacity. The Vander Lugt correlator, on the other hand, has good SNR due to its large processing gain. However, it is not very useful as an associative memory because it maps input objects into autocorrelation peaks in the output plane instead of associating one optical image or object with another.

The NHAM is an optical associative memory which combines the fully-parallel image-to-image heteroassociative capabilities of ghost image holography with the high SNR, processing gain, and storage capacity of thresholded Vander Lugt correlators. In addition, nonlinearities allow an NHAM to select a particular stored memory over all others on the basis of incomplete input data. A schematic diagram of a representative NHAM system is shown in Fig. 1. The heart of the system is a hologram in which Fourier transforms of objects a^{m} are recorded sequentially using angularly multiplexed reference beams b^{m}, as shown in Fig. 1. For readout of the NHAM, phase conjugate mirrors (PCM's) or other means of forming retroreflected time-reversed beams are positioned on both sides of the hologram, forming a phase conjugate resonator. The hologram divides the resonator into the object and reference legs. When a partial or distorted version of object $mo(a^{m'})$ addresses the hologram via the beamsplitter, a set of partially-reconstructed ref-

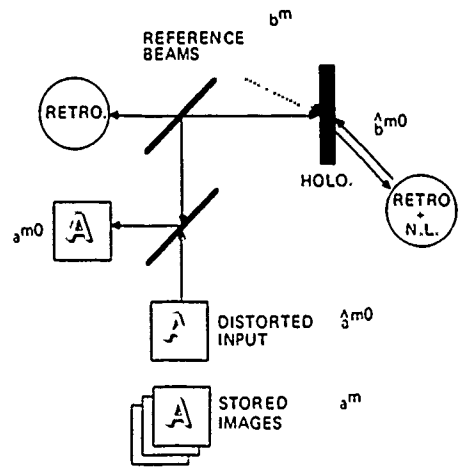

Fig. 1. Recording and readout of objects in reference-based NHAM

erence beams (b^{m0}) is generated. Each reconstructed reference beam is convolved with the correlation of the input object with the stored object associated with that particular reference beam. This part of the system is identical to a matched filter Vander Lugt correlator. The distorted reconstructed reference beams are phase conjugated by the reference leg PCM and retrace their paths to the hologram. These beams then reconstruct the complete stored objects. The reconstructed objects are phase conjugated by the object leg PCM and the process is iterated until the system settles into a self-consistent solution or eigenmode, assuming the gain of the PCM's is sufficient for oscillation. In the absence of the hologram the phase conjugate resonator can support a continuum of different resonator modes. The eigenmodes of the NHAM resonator are defined by the stored wavefronts in the hologram.

An important common feature of NHAM's is nonlinearity. Without it NHAM's could not "choose" a particular memory over all others and the output would be a linear superposition of multiple recalled memories. If the stored objects are considered to be vectors in state space, then NHAM nonlinearities form regions of attraction around the stored object vectors in a manner analogous to neural network formulations of associative memory. The nonlinear response and multiple stable states of the NHAM allow selections between patterns to be made on the basis of incomplete data since gain will exceed loss only for the stored pattern with the largest overlap with the input pattern. Nonlinearities also improve the SNR and storage capacity over ghost image holography or linear matched filter correlators. The output association is available in two forms depending on where the output is coupled out. The reference side of the NHAM is essentially a Vander Lugt correlator where a correlation peak marks the location of the recognized object in the input plane. In the object leg an undistorted version of the associated stored object is superimposed over the partial input object. The output can be separated from the input with a beamsplitter.

2) Storage Capacity. In this section I will discuss the effects of nonlinearities in the reference leg on the SNR

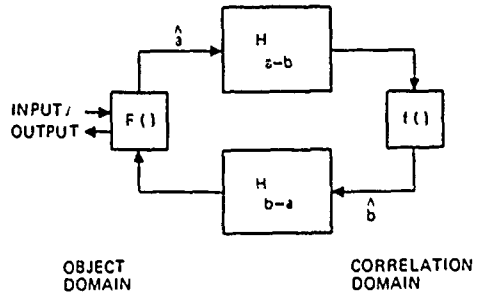

Fig 2. Block diagram of iterative model of NHAM.

and storage capacity of NHAM's. The resonator nature of the NHAM is illustrated in the block diagram of Fig. 2. Assuming thin Fourier transform holograms and using the same approach as in (1)–(3), an iterative equation can be written for the NHAM output:

$$a_n^{m0} = F\left[\sum_{m'}\left(f\left\{\sum_{m}(a_{n-1}^{m0} \odot a^{m}) * b^{m}\right\}\right) \odot b^{m'} * a^{m'}\right], \tag{4}$$

where a_n^{m0} is the amplitude in the object leg after the nth round-trip through the resonator, a^m are the objects stored in the hologram, b^m are the reference beams used in holographically recording the objects, $f(\ )$ represents the nonlinear reflectivity of the reference leg, and $F(\ )$ represents an output plane point nonlinearity. The input "seed" a_0^{m0} for the resonator is a partial or distorted version of object $m0$. The output in the nth round-trip consists of a double sum of cascaded correlations–convolutions. The double sum over the object indexes m and m' is due to the double-pass through the hologram. Assuming the reference beams are angularly multiplexed plane waves, the b^m functions are spatially displaced delta functions:

$$b^m = \delta(x - x_m). \tag{5}$$

(It should be noted that although all the calculations here are being done in one dimension, these results are readily extended to the two-dimensional images in NHAM associative memories.) Substituting (5) in (4) results in the following iterative equation for the object leg optical amplitude distribution after the first round-trip through the resonator:

$$a_n^{m0}(x) = F\left\{\sum_{m'}\sum_{m} f\left[C_{n-1}^{m}(x - x_m + x_{m'})\right] * a^{m'}(x)\right\} \tag{6}$$

where

$$C_n^m(x) = a_{n-1}^{m0} \odot a^m$$

$C_n^m(x)$ is the correlation between the stored object m and the resonator amplitude distribution in the nth iteration. I have assumed that the angular separation between reference beams is large enough to separate the correlation–convolution terms in the reference leg, which permits me to disregard cross terms due to the nonlinear reflectivity $f(\ )$. To facilitate the analysis and allow direct comparisons with some outer-product type neural network models of associative memory, I will assume objects consist of N-dimensional vectors whose components assume values of $+1$ or -1. (Objects consisting of analog vectors can also be stored in NHAM's. This binary representation is used to simplify the analysis.) I will further assume that the reference functions b^m are uniformly distributed and equally spaced in the object plane. If these spacings are wider than the widths of the objects, then by placing an aperture over the output plane only reconstructions for which $m = m'$ in (6) are retained. This aperture prevents ambiguities in the output plane which would otherwise occur if a thin hologram is used. The reference beam reconstructs not only object $m0$ centered on the input object but also all other stored objects. The aperture blocks these other objects since they are displaced from object $m0$, but at the cost of a reduced amount of shift invariance in the field of view (FOV). As more objects are stored the amount of unambiguous shift invariance is decreased proportionally. The hologram can store only a single object with shift invariance over the entire FOV. (Another limitation on the shift invariance and storage capacity is that the total space-bandwidth product of all shifted versions of the stored objects cannot exceed the space-bandwidth product of the hologram [22], [23].)

An estimate can be made of this FOV tradeoff between the number of stored objects and degree of shift invariance. For example, assuming a Fourier transform lens focal length of F, a shift invariance of X implies an angular spectrum range at the hologram of

$$\theta = X/F. \tag{7}$$

If we further assume the hologram has good diffraction efficiency for a range Φ of reference-object beam angles, then the number of objects that can be stored with shift invariance X in two dimensions is limited by FOV ambiguity to

$$M = (\Delta\phi/\theta)^2. \tag{8}$$

For parameter values of $F = 500$ mm, $X = 10$ mm, $\Phi = 30°$, and out-of-plane reference beams, the maximum number of stored objects limited by FOV ambiguity is $M = 680$. The FOV ambiguity issue is moot for volume holograms because Bragg selectivity prevents reconstruction of beams angularly shifted in the same plane as the original reference and object beams. (The selectivity is much less, however, for out-of-plane shifts [24].)

Assuming an aperture which eliminates the ambiguous reconstruction, only terms for which $m = m'$ are retained in (6):

$$a_n^{m0}(i) = F\left[\sum_{m}\sum_{p} f(C_{n-1}^{m}(p))\, a^{m}(i - p)\right]. \tag{9}$$

The SNR for NHAM in the first iteration or at the end of the first round-trip [before pointwise nonlinear transformation in the object domain by $F(\ )$] can be calculated from

$$\mathrm{SNR} = \frac{\left|f[C_0^{m0}(0)]\right|}{\sqrt{\sum_{p\neq 0}\left|f[C_0^{m0}(p)]\right|^2 + \sum_{m\neq m0}\sum_{p}\left|f[C_0^{m}(p)]\right|^2}}. \tag{10}$$

I will now make some assumptions concerning the statistical properties of the stored objects in order to calculate the $C^m(p)$ cross correlation coefficients. In particular, I will assume the objects are random and not orthogonalized so that the statistics can be described by a balanced binary phase diffuser model [25]:

$$\begin{aligned} C_0^m(p) &= N\delta(p) + \sqrt{2(N-|p|)/3}, && \text{if } m = m0 \\ &= \sqrt{2(N-|p|)/3}, && \text{if } m \neq m0 \end{aligned} \tag{11}$$

where N is the size of the stored object vectors. Assume further that $f(x)$, the point nonlinearity in the reference or correlation domain, has the form $f(x) = x^n$. (The effects of arbitrary nonlinearities can then be estimated by using a polynomial approximation and superposition.) Substituting these expressions in (10) and performing the summations over m and p results in the following expression for the SNR:

$$\mathrm{SNR}_{\mathrm{NHAM}} = \beta(3/2)^{n/2}\sqrt{(n+1)/2}\,\frac{N^{(n-1)/2}}{\sqrt{M}}, \qquad N \gg 1 \tag{12}$$

where β is the fraction of a^{m0} used as the input object and M is the number of stored vectors. A heuristic estimate for the storage capacity can be obtained by solving (12) for M in terms of N. Assuming a minimum SNR required for successful associative recall, M should be proportional to N^{n-1}. The proportionality constant is given by the minimum SNR required by the particular NHAM system for successful convergence. Therefore, within limits set by the available dynamic range, we can conclude that the storage capacity of an NHAM can be increased by increasing the nonlinearity in the correlation domain. A similar analysis for the outer-product associative memory results in

$$\mathrm{SNR}_{\text{outer-product}} = |2\beta - 1|\sqrt{N/M} \tag{13}$$

which, using the above SNR arguments, implies that M, the number of stored objects, should be linearly proportional to N. The storage capacity of an outer-product model was reported by Hopfield as linear in N based on empirical evidence for small N values [12]. Using a hyperplane counting argument, Abu-Mostafa and St. Jacques have shown that the capacity of the outer-product model is bounded from above by N [26]. McEliece *et al.* [27], Bruce *et al.* [28], and Weisbuch and Fogelman [29] applied techniques from coding theory to the outer-product model and showed that for random objects the maximum asymptotic value of M for which all objects can be recovered exactly is $N/(4 \log N)$ as N approaches infinity. Their results also implied that if a specified nonzero error rate in recall can be tolerated, the asymptotic storage capacity becomes linear in N. Gardner [30] extended these results to a higher order generalization of the outer-product model. Owechko *et al.* [31] performed computer simulations of the storage capacity of the outer-product and NHAM models. The results are shown in Fig. 3 for the number of vectors stored as a function of N for power law nonlinearities with $n = 2$, 3, and 4. Each curve was averaged over many runs using randomly selected vectors. Because the input vectors did not contain any errors, the simulations in effect tested the stored vectors for being eigenvectors of the system.

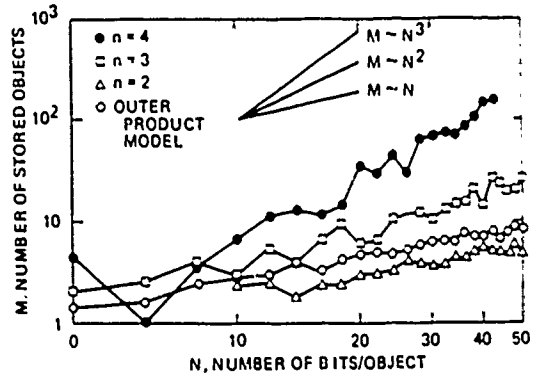

Fig. 3. Comparison of storage capacity of reference-based NHAM with the outer-product model for nonlinearities in correlation domain of form $f(x) = x^n$. Error-free input objects assumed. (After [31].)

Combining (12) and (13) and solving for the nonlinearity $n = n_{\mathrm{op}}$ which results in an NHAM storage capacity equal to the outer-product model gives n_{op} approximately equal to 2. This is verified in Fig. 3 as the slopes of the M versus N curves plotted on logarithmic scales equal $n - 1$ and the capacity for $n = 2$ is approximately equal to the outer-product model. Although the above SNR arguments and simulation results demonstrate the improvement in storage capacity caused by nonlinearities in the correlation domain, the heuristic nature of the arguments are evident in light of the asymptotic results of McEliece *et al.* for the outer-product model capacity.

The improvement in storage capacity of an NHAM over an outer-product associative memory is due to its close analogy to certain higher order discriminant models. One form of the nth order discriminant model can be defined as a generalization of the outer-product associative memory model in which the W_{ij} weight matrix is a tensor of order $n + 1$:

$$W_{ij_1j_2,\cdots,j_n} = \sum_m X_i^m X_{j1}^m X_{j2}^m, \cdots, X_{jn}^m \tag{14}$$

where the X^m are one-dimensional stored vectors. The

output is calculated by forming a tensor product:

$$X_i^{\text{output}} = F\left[\sum_{j_1}\sum_{j_2}\cdots\sum_{j_n} W_{ij_1j_2\cdots j_n} X_{j_1}^{\text{input}} \cdot X_{j_2}^{\text{input}} \cdots X_{j_n}^{\text{input}}\right] = F\left[(X^{m0}, X^{\text{input}})^n X_i^{m0} + \sum_{m \neq m0} (X^m, X^{\text{input}})^n X_i^m\right]. \quad (15)$$

The tensor generalization greatly increases the number of degrees of freedom which results in dramatically increased storage capacities [32]–[34]. Comparing (15) and (9) shows that a power law nonlinearity of degree n in the correlation plane of an NHAM is analogous to an nth order discriminant function. A polynomial nonlinearity in the correlation plane is analogous to a weighted sum of higher order discriminant functions. They are not completely equivalent because inner products are used in the outer product model as opposed to correlation in the NHAM. This results in additional noise terms in the NHAM arising from the wings of the correlation function.

Other sources of noise will also be present in practical NHAM systems. These noise sources include dielectric inhomogeneities in the holographic medium and detector noise [35]. For photorefractive materials, erasure of previously recorded holograms during recording and subsequent readout may also limit the storage capacity [36], although fixing techniques [37] may remove the later limitation. These factors will reduce the storage capacity from the theoretical diffraction-limited estimates of Van Heerden. Accurate estimates will be specific to the particular system being considered.

III. Implementations

A. NHAM Categories

NHAM implementations can be categorized based on the resonator geometry and the method used for generating the reference beams used in recording the holograms. They can be further differentiated by the form and implementation of the nonlinearities. Most of the systems reported to date have been based on a double PCM resonator configuration similar to the one described above in which a separate independent reference beam is associated with each object beam. The reference beams are generally plane waves, so that the reconstruction quality can be controlled by adjusting the nonlinearities in the correlation domain without loss of gray scale fidelity in the object. (In general, most NHAM implementations to date have not relied on the nonlinearity of the PCM's, instead various external nonlinear mechanisms have been used.) Ring resonator geometries have also been proposed and demonstrated which derive the reference beam from the object beam. Although such systems lack some of the discrimination obtainable using separate reference beams, they do incorporate competition between stored modes using nonlinear gain saturation. Some specific implementations of these categories of NHAM, which vary mostly in the nature of the feedback and thresholding mechanisms, will now be described.

B. Multipass NHAM Configurations

1) Phase Conjugate Mirrors: Soffer *et al.* [38], [39] have demonstrated NHAM's which use thin thermoplastic Fourier transform holograms as the storage medium. Advantages of this approach include shift-invariance and the capability of programming heteroassociations by manipulating the correlation plane. A disadvantage is the lack of Bragg selectivity which results in low information storage capacity compared to volume holograms.

This NHAM structure is identical to Fig. 1 and the theory of the previous section is applicable without modification. In experimental demonstrations a single iteration nonresonating configuration was used, as shown in Fig. 4. Two objects were recorded sequentially in the hologram, each with its respective angularly-shifted plane wave reference beam. The hologram was recorded at 514.5 nm using a Newport Corporation thermoplastic holographic camera. A partial version of one of the stored objects was then used to address the hologram. A lens was used to focus the correlation plane output of the hologram into a PCM based on degenerate four-wave mixing (DFWM) in $BaTiO_3$. Typical parameters for PCM operation were wavelength 514.5 nm; forward and backward pump fluxes 3.3 and 11.5 W/cm^2, respectively; internal pump-probe angle 26°; and internal angle of grating k vector to c axis 13°. The output of the hologram acted as a probe for the DFWM system, generating an amplified phase conjugate of the correlation plane. The conjugated backward propagating beam illuminated the hologram, recreating a complete version of the stored object. Examples of stored objects, partial inputs, and reconstructed outputs are shown in Figs. 5 and 6. The capability of a reference based NHAM to handle gray scale objects is demonstrated in one of the examples. In this series of experiments a single pass nonresonator configuration was used and the PCM was operated in the linear reflectivity regime of DFWM. Thresholding, whether due to competition between resonator modes caused by gain saturation or to nonlinearities in the PCM reflectivity, was not demonstrated in this system. The quality of the reconstructions using what was basically a linear associative memory was due to the coding of the objects using high spatial frequency diffusers in contact with the objects. The sharpened autocorrelation peaks of the diffusers improved the resolution of the objects.

2) Electronic Lookup Tables: In order to address the issues of implementing controllable arbitrary nonlinearities in the correlation plane and making diffusers unnecessary, increasing the optical gain in order to achieve resonator oscillation, and facilitating the interfacing of an NHAM to an electronic host computer, Owechko [40] suggested and implemented a hybrid optical-electronic NHAM based on liquid crystal light valves (LCLV's). A

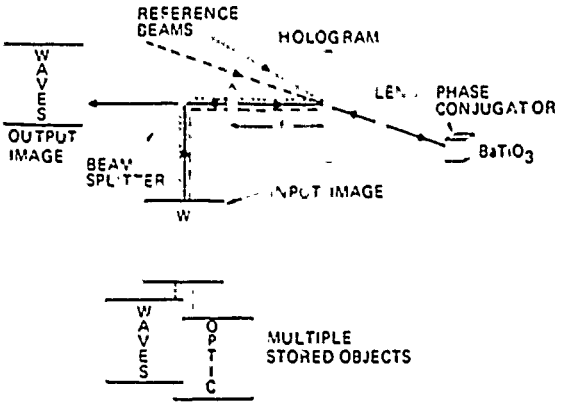

Fig. 4 Configuration used in associative memory experiments by Soffer *et al.* (After [39].)

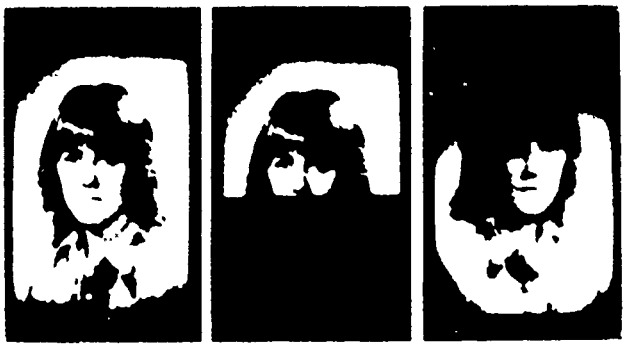

Fig. 5. Reconstruction of gray scale image from partial input: (a) image stored in hologram; (b) partial input image; (c) associated output image (inversion due to mirror reflection). (After [39].)

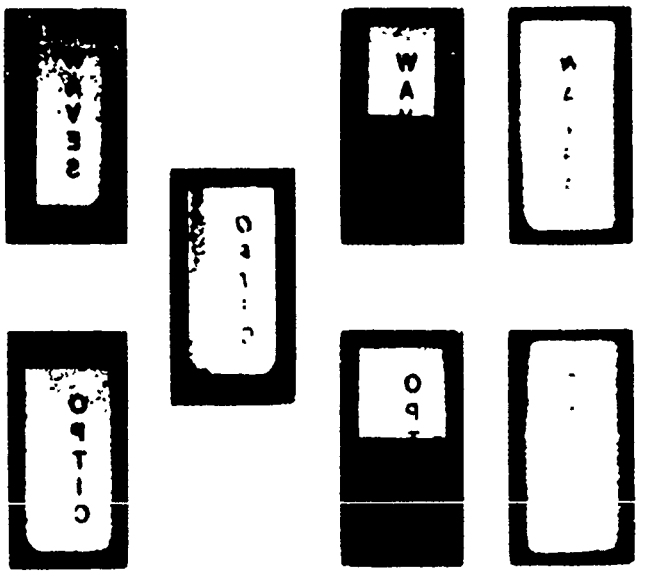

Fig. 6 Reconstruction of complete objects from partial input objects for multiple stored objects (a) images stored in hologram, (b) superimposed images shown as recorded; (c) partial input images; (d) corresponding output images. (After [39].)

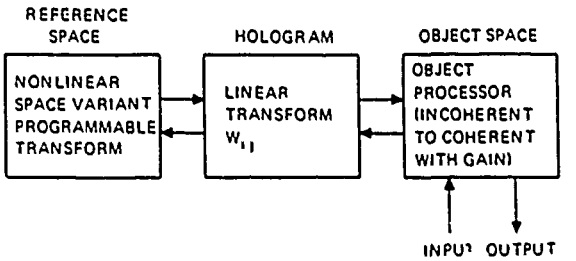

Fig. 7. Block diagram of hybrid NHAM. (After [40].)

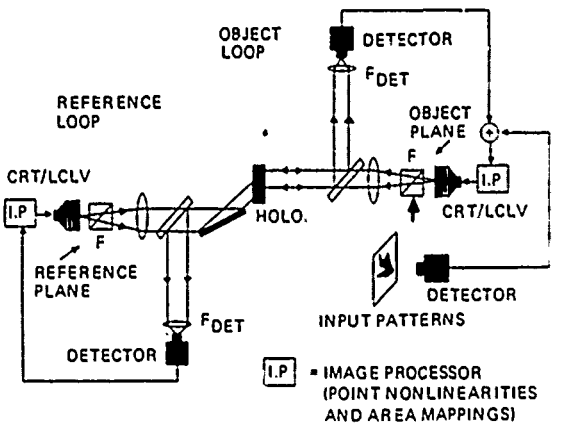

Fig. 8. Schematic diagram of hybrid NHAM. (After [40].)

block diagram of the hybrid NHAM is shown in Fig. 7 and a detailed schematic in Fig. 8. The basic principles of the hybrid NHAM are the same as described for the all-optical NHAM. The implementation of the input and feedback mechanisms are, however, quite different. Instead of using DFWM in $BaTiO_3$ to create true phase conjugates of the reconstructed reference and object beams, a pseudoconjugation system using video detectors and CRT-addressed LCLV's was used. Referring to Fig. 8, the partial input image is focused onto an object loop video detector and transfers the image to a CRT-addressed LCLV. The optical output of the object loop LCLV addresses the thermoplastic hologram and reconstructs the correlation plane which is focused on the reference loop video detector. A one-to-one mapping is performed between the detector and the output of reference loop LCLV, which is positioned in the back focal plane of the correlation lens. Thresholded correlation peaks on the reference loop LCLV are converted into backward propagating plane wave reference beams by the correlation lens. These beams address the hologram, reconstructing recorded objects which are in turn focused on the object loop video detector, closing the resonator loop. The combined gain of the detector/CRT/LCLV loops is more than sufficient to overcome the optical losses, resulting in a feedback system. The advantage of this approach is that general nonlinear feedback functions can be easily programmed. Between the reference loop video detector and the LCLV, the correlation plane is nonlinearly processed in electronic form using digital lookup tables in a PC board level image processor. The image processor can also be used

to program heteroassociations or multilayer optical neural networks by shuffling subregions of the correlation plane [32].

In preliminary experiments using a 20 mW HeNe laser at 632.8 nm, a single object-reference pair was recorded in the hologram. This demonstration showed that the hybrid resonator has at least one stable state which can be reached only if the injected signal is sufficiently similar to the stored image. As shown in Fig. 9, if more than 50 percent of the object were injected into the system, resonance would occur and the system would latch onto the stored object. The object would continue to circulate in the resonator after removal of the input, demonstrating bistability. Interruption of the circulating beam would return the resonator to its initial zero state. The hybrid NHAM demonstrated robustness in the face of input distortions. For example, if the input object was rotated by up to 10°, the output would still switch to the resonator state consisting of a circulating undistorted version of the stored object. The amount of tolerable distortion increased as the sharpness of the nonlinearity in the correlation plane was increased. The system would not latch for different input objects, indicating the resonator was recognizing the input object and not merely being switched by stray scattered light.

3) Pinhole Array: Paek and Psaltis [41] have demonstrated two different NHAM systems. In the first system, a single-pass passive system shown in Fig. 10, a set of spatially multiplexed objects are holographically recorded, all simultaneously using a single reference beam. In other words, a single "macro object" is recorded in the hologram which consists of many subregions, each containing a single object. The macro object and the hologram are located in the front and back focal planes of a lens, which results in the formation of a Fourier transform hologram. During readout an aperture equal in size and shape to the subregions in the macro object is centered in the input plane and input objects are placed inside it, as shown in Fig. 11. (See discussion of FOV ambiguity in the previous section.) This approach is equivalent to sequentially recording objects centered in the same aperture but with angularly-shifted plane wave reference beams. Both approaches divide the correlation plane into subregions. During readout, the presence of a correlation peak in a particular subregion is a unique label for which the stored object is being recognized. The location of the correlation within the subregion has a one-to-one correspondence to the location of the object in the input aperture.

Thresholding was implemented using a pinhole array in contact with a mirror placed in the back focal plane of a correlation lens. The correlation lens, in turn, was positioned so that its front focal plane coincided with the Fourier transform hologram. The correlation lens and mirror acted as a "cat's eye" pseudo-conjugator which retroreflected the reconstructed reference beams back to the hologram for readout of the hologram. The appropriate stored object was reconstructed centered on the input aperture. Thepinhole array passed only the peaks of the correlations, suppressing the sidelobe noise and improving the reconstruction quality. Such an approach to correlation plane nonlinearities has the advantage of simplicity, but it also destroys the natural shift invariance of the Fourier transform hologram. Shifts of the input object within the input aperture shifts the correlation peak as well. Since the pinholes are spatially fixed, no object shifts can be tolerated. (Paek and Psaltis have discussed approaches for restoring shift invariance by eliminating the pinhole array and using quadratic nonlinearities in the correlation plane [e.g., $n = 2$ in (15)], but have not discussed specific implementations.) Their experimental results using the pinhole system are shown in Fig. 12. Four objects were stored in the hologram. The reconstructed outputs and their associated partial inputs are shown. The poor reconstruction quality may have been due to the relatively large size of the pinholes (350 microns). Because of the passive nature of the pinhole-mirror pseudoconjugator and the resultant lack of gain, a resonator architecture was not implemented.

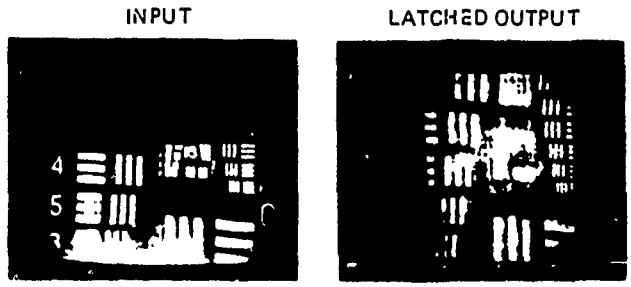

Fig. 9. Hybrid NHAM latched output for partial input. (After [40].)

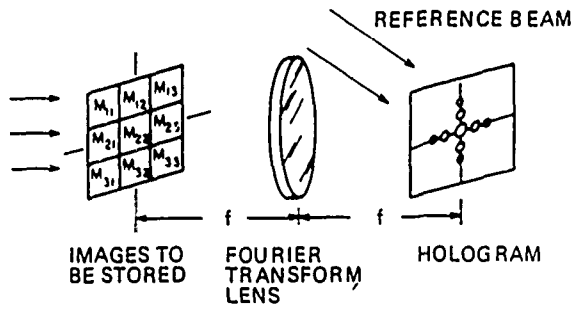

Fig. 10 Recording of multiple objects in a thin Fourier transform hologram using spatial multiplexing of the objects. (After [41].)

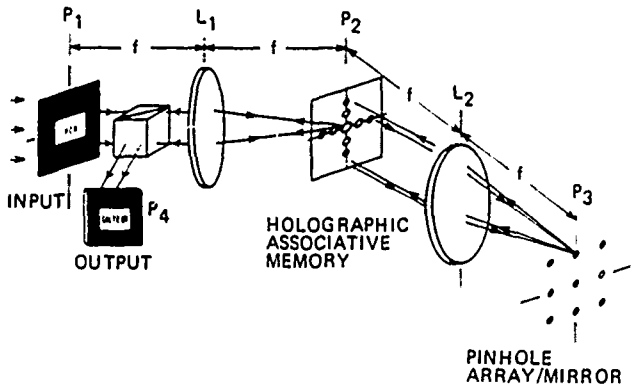

Fig. 11 Schematic diagram of the pinhole array-mirror holographic associative memory system. (After [41].)

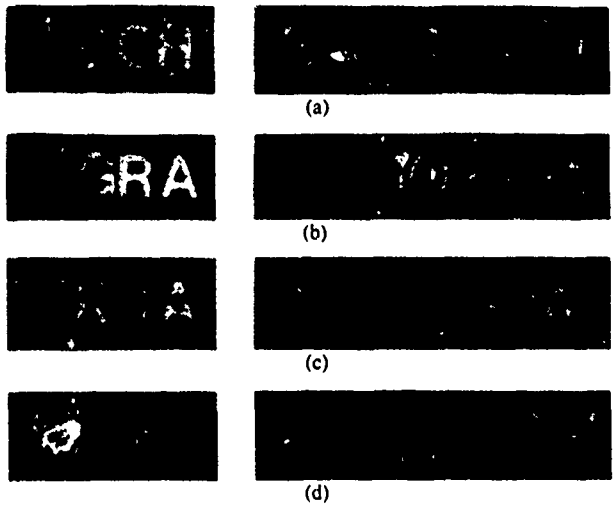

Fig. 12. Pinhole array–mirror associative memory: partial inputs (left) and outputs (right). (After [41].)

In order to improve the reconstruction quality, in their second system Paek and Psaltis separated the functions of identification and reconstruction and used a separate hologram for each function. This second NHAM is shown in Fig. 13. A thresholding spatial light modulator (microchannel spatial light modulator or MSLM) was also added in the input path. Thresholding the input image [the $F(\ )$ function in (9)] can sharpen the correlation peak and improve the reconstruction quality. The first Fourier transform lens, hologram, correlation lens, and pinhole array combination is identical to the thresholded Vander Lugt correlator portion of their first system. However, now instead of retroreflecting the correlation peak back toward the first hologram, it is passed on to a second correlation lens which converts it to a plane wave reference beam which reads out a second hologram. The second hologram is recorded in the same setup as the first using the same objects and reference beam. The second hologram therefore reconstructs the associated object when addressed by the thresholded reference beam. During recording each hologram is optimized for its particular function. The relative intensities of the reference and object beams were adjusted during recording of the first hologram to emphasize high spatial frequencies in the object. This tended to orthogonalize the objects and increase the autocorrelation peak relative to its sidelobes and cross-correlations. The second hologram, on the other hand, was recorded with diffuse illumination to improve the display quality when it is addressed by a restored plane wave reference beam. The combination of object thresholding, orthogonalization, and display optimization (which was made possible by the separation of recognition and reconstruction functions between the two holograms) greatly improved the reconstruction quality, as shown in Fig. 14.

4) Optical Fibers and Mirrors: An alternative, but closely-related approach to thresholding the correlation plane is the use of optical fibers coupled to mirrors to retroreflect the central peak of the correlation function back to the hologram. This approach was demonstrated by Yariv, Kwong, and Kyuma [42]. In their experiment, shown in Fig. 15, two objects were recorded in a volume holographic material using angularly-multiplexed refer-

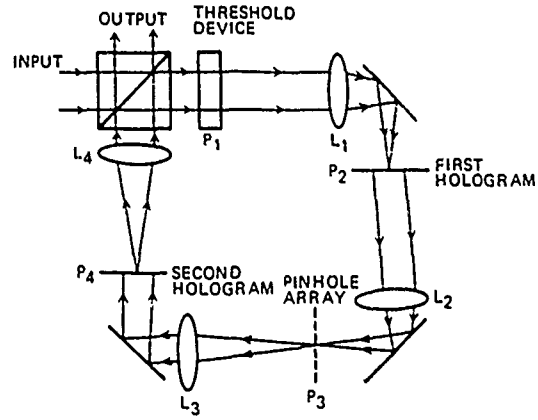

Fig. 13. Pinhole array optical associative loop. (After [41].)

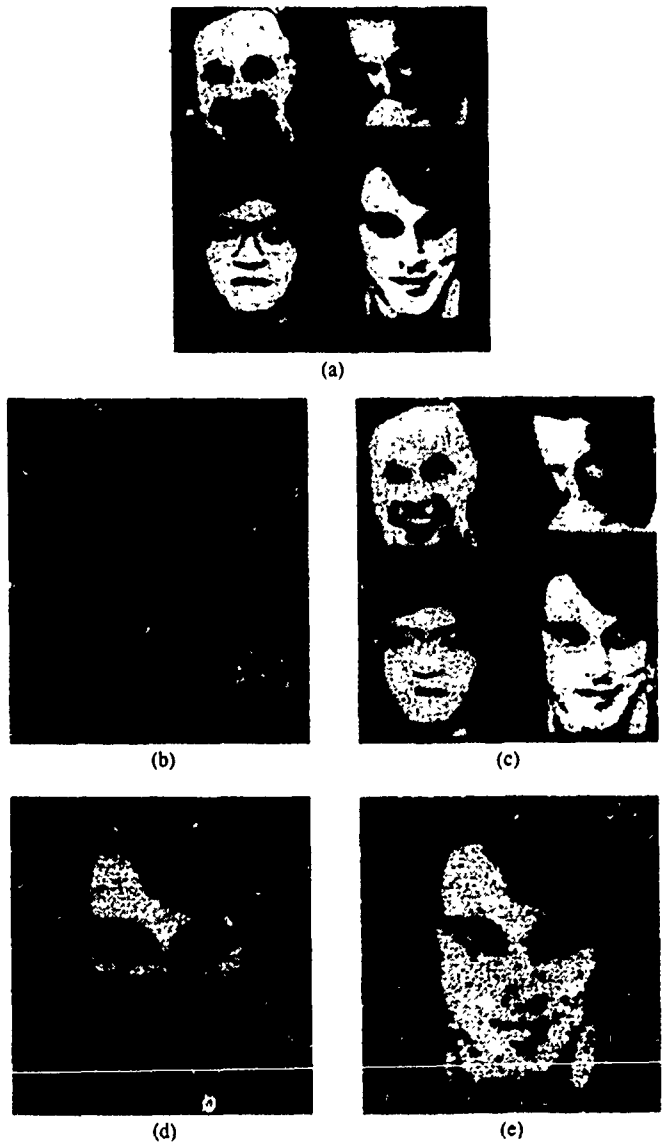

Fig. 14. Pinhole array optical associative loop: (a) four stored memories; reconstructed images from (b) the first hologram and (c) the second hologram, and (d) partial input and (e) recalled output (After [41].)

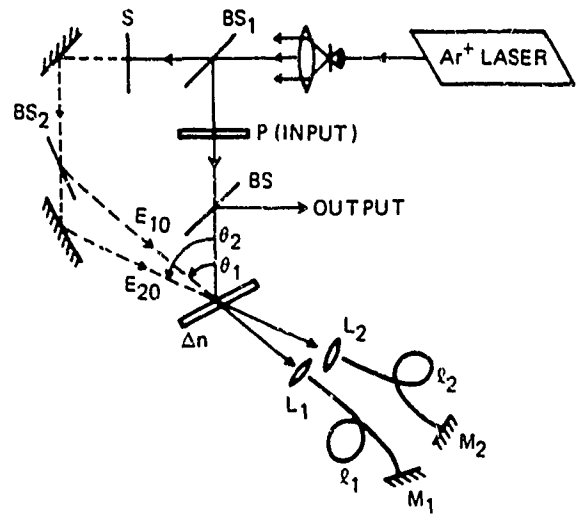

Fig. 15. Experimental arrangement of associative memory using feedback from optical fibers. (After [42].)

ence beams. Taking into account the volume nature of the holographic medium and assuming that the induced index variations are linearly proportional to the optical exposure, the volume index variation can be written as

$$\Delta n \propto \sum_{i=1}^{N} (E_i^* E_{io} + \text{c.c.}) \tag{16}$$

where E_i are the recorded objects E_{io} are the angularly multiplexed reference beams, and N is the total number of recorded objects. When the hologram is addressed by a partial input object E', the diffracted field is given by

$$E_{\text{diff}}(r) \propto \sum_j \int_V A'(r')\, A_j^*(r')\, A_{jo}(r') e^{-i(k/r)(xx'+yy')} \cdot dx'\, dy'\, dz' \tag{17}$$

where the integral is performed over the volume of the hologram and $r = |r|$, and r is a point in the observation plane. The A's are the slowly varying amplitudes of the input object, stored objects, and reference beams. The above quantity represents a sum of distorted versions of the original plane wave reference beams. It is analogous to (3), which was derived for a thin hologram. When these beams are spatially filtered and retroreflected in the correlation plane the result is a sum of plane-like waves propagating back along the direction of E_i^{o*} with complex field amplitudes proportional to the overlap integral

$$J_i(r) = \int_V A'(r')\, A_i^*(r')\, A_{io}(r')\, dx'\, dy'\, dz'. \tag{18}$$

The above overlap integral is analogous to the inner-product formed in the thin hologram case when the correlation function is sampled at its central peak. It is a measure of the similarity of the input object to the stored objects. The set of retroreflected plane wave references is given by

$$E_{\text{refl}} \propto \sum_i E_{io}^* J_i. \tag{19}$$

If a nonlinearity is used to enhance the strongest J_i and completely suppress the weaker ones, and if this J_i is allowed to illuminate the hologram, the reconstructed output will be given by

$$E_{\text{recons}}(r) \propto J_i |A_{io}|^2 A_i^*(r) \tag{20}$$

which is proportional to the conjugate of the stored object $A_i(r)$. Therefore, with the proper nonlinearities in the correlation domain, a volume hologram NHAM will display the one stored object that has the largest spatial overlap integral with the input object.

In the system shown in Fig. 15, Yariv, Kwong, and Kyuma used optical fibers to sample the peak in the correlation plane and generate the J_i. The opposite ends of the fibers were butted against mirrors which retroreflected the light back to the hologram. Since the fiber ends were located in the back focal planes of correlation lenses, reconstructed plane wave reference beams illuminated the hologram. (This spatial filtering technique is conceptually identical to the pinhole–mirror technique used by Paek and Psaltis.) Experimental results for storing two overlapping, nonorthogonal objects using this system are illustrated in Fig. 16. In a modification of the system, the mirrors were replaced with a conjugating–thresholding element. This element consisted of a bistable oscillation [43] using a ring resonator passive phase conjugate mirror [44]. The bistable oscillator utilizes mode competition to selectively enhance the strongest mode at the expense of weaker ones and retroreflect it back to the hologram. The bistable oscillator was added to the NHAM, as shown in Fig. 17, to further enhance the discrimination between reconstructed reference beams. Experimental results using this thresholding system are also shown in Fig. 16.

5) Pinhole Array and PCM: White, Aldrige, and Lindsay [45] have constructed an NHAM which utilizes a pinhole array and PCM combination for thresholding the correlation plane. Their system is illustrated in Fig. 18. The correlation plane is sampled using a fixed pinhole array in a manner similar to that of Paek and Psaltis, but the restored reference beam is retroreflected back along its path to the hologram using a PCM rather than an ordinary mirror. The PCM consists of DFWM in $BaTiO_3$ which results in the system having net optical gain. The storage medium consisted of Fourier transform holograms in dichromated gelatin. In their experiments, two objects were sequentially recording using angularly-multiplexed plane wave reference beams. During recording the reference–object beam ratio was adjusted to enhance the high spatial frequencies of the object, resulting in edge enhancement. This edge enhancement sharpened the autocorrelation peaks and improved object discrimination.

Their experimental results are shown in Fig. 19. Each object consisted of four geometric shapes. The only common element between the two objects was a circle in the lower left quadrant. As shown in Fig. 19(a) and (b), if a unique subset of an object addressed the NHAM, a complete, albeit edge-enhanced, version of that object was reconstructed. When the circle addressed the hologram [Fig.

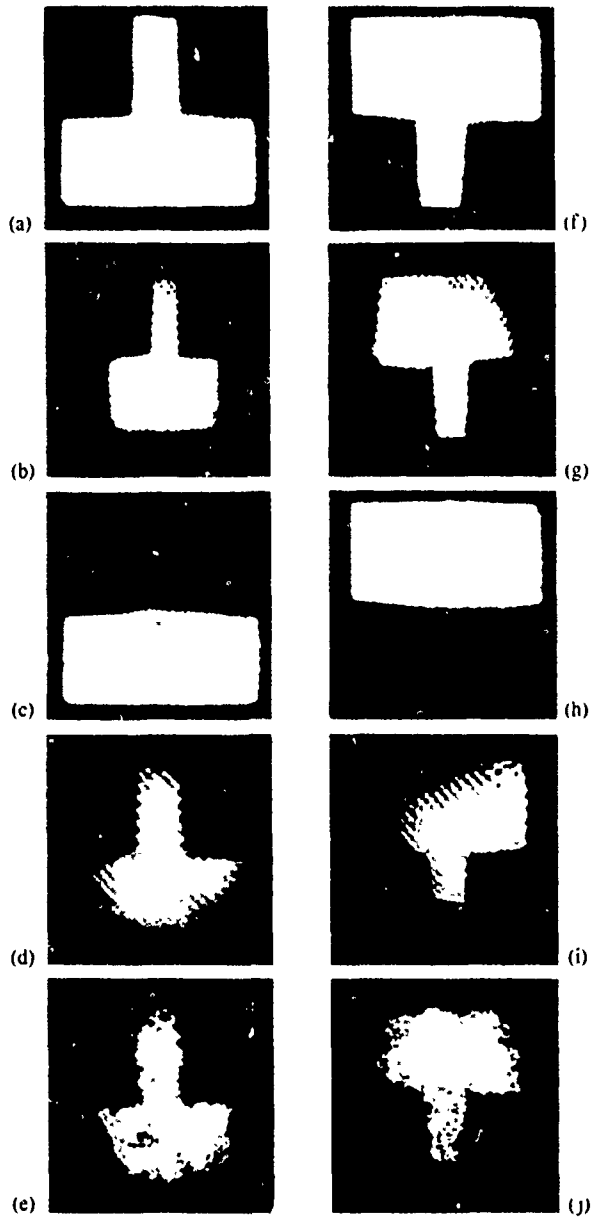

Fig. 16. Associative memory using feedback from optical fibers: (a) stored image E_1, (b) image E_1 diffracted off the hologram by a plane wave input at plane P, (c) partial input image E_1', (d) retrieval of the stored image E_1 by the partial image E_1' using the system of Fig. 15; (e) retrieval of the stored image E_1 by the partial image E_1' using the system of Fig. 17; (f) stored image E_2, (g) image E_2 diffracted off the hologram by a plane wave input at plane P, (h) partial input image E_2', (i) retrieval of the stored image E_2 by the partial image E_2' using the system of Fig 15; (j) retrieval of the stored image E_2 by the partial image E_2' usi' 'he system of Fig. 17. (After [42].)

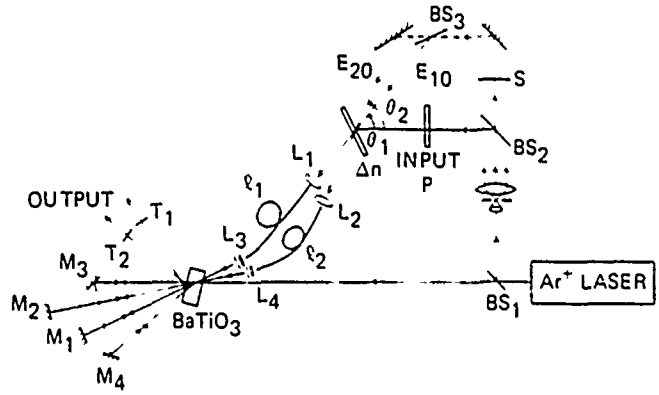

Fig. 17 Associative memory using bistable oscillator based on passive ring phase conjugate mirror. (After [42].)

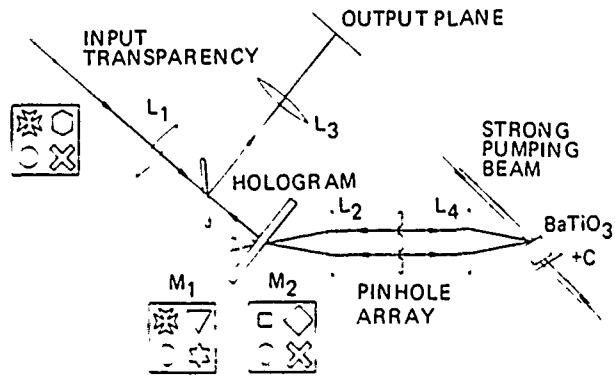

Fig 18. Associative memory using pinhole array and phase conjugate mirror based on four-wave mixing in $BaTiO_3$. (After [45].)

19(c)], the correlations with the two memories were equal and a superposition of the two stored objects was reconstructed. In order to test the discrimination of the NHAM the symmetry was broken by including additional subobjects to favor one of the memories (Fig. 20). This did tend to enhance the memory with the larger correlation, but the discrimination was not complete as a faint image of the other memory can still be seen. The authors attributed this to a lack of nonlinearity in the PCM, since the reflectivity of DFWM is essentially linear for low probe beam intensities (no pump depletion regime). No object was reconstructed when the input consisted of a geometric shape not present in either of the memories [Fig. 19(d)].

6) Nonlinear Etalons: A novel method of thresholding the correlation plane in an NHAM was demonstrated by Wang *et al.* [46]. The NHAM system was similar to the single-pass systems described above with a dichromated gelatin holographic storage element except that the thresholding element was a ZnS bistable etalon. As shown in Fig. 21, holding beams were used to bias the etalon just below the threshold point where it would switch from nontransmitting to transmitting. The etalon was positioned in the back focal plane of the correlation lens. If the peak of the autocorrelation function was sufficient to switch the etalon, the holding beam at that point would be transmitted. Since the holding beams were aligned to be counterpropagating with the reference beams, the transmitted holding beam read out the hologram and reconstructed the associated image. The need for a PCM was therefore avoided. Both auto- and heteroassociation could be implemented by directing the holding beams to the same or different holograms. Associations of two stored fingerprint images have been demonstrated. Wang *et al.* have discussed various practical limitations of this approach, including the high power requirements and nonuniformity of the ZnS etalon. Moreover, a PCM or pseudoconjugator would have to be added on the object

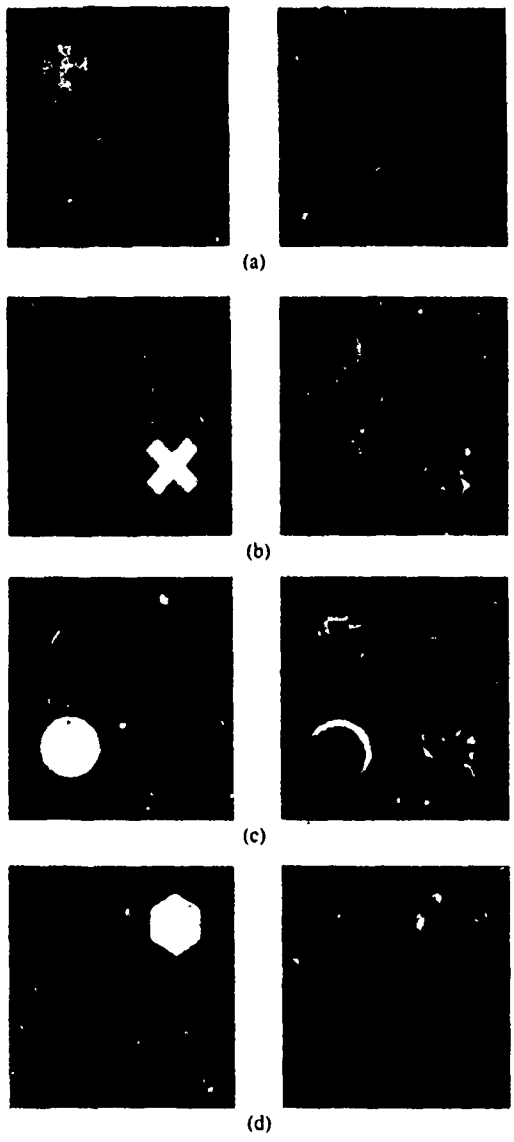

Fig. 19. Associative recall (right) for single test inputs (left) using associative memory system of Fig. 18: (a) Maltese cross; (b) diagonal cross; (c) circle; (d) hexagon (not in training set). (After [45].)

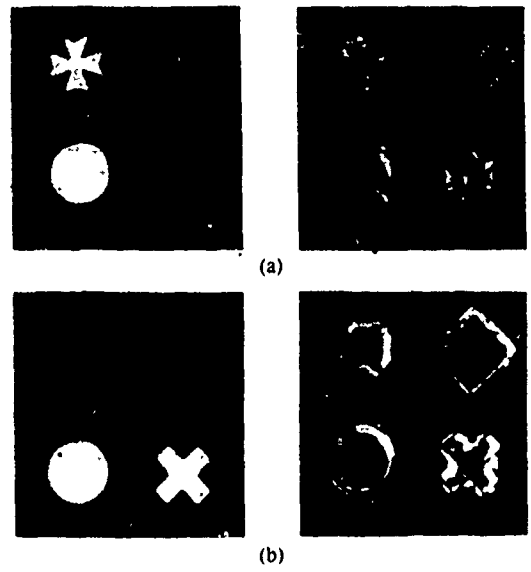

Fig. 20. Associative recall (right) for pairs of test inputs (left) using associative memory system of Fig. 18: (a) circle and Maltese cross, (b) circle and diagonal cross. (After [45]).

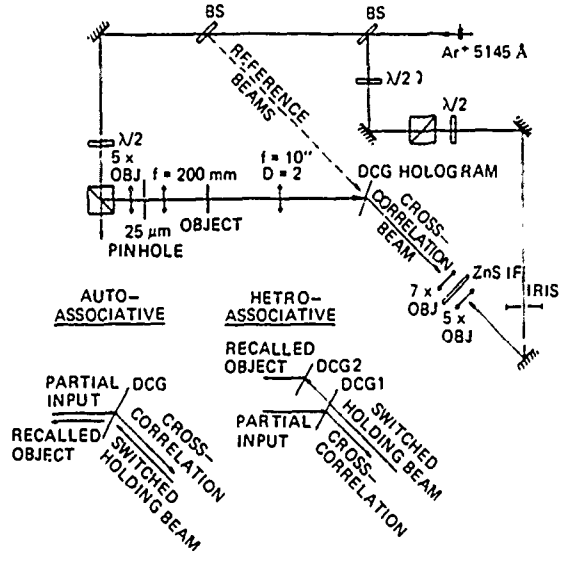

Fig. 21. Associative memory apparatus using nonlinear ZnS etalons. (After [46].)

side of the hologram in order to form a multipass resonator.

C. Ring Resonator NHAM Configurations

An alternative type of optical associative memory is the ring resonator NHAM described and demonstrated by Anderson [47]. In the ring resonator NHAM, the reference beam for recording the hologram is derived from the object beam in a ring configuration, as shown in Fig. 22. After the hologram is recorded, each stored pattern defines an eigenmode of the resonator in the same manner as for the linear resonator NHAM's described previously. An association is made by injecting a portion of the original pattern. A gain medium inside the resonator amplifies the eigenmode with the largest overlap with the injected field. The other eigenmodes are suppressed by a gain competition mechanism.

Anderson and Saxena [48] have performed a perturbative analysis of the evolution of the fields inside the ring resonator NHAM. In their analysis the equation of motion for eigenmode n is

$$\dot{I}_n = \alpha_n I_n - \theta_{nn} I_n^2 - \sum_{n \neq m} \theta_{nm} I_n I_m \qquad (21)$$

where θ_n is a linear gain coefficient, θ_{nn} is a self-saturation coefficient describing how much the presence of a mode suppresses itself, and θ_{nm} is a cross-saturation coefficient indicating to what degree one mode suppresses another. The cross-saturation term is proportional to the mode intensity overlap integral:

$$\theta_{nm} \propto \int_{\text{gain volume}} |U_n(r)|^2 |U_m(r)|^2 d^3r \qquad (22)$$

where $U_n(r)$ is the amplitude distribution of mode n. For

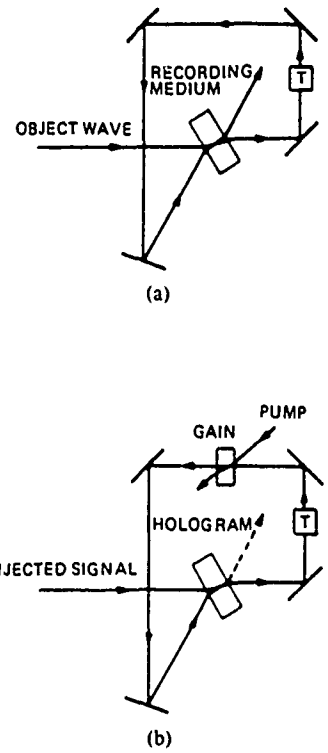

Fig 22 Holographic ring resonator memory (a) recording of hologram, (b) recall by injected signal Gain is supplied by a pumped photorefractive medium. (After [47].)

the case of two stored eigenmodes, the gain competition between modes is described by the ratio of cross- to self-saturation:

$$C = \frac{\theta_{12}\theta_{21}}{\theta_{11}\theta_{22}}. \tag{23}$$

If $C \ll 1$, then overlap between different modes is low, competition is weak, and one mode does not influence the other. If $C \gg 1$, then competition is strong and one mode will dominate over the other. Anderson and Saxena's theoretical results indicate that for a gain medium based on photorefractive two-wave mixing in barium titanate, C can be at most 1. The ring resonator NHAM is adjusted until C is approximately 1 for all pairs of modes. The competition between modes can then be biased with an injected signal. Anderson and Erie [49] have demonstrated this concept using both simple plane waves and printed characters as the recorded eigenmodes. An example of an image stored in a ring resonator NHAM is shown in Fig. 23.

This approach is different from the previously-described NHAM architectures in that the reference beam is derived from the object beam for recording the hologram. During readout no separate thresholding is performed on the reconstructed reference beam. Instead a nonlinear gain competition mechanism is relied on to favor one reconstruction over other possible ones. This results in a simpler design and automatic generation of reference beams for recording, but at the cost of losing some of the flexibility and storage capacity advantages of the plane wave reference based NHAM described in Section II-B.

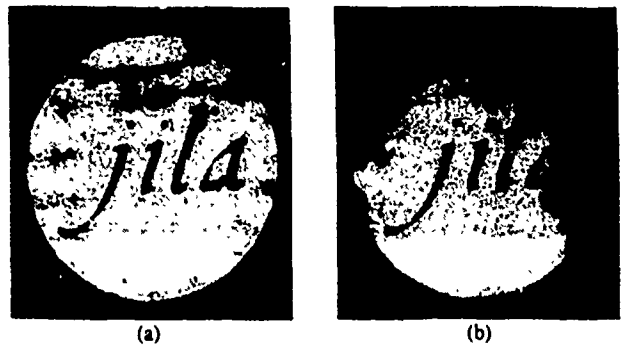

Fig. 23. Image storage and recall in the ring resonator of Fig. 22: (a) output of resonator during writing; (b) output of resonator during recall without an injected signal. (After [49].)

IV. Discussion

Nonlinear holographic associative memories represent a novel innovation on older linear holographic memories. Nonlinearities and feedback improve the reconstruction quality compared to ghost image holography, but beyond that they make possible new optical computation tools, such as image vector quantization and programmable heteroassociations. These operations can be implemented on large scale-bandwidth-product images with the parallelism characteristic of optics. Potential applications include multiple target identification and optical computing using symbolic substitution [50]. Modified versions of these architectures may have applications in optical neural network computers [51]. The parallelism and large interconnectivity make NHAM's especially attractive for this application.

It is interesting that most of the experimental systems reviewed did not utilize the nonlinearity of photorefractive PCM's to improve storage capacity and perform error-correcting associations. In most cases the PCM's were used as linear phase conjugating elements only and external supplemental nonlinearities were added. The external nonlinearities included pinhole arrays, optical fibers, bistable ring resonators, nonlinear etalons, and electronic lookup tables. Even when a thresholding PCM based on a bistable ring resonator was used, it was supplemented by spatial filtering using optical fibers. The use of external nonlinearities is due to experimental difficulties in controlling the nonlinear reflectivity of a PCM. For example, a photorefractive PCM based on four-wave mixing using external pumps can have a nonlinear reflectivity when operated in the pump depletion regime [52]. However, since pump depletion is a nonlocal effect, the threshold level of an incident beam is affected by other incident beams. (In addition the reflectivity of a self-pumped photorefractive PCM is a function of the angle of incidence.) This interaction between beams makes control of the optical nonlinearities difficult using only a photorefractive PCM, making external nonlinearities a practical necessity for consistent results. Pepper has discussed an alternative method for thresholding and conjugating an optical wavefront in an NHAM which uses a PCM for conjugation and a liquid crystal light valve for controllable external thresholding [53].

The experimental systems discussed here demonstrate the potential of NHAM's but they are also evidence of the immature state of NHAM implementations to date. Besides finding the optimum nonlinear mechanism, issues remaining include demonstrating better image quality, larger storage capacity, and programmability. Permanent storage by fixing of holograms in photorefractive materials is an important issue, although much work has already been done in this area [54]–[56]. Interfaces to conventional electronic host computers need to be developed for these systems to become practical. In order to implement higher order tasks (such as rotation and scale invariant recognition of patterns) NHAM modules need to be incorporated in general purpose optical neural network architectures. Nevertheless, these first generation systems have demonstrated several design principles which will doubtless be incorporated in future optical associative memory and neural network processors.

Acknowledgment

I would like to thank G. Dunning, E. Marom, B. H. Soffer, D. M. Pepper, and U. Efron for helpful discussions.

References

[1] See, for example, *Proc IEEE 2nd Int. Conf. Neural Networks*, San Diego, CA, 1988.
[2] S. Grossberg, "Competitive learning: From interactive activation to adaptive resonance," *Cog. Sci.*, vol. 11, pp. 23-63, 1987.
[3] D. E. Rumelhart and J. L. McClelland, *Parallel Distributed Processing*. Cambridge, MA: M.I T., 1986.
[4] G. A. Carpenter and S Grossberg, "A massively parallel architecture for a self-organizing neural pattern recognition machine," *Comput. Vision, Graphics, Image Process.*, vol 37, pp. 54-115, 1987
[5] T Kohonen, *Self-Organization and Associative Memory*. New York: Springer, 1984.
[6] D. H. Ackley, G. E. Hinton, and T. J. Sejnowski, "A learning algorithm for Boltzmann machines," *Cog. Sci.*, vol. 9, pp. 147-169, 1985.
[7] J. J. Hopfield and D W Tank, "'Neural' computation of decisions in optimization problems," *Biol. Cybern.*, vol. 52, pp. 141-152, 1985.
[8] M. L. Minsky and S. A. Papert, *Perceptrons: Expanded Edition*. Cambridge, MA: M.I.T., 1988.
[9] D. Gabor, "Associative holographic memories," *IBM J. Res. Dev.*, vol. 156, 1969.
[10] J. A. Anderson, J. W. Silverstein, S. A. Ritz, and R. S. Jones, "Distinctive features, categorical perception, and probability learning: Some applications of a neural model," *Psych. Rev.*, vol. 84, pp. 413-451, 1977.
[11] J. J. Hopfield, "Neural networks and physical systems with emergent collective computational abilities," in *Proc Nat. Acad. Sci U.S.A. '79*, 1982, pp. 2554-2558.
[12] S. Grossberg, "Nonlinear neural networks: Principles, mechanisms, and architectures," *Neural Networks*, vol. 1, pp. 17-61, 1988.
[13] N. H. Farhat, D Psaltis, A. Prata, and E. Paek, "Optical implementation of the Hopfield model," *Appl Opt.*, vol 24, pp 1469-1475, 1985
[14] K. Wagner and D Psaltis, "Multilayer optical learning networks," *Appl. Opt.*, vol 26, pp. 5061-5076, 1987
[15] D. Gabor, "A new microscopic principle," *Nature*, vol. 161, p. 777, 1948.
[16] P J van Heerden, "A new optical method of storing and retrieving information," *Appl. Opt.*, vol. 2, pp. 387-392, 1963.
[17] G. W Stroke, R. Restrick, A Funkhouser, and D Brumm, "Resolution-retrieving compensation of source effects by correlative reconstruction in high resolution holography," *Phys. Lett.*, vol. 18, pp. 274-279, 1965.
[18] E. N. Leith and J. Upatnieks, "Reconstructed wavefronts and communications theory," *J. Opt. Soc. Amer.*, vol. 52, pp. 1123-1130, 1962.
[19] R. J. Collier and K. S Pennington, "Ghost imaging by holograms formed in the near field," *Appl. Phys. Lett.*, vol. 8, pp. 44-46, 1966.
[20] A B Vander Lugt, "Signal detection by complex spatial filtering," *IEEE Trans. Inform. Theory*, vol. IT-10, p. 2, 1964.
[21] G. R Knight, "Page-oriented associative holographic memory," *Appl. Opt.*, vol. 13, pp. 904-912, 1974.
[22] D Psaltis, J. Hong, and S. Venkatesh, "Shift invariance in associative memories," *Proc. SPIE*, vol. 625, pp. 189-195, 1986.
[23] J Hong and D Psaltis, "Storage capacity of holographic associative memories," *Opt. Lett.*, vol. 11, pp. 812-814, 1986.
[24] J. Yu, F. Mok, and D. Psaltis, "Capacity of optical correlators," *Proc. SPIE*, vol. 825, pp. 128-135, 1987.
[25] E L Kral, J F Walkup, and M O Hagler, "Correlation properties of random phase diffusers for multiplex holography," *Appl. Opt.*, vol 21, pp. 1281-1290, 1982.
[26] Y S Abu-Mostafa and J N St Jacques, "Information capacity of the Hopfield model," *IEEE Trans. Inform. Theory*, vol IT-31, pp. 461-464, 1985.
[27] R J McEliece, E. C. Posner, E. R. Rodemich, and S. S. Venkatesh, "The capacity of the Hopfield associative memory," *IEEE Trans. Inform. Theory*, vol. IT-33, pp. 461-482, 1987.
[28] A. D. Bruce, E. Gardner, and D. J. Wallace, "Dynamics and statistical mechanics of the Hopfield model," *J. Phys. A: Math. Gen.*, vol. 20, pp. 2909-2934, 1987.
[29] C. Weisbuch and S. F. Fogelman, *J. Phys. Lett.*, vol. 46, p. L623.
[30] E. Gardner, "Multi-connected neural network models," *J. Phys. A. Math. Gen.*, vol. 20, pp. 3453-3464, 1987.
[31] Y. Owechko, G. J. Dunning, E. Marom, and B. H. Soffer, "Holographic associative memory with nonlinearities in the correlation domain," *Appl. Opt.*, vol. 26, pp. 1900-1910, 1987.
[32] R. A. Athale, H. H. Szu, and C. B. Friedlander, "Optical implementation of associative memory with controlled nonlinearity in the correlation domain," *Opt. Lett.*, vol. 11, pp. 482-484, 1986.
[33] D. Psaltis and C. H. Park, "Nonlinear discriminant functions and associative memories," in *Neural Networks for Computing*, J. Denker, Ed. New York: Amer. Inst. Phys., 1986, pp. 370-375.
[34] H. H. Chen, Y. C. Lee, G. Z. Sun, H. Y. Lee, T. Maxwell, and C. L. Giles, "High order correlation model for associative memory," in *Neural Networks for Computing*, J. Denker, Ed. New York: Amer. Inst. Phys., 1986, pp. 86-89.
[35] R. G. Zech, "Data storage in volume holograms," Univ Michigan, Ann Arbor, Ph.D. dissertation, 1974.
[36] K. Blotekjaer, "Limitations on holographic storage capacity of photochromic and photorefractive media," *Appl. Opt.*, vol. 18, pp. 57-67, 1979.
[37] J. J. Amodei and D. L. Staebler, "Holographic pattern fixing in electrooptic crystals," *Appl. Phys. Lett.*, vol. 18, pp. 540-542, 1971.
[38] B. H. Soffer, G. J. Dunning, Y. Owechko, and E. Marom, "Associative holographic memory with feedback using phase-conjugate mirrors," *Opt. Lett.*, vol. 11, pp. 118-120, 1986.
[39] G. J. Dunning, E. Marom, Y. Owechko, and B. H. Soffer, "All optical associative memory with shift invariance and multiple image recall," *Opt. Lett.*, vol. 12, pp. 346-348, 1987.
[40] Y. Owechko, "Optoelectronic resonator neural networks," *Appl. Opt.*, vol. 26, pp. 5104-5111, 1987.
[41] E. G. Paek and D. Psaltis, "Optical associative memory using Fourier transform hologram," *Opt. Eng.*, vol. 26, pp. 428-433, 1987.
[42] A Yariv, S. Kwong, and K. Kyuma, "Demonstration of an all-optical associative holographic memory," *Appl. Phys. Lett.*, vol. 48, pp. 1114-1116, 1986.
[43] S. K. Kwong and A. Yariv, *Tech. Dig. Opt. Soc. Amer. Annu. Meet.*, Washington, DC, paper THU3, 1985.
[44] M. Cronin-Golomb, B. Fisher, J O. White, and A. Yariv, "Passive phase conjugate mirror based on self-induced oscillations in an optical ring cavity," *Appl. Phys. Lett*, vol. 42, pp. 919-921, 1983.
[45] H. J. White, N. B. Aldrige, and I. Lindsay, "Digital and analogue holographic associative memories," *Opt. Eng.*, vol. 27, pp. 30-37, 1988.
[46] L. Wang, V. Esch, R. Feinleib, L. Zhang, R. Jin, H. M. Chou, R. W. Sprague, H. A. Macleod, G. Khitrova, H. M. Gibbs, K. Wagner, and D Psaltis, "Interference filters as nonlinear decision-making elements for three-spot recognition and associative memories," *Appl Opt.*, vol. 27, pp. 1715-1720, 1988.
[47] D. Z. Anderson, "Coherent optical eigenstate memory," *Opt. Lett.*, vol. 11, pp. 56-58, 1986.
[48] D. Z. Anderson and R. Saxena, "Theory of multimode operation of

a unidirectional ring oscillator having photorefractive gain. Weak field limit," *J. Opt. Soc. Amer. B*, vol. 4, p. 164, 1987.
[49] D. Z. Anderson and M. C. Erie, "Resonator memories and optical novelty filters," *Opt. Eng.*, vol. 26, pp. 434-444, 1987.
[50] F. T. S. Yu and S. Jutamulia, "Implementation of symbolic substitution logic using optical associative memories," *Appl. Opt.*, vol. 26, pp. 2293-2294, 1987.
[51] Y Owechko and B H. Soffer, "Optical neural networks using holographically interconnected image processors," in *Proc Int. Conf. Neural Networks*, San Diego, CA, 1988.
[52] P Gunter, "Holography, coherent light amplification and optical phase conjugation with photorefractive materials," *Phys. Rep.* (Review Section of *Phys. Lett.*), vol. 93, pp. 199-299, 1982.
[53] D M Pepper, "Optical phase conjugator with spatially resolvable thresholding utilizing liquid crystal light valve," U.S. Patent no. 4 762 397, Aug. 9, 1988.
[54] J. P Herriau and J P. Huignard, "Hologram fixing process at room temperature in photorefractive $Bi_{12}SiO_{20}$ crystals," *Appl Phys Lett*, vol. 49, pp. 1140-1142, 1986.
[55] D L Staebler, W J Burke, W Phillips, and J. J Amodei, "Multiple storage and erasure of fixed holograms in Fe-doped $LiNbO_3$," *Appl. Phys. Lett.*, vol. 26, pp. 182-184, 1975.
[56] F. Micheron, C. Mayeux, and J. C. Trotier, "Electrical control in photoferroelectric materials for optical storage," *Appl. Opt.*, vol. 13, pp. 784-787, 1974.

Yuri Owechko was born in Sao Paulo, Brazil, in 1956. He received the B.S. degree in applied physics from the California Institute of Technology, Pasadena, in 1978 and the Ph.D. degree in materials science from the University of Southern California, Los Angeles, in 1983, where he conducted research on the optical characteristics of the PROM and PRIZ spatial light modulators.

Since 1984 he has been a member of the technical staff at Hughes Research Laboratories, Malibu, CA, where he has been active in optical data processing research. His present research interests include optical neural networks and associative memories, optical linear algebraic processors, optical beam forming, and the physics of spatial light modulators.

Dr. Owechko is a member of the Optical Society of America and Sigma Xi.

Reprinted from SPIE Vol 882—Neural Network Models for Optical Computing
1988 by the Society of Photo-Optical Instrumentation Engineers, Box 10 Bellingham WA 98227-0010 USA

APPENDIX C

Optoelectronic Neural Networks Based On Holographically Interconnected Image Processors

Y. Owechko, B. H. Soffer, and G. J. Dunning

Hughes Research Laboratories
Malibu, CA 90265

Abstract

We describe an optoelectronic resonator associative memory system which utilizes holographic interconnects. Image processing techniques are used to implement nonlinearities and feedback. We show using numerical models that both power law and sigmoidal nonlinearities improve the storage capacity. Our experimental results lead us to be optimistic that this hybrid optical/electronic approach can be extended to adaptive neural network models.

1.0 Introduction

The self-organizing, adaptive features of neural network models developed by biologists and mathematicians has in recent years piqued the interest of engineers who are interested in applying them to problems in signal processing, pattern recognition, and multi-variable optimization (1). Neural network models offer a data-driven unsupervised computational approach which is complementary to the algorithm-driven approaches of traditional information processing and artificial intelligence. The fine granularity, massive interconnectivity, and high degree of parallelism set neural network models apart from traditional electronic serial computing. These same features are the hallmarks of optical computing architectures which have led many workers to consider optical implementations of neural network models (1-12).

As reported in (2-4), we have constructed and demonstrated a resonator-based nonlinear holographic associative memory (NHAM) which can be described as an optical neural network. A diagram of a generic NHAM is shown in Fig. 1. In this paper we describe a hybrid optical/electronic version of the associative memory in which the nonlinearities are implemented electronically. We also discuss some initial numerical results from computer simulations which show the effects of various nonlinearities on NHAM performance.

The all-optical NHAM reported in (2) consisted of a hologram situated in a phase conjugate resonator cavity formed by two phase conjugate mirrors (PCMs). The PCMs were formed by four wave mixing in $BaTiO_3$. An intra-cavity thermoplastic hologram defined the self-consistent low-loss transverse modes of the resonator. These modes corresponded to images stored in the hologram. Several images were recorded as superimposed Fourier transform holograms, each with a unique angularly shifted plane wave reference beam (which corresponds to spatially separated delta functions in the input plane). If the hologram was subsequently addressed by a partial or distored version of one of the stored images, a set of distorted reference beams was reconstructed. The oscillation threshold of the NHAM and the nonlinear reflectivity of the phase conjugate mirrors act to enhance the strongest reconstructed reference relative to the weaker ones. The stored image with the largest correlation with the input survives at the expense of the less correlated images. A method for adjusting the threshold level of a PCM was reported in (13). These nonlinear mechanisms perform functions analogous to "winner-take-all" competitive neural networks. The output of the associative memory after presentation with a distorted input is an undistorted version of the input.

The storage capacity of such a nonlinear associative memory was shown in (3) to be superior to a linear holographic associative memory when a power law nonlinearity is used in the correlation domain. These results are reviewed in Section 2 and extended to sigmoidal nonlinearities using numerical simulations. They indicate that the theoretical storage capacity of an NHAM can be much greater than outer-product or simple correlation matrix formulations of associative memory because of the superior cross-talk suppression characteristics of the NHAM.

A hybrid optical/electronic version of the all-optical NHAM is described in Section 3. In the hybrid NHAM the $BaTiO3$ based phase conjugate mirrors are replaced with video detectors and spatial light modulators arranged in a pseudo-conjugating configuration. Although the self-aligning feature of the all-optical phase conjugate resonator is lost with this change, other desirable features are gained. Greater gain is possible due to the combination of the electronic gain of the video detector and the optical gain of the spatial light modulators (in this case Hughes Liquid Crystal Light Valves (LCLV)). Large

gains are desirable since the diffraction efficiency of the hologram becomes less as more gratings are recorded. The hologram diffraction efficiency is an optical loss which must be overcome in order to form a resonator. Using this hybrid approach, we have demonstrated such an associative resonator. Another feature of the hybrid resonator associative memory is that programmable digital video processing can be used to implement nonlinearities and hetero-associative operations. The nonlinearities are point operations and can be implemented at video rates using fast lookup tables. In this hybrid approach the strengths of optics: linear transformations, massive interconnectivity and parallelism; and the strengths of electronics. point nonlinearities and programmability; are both used to advantage.

The NHAM can be interpreted as a single layer optical neural network in which the interconnection weights are established permanently and non-adaptively during recording of the hologram. Feedback is used during readout but not in the recording of the weights. A hybrid opto-electronic two-layer neural network is described in Section 4 in which the weights can be adjusted adaptively. This system is a straightforward extension of the hybrid NHAM which uses photorefractive crystals as the holographic storage medium

2.0 NHAM Storage Capacity

The storage capacity of the NHAM is limited by such factors as the resolution, area, and dynamic range of the holographic storage medium and the overall system gain. A more fundamental limitation, however, which is independent of such material issues, s correlation noise. Correlation noise is especially bothersome for an NHAM which, in order to maintain shift-invariance, is based on a thin hologram. The root cause is cross-talk between non-orthogonal stored image vectors and it is similar to the storage limitation mechanisms in the outer-product matrix type associative memories which have been described by many workers. Fortunately, correlation noise can be greatly reduced in the reference-based NHAM by utilizing the proper nonlinearities in the correlation domain. The effects of such nonlinearities will be described in this section using examples from numerical simulations.

A block diagram of an NHAM from which we will derive an iterative equation for the NHAM resonator is shown in Fig. 2. The operators H_{A-B} and H_{B-A} represent forward and backward paths through the hologram. The functions h() and f() represent point nonlinearities in the image or object domain and in the reference or correlation domain, respectively. Based on this diagram, an iterative equation can be written for the object distribution $\hat{A}_n(x)$ after the n-th iteration around the loop based on the previous iteration distribution $\hat{A}_{n-1}(x)$:

$$\hat{A}_n = G\,[\,\hat{A}_{n-1}\,]$$

where

$$G\,[\,\hat{A}_n\,] = h\,\{\,\sum_m f\,(\,\hat{A}_n \circledast A^{(m)}\,) * A^{(m)}\,\}$$

(In this paper $\circledast$ and * denote correlation and convolution, respectively.) We derived the above equation by assuming a thin hologram and angularly shifted plane wave reference beams, which correspond in the correlation domain to references $B^{(m)}$ which are spatially shifted delta functions. The correlation domain nonlinearity f() operates on each term separately because the terms are spatially separated due to the angular multiplexing of the reference beams. The stored images $A^{(m)}$ are the eigenfunctions of the operator G, e.g.

$$G\,[\,A^{(m)}\,] = A^{(m)}$$

The correlation/convolution operations inherent in G serve to "recognize" inputs to the system as members of the stored set of images. These operations are also the source of capacity-limiting correlation noise when non-orthogonal images are stored. The nonlinear functions f() and h() can be used to reduce the correlation noise.

In (3) we showed that when the correlation domain nonlinearity f() is of the form

$$f\,(\,x\,) = x^n$$

then the storage capacity in terms of the number, M, of images that can be stored with an arbitrary "acceptable" level of cross-talk is proportional to

$$M \sim N^{n-1}$$

where N is the size of the stored image vectors. This result was derived assuming random non-orthogonal binary image vectors and it was verified using computer simulations. The above result indicates that the cross-talk among stored vectors can be reduced to an arbitrarily small value by increasing the nonlinearity of the correlation domain function f().

However, in physically realizable systems the degree to which this can be achieved is limited by the finite dynamic range of analog systems. Therefore, we have performed computer simulations in which the f() and h() functions are sigmoidal (incorporating saturation) and noise is added to the updated image vector after each iteration or round trip through the NHAM resonator (simulating limited NHAM dynamic range).

The dynamic behavior of the NHAM simulation is illustrated in Figs. 3a-c using phase diagrams. In the phase diagrams the horizontal coordinate represents the "distance" of the current state of the system from the target image vector. The vertical coordinate represents the distance in the next iteration. Distance D(k) in the k-th iteration is defined here as $1-\cos(\theta)$ where $\cos(\theta)$ is the direction cosine between the state of the system and the target image vector. We use the direction cosine as a distance measure rather than Hamming distance because it is a normalized quantity which measures the orientation of image vectors in state space and is independent of the vector norm. It is a better measure of image similarity. The dynamic evolution of the system for a particular initial input is represented by a series of points which head toward the origin when the system successfully converges to the target image vector. An "equilibrium line" which passes through the origin with unity slope represents the projection of equilibrium points (possibly unstable) in state space onto the phase diagram. If the output of the NHAM evolves to an eigenfunction of the operator G, the distance D(k) from the target vector will be constant for succeeding iterations k, hence the system will be "stuck" on the equilibrium line. Recall of false or incorrect memory states is represented by system trajectories which come to rest on the equilibrium line anywhere other than the origin. Trajectories which monotonically approach the target vector are confined below the equilibrium line.

In all of the following examples the image vectors are 50 bit long binary vectors whose entries are +-1. The sigmoidal nonlinearity in the correlation plane in all cases was

$$f(x) = \frac{10}{1 + \exp[\,0.23\,(x - 44)\,]}$$

which set the correlation threshold level at 44 (the maximum possible correlation peak value was 50). In the phase diagram shown in Fig. 3a the following nonlinearity was used in the object domain:

$$h(x) = \frac{1}{1 + \exp[\,1.5\,x\,]}$$

In all of the following examples the parameters for h() and f() were determined empirically using numerical "experiments." No optimizations were done. A total of 100 random 50 bit long image vectors was generated and stored in the NHAM operator G. The input vector was generated by reversing nine of the bits in a randomly chosen stored vector. As evidenced by the eventual path of the system toward the origin, the target vector was successfully associated with the distorted input vector. In this case M=2N where M is the number of stored vectors and N is the vector size. Even with this number of stored vectors an error in the input of 18% (nine bits in error) was successfully corrected. This capacity and error-correction ability is far in excess of outer-product matrix-based associative memories where M=0.15N (14,15). Note that the system spent several iterations close to the equilibrium line where progress toward convergence on the target vector is slow. The trajectory can be pushed away from the equilibrium line and faster convergence obtained by sharpening the object domain nonlinearity. In Fig. 3b the only change was a h() with a slightly sharper threshold:

$$f(x) = \frac{1}{1 + \exp[1.9x]}$$

Note the faster convergence Finally, in Fig 3c noise was added after each iteration The magnitude of the noise was 10% of image vector magnitude. In this case the system initially started to diverge until a random perturbation pushed the system into the basin of attraction of the target vector

3.0 Hybrid NHAM

A block diagram of the hybrid associative memory is shown in Fig. 4 and a detailed schematic in Fig. 5 As in the all-optical NHAM, thin Fourier transform holograms were recorded in thermoplastic film Angular multiplexing of the reference beams acts to separate correlation noise from the desired signal, improving the efficacy of thresholding to remove the correlation noise and increase the signal to noise ratio of the reconstructed image. The number of interconnection weights that can be stored in a thin hologram is much less than in a thick hologram. However, because of the shift-invariance of the Fourier transform, the relatively small number of interconnections are used very efficiently to implement position independent pattern recognition. In this case the mapping for shift-invariance is built into the system by the physics of lenses and diffraction. In a true neural network with adaptable weights the system would have to "learn" the required mappings from examples supplied by its environment or an external teacher.

Thresholding, feedback, and gain are provided electronically by two sets of vidicon detectors, cathode ray tubes (CRTs), and LCLVs. A partial or distorted input image is focused onto an object loop vidicon detector which transfers the image to an LCLV via a CRT. The dashed lines in Fig. 5 indicate conjugate planes which are in one-to-one correspondence with unity magnification The output from the object loop LCLV addresses the hologram and reconstructs distorted versions of the angularly multiplexed plane wave reference beams used in recording the stored images. Each of the original delta functions references is convolved with the correlation of its respective associated object with the input object. The distorted references are, therefore, simply the correlation functions of the input object with the stored objects, each of which comes to a focus on a unique subregion of the correlation plane. The locations of these subregions in the correlation plane are determined by the angular shifts of the reference beams used during recording of the hologram. The correlation functions are focused onto a reference leg vidicon detector A one-to-one mapping is performed between points on the detector and points on the output of the LCLV A pseudo-conjugate of the incident reference beam is generated by aligning the LCLV in the back focal plane of the correlation lens. The activated pixels on the LCLV which represent the thresholded correlation function are illuminated by a readout beam The activated spot on the LCLV is converted into a back-propagating undistorted reference beam by the correlation lens. This restored reference beam addresses the hologram and reconstructs its associated stored object as a real image which focuses on the vidicon detector in the object loop of the resonator. Again, a one-to-one mapping is made of the light incident on the vidicon to the readout side of the object LCLV. The restored object image is then directed to the hologram, closing the resonator loop. The combined gain of the vidicon/CRT/LCLV units are adjusted to overcome the optical losses of the system. General nonlinear feedback functions can be easily implemented. The correlation functions are processed in electronic form using an image processor with a programmable digital look-up table before being sent to the reference leg LCLV.

In our initial experiment, a single object/reference pair was recorded in the hologram Although this was obviously insufficient to demonstrate discrimination between objects, it does serve to demostrate that the resonator has a stable state which can be reached only if the injected signal is sufficiently similar to the stored image. The results are shown in Fig. 6 The input object was a partial version of the stored object, an Air Force resolution chart. If more than approximately 50% of the object was injected into the system, resonance was achieved and the system would latch onto the stored image. The system would stay latched after removal of the input, demonstrating bistability Interrupting the circulating beam in the resonator would return it to its initial zero state If the input object was rotated by up to 10°, the output would still switch to its other stable state The output would be an undistorted (unrotated) version of the stored object. The system would not recognize the object if it was rotated more than 10°, indicating that the system was not merely being brought above threshold by noise.

4.0 Extension of NHAM to Adaptive Neural Networks

The opto-electronic resonator associative memory can be extended to implement an adaptable and reconfigurable multi-layer optical neural network (ONN) with large storage capacity and parallel weight update capability. A block diagram of the system is shown in Fig. 7. A two-dimensional neural activation pattern (object OA) addresses subhologram H1 and reconstructs another activation pattern (reference R). Reference R is nonlinearly processed and then shifted so that it addresses a second subhologram H2 and reconstructs a third pattern (object OB) The two subholograms H1 and H2 are physically adjacent on the same substrate and form the link weights between the input/output layers, OA and OB, and the hidden layer, R The hologram substrate is a volume photorefractive crystal such as LiNbO3 in which link weights can be continuously reinforced or inhibited. The optical pathways or links are bidirectional so that light can propagate not only in the direction OA-R-OB but also OB-R-OA. An error signal is back-propagated through the ONN with its phase shifted by 0 or π so that grating which contribute to a large error signal can be enhanced or inhibited. Thus this system can implement an optical version of the back-propagation algorithm. The three activation patterns and two subholograms form a two-layer optical neural network. OA is the input activation pattern, R is a "hidden" layer, and OB is the output layer.

Although the number of interconnects that can be stored is proportional to the volume of the hologram, which scales as the linear dimension cubed; the number of possible interconnections between two NxN neural planes is N^4, which scales as the linear dimension to the fourth power. This reflects the fact that each grating wavevector can be read out by a multiplicity of input/output wavevector pairs, which can result in unwanted cross-talk between neurons (9). This is illustrated in Fig. 8 which shows that each grating wavevector K_g can be read out by a set of input/output wavevector pairs which forms two cones touching at their apexes. In other words, all wavevector pairs lying on the surfaces of the two cones satisfy the Bragg condition for diffraction off the grating represented by K_g, which can result in unwanted cross-talk between the K_g "weights".

Several approaches can be used to resolve this readout ambiguity, including sampling of the neuron planes using fractal grids (9). In our preferred approach, the object wavevectors are free to vary in both θ and ϕ (two-dimensional pixel arrays), but the reference wavevectors are confined to a plane using cylindrical lenses (one-dimensional line pixel arrays). This results in the volume filling of K space with grating wavevectors and a total number of possible interconnects which scales as the linear dimension cubed. The degrees of freedom in the volume hologram are then matched to the number of required interconnects and cross-talk is automatically avoided. This arrangement also maps well to many neural network models in which a number of neurons in one layer are connected to smaller or larger numbers of neurons in succeeding layers. In the hybrid NHAM this type of partitioning also results in larger gain because one-dimensional pixel lines rather than points are used in the reference plane. The pixel lines intercept a greater fraction of the readout beam which results in brighter retroreflected reference beams. If N_1 is the number of pixels that can be resolved along a line by an LCLV, then the number of noninterfering interconnections between two planes is N_1^3 using this partitioning method, which is the same as the fractal partitioning method.

A detailed drawing of the proposed optical back-propagation system is shown in Fig. 9. This system is virtually identical to the opto-electronic resonator associative memory system described in the previous section except for the substitution of a LiNbO3 volume hologram for the thin thermoplastic film hologram and the addition of a few lenses and an SLM. The "top" and "bottom" activation patterns OA and OB are located side by side in the input plane. An incoherent-to-coherent conversion is performed in the object loop using a vidicon detector and LCLV.

5.0 Summary

A hybrid opto-electronic nonlinear holographic associative memory (NHAM) was described and theoretical and experimental results discussed. The NHAM consists of a hologram in an opto-electronic cavity. Gain, feedback, and nonlinear processing of the reference beams are provided by vidicon detectors, an image processor, and liquid crystal light valves. Numerical simulations demonstrated the beneficial effects of nonlinearities in the correlation domain on the storage capacity and object discrimination of NHAM. Operation of the system as a resonator was experimentally demonstrated. The error-correction properties were evident as the input image could be rotated over a range of 10° with no observable degradation in the associated output image.

A design for a hybrid opto-electronic resonator neural network architecture based on volume holograms and capable of learning using error back-propagation was also discussed. The design is a direct extension of the opto-electronic nonlinear holographic associative memory. The use of spatially multiplexed subholograms in photorefractive crystals should allow the implementation of a multi- layer optical neural network consisting of millions of

neurons with potential processing rates of 1×10^9 interconnects per sec. This optical neural net can be constructed from standard components and would not require the development of new devices or the use of excessive optical power levels. The use of video electronics in the feedback and back-propagation paths simplifies interfacing to an outside computer host and allows the implementation of general nonlinear activation functions. In this hybrid system, optics provides the massive connectivity and parallelism necessary in a neural network, while electronics provides the nonlinear processing. Both are therefore used in the roles to which they are best suited. Such a system would find numerous applications in adaptive information processing and control systems.

This work was supported in part by the Air Force Office of Scientific Research. The authors wish to thank C. DeAnda for expert technical assistance.

References

1. Proceedings of the International Conference on Neural Networks, San Diego, June, 1987

2. B. Soffer, G. Dunning, Y. Owechko and E. Marom, "Associative holographic memory with feedback using phase-conjugate mirrors," Optics Letters, Vol. 11, Page 118, February 1986

3. Y. Owechko, G. Dunning, E. Marom and B. Soffer, "Holographic associative memory with nonlinearities in the correlation domain," Applied Optics, Vol. 26, Page 1900, May 1987

4. Y. Owechko, G. Dunning, B. Soffer, and E. Marom, "Video rate optical associative memory with shift invariance," International Conference on Neural Networks, San Diego, June, 1987

5. D Z. Anderson, "Coherent Optical Eigenstate Memory," Opt. Lett. 11, 45 (1986).

6. A Yariv and S K. Kwong, "Associative Memories Based on Message-Bearing Optical Modes in Phase-Conjugate Resonators," Opt. Lett. 11, 186 (1986).

7. R. A. Athale, H. H. Szu, and C. B. Friedlander, "Optical Implementation of Associative Memory with Controlled Nonlinearity in the Correlation Domain," Opt. Lett. 11, 482 (1986)

8. N. H. Farhat, D. Psaltis, A. Prata, and E. Paek, "Optical Implementation of the Hopfield Model," Appl. Opt. 24, 1469 (1985).

9. D. Psaltis, J. Yu, X. G. Gu, and H. Lee, "Optical Neural Nets Implemented with Volume Holograms," OSA Topical Meeting on Optical Computing, Lake Tahoe, March, 1987.

10. K. Wagner and D. Psaltis, "Multilayer Optical Learning Networks," SPIE Vol. 752 (1987) 86.

11. M. Cohen, "Design of a new medium for volume holographic information processing," Appl. Opt., Vol. 25 (14), p. 2288 (1986).

12. See also Applied Optics, May 15, 1987 issue on optical artificial intelligence.

13. K. Sayano, G. A. Rakuljic, and A. Yariv, "Thresholding semilinear phase-conjugate mirror," Opt. Lett. 13, 143 (1988).

14. T. Kohonen, **Self-Organization and Associative Memory**, (Springer-Verlag, New York, 1984).

15. J. J. Hopfield, "Neural Networks and Physical Systems with Emergent Collective Computational Abilities," Proc. Natl. Acad. Sci. USA 79, 2554 (1982).

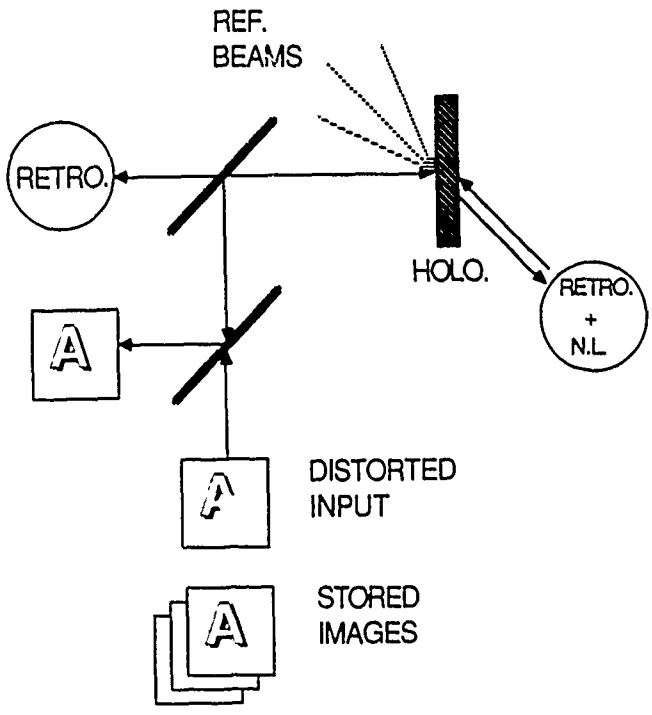

Figure C-1. Generic NHAM

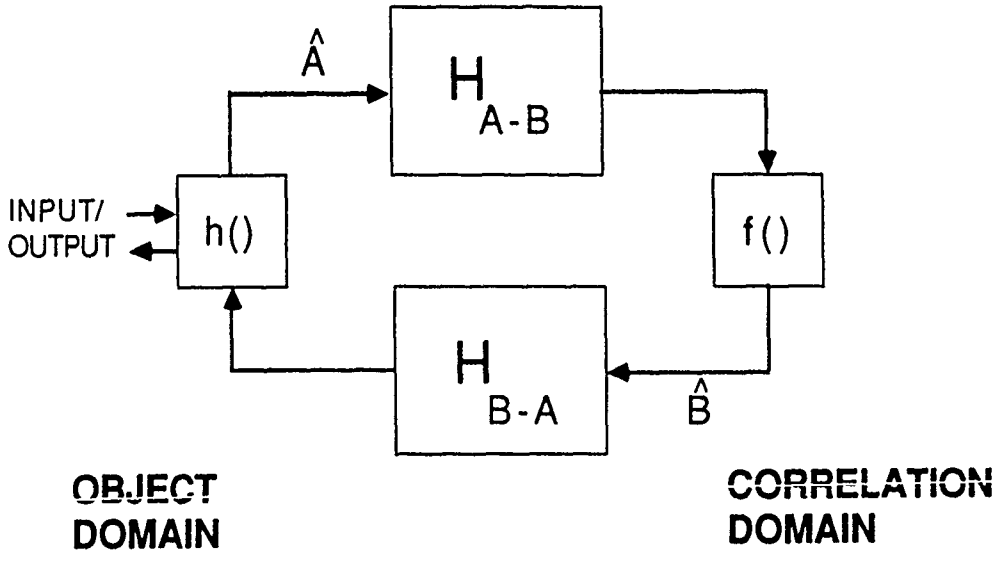

Figure C-2. Nonlinear correlation model of NHAM

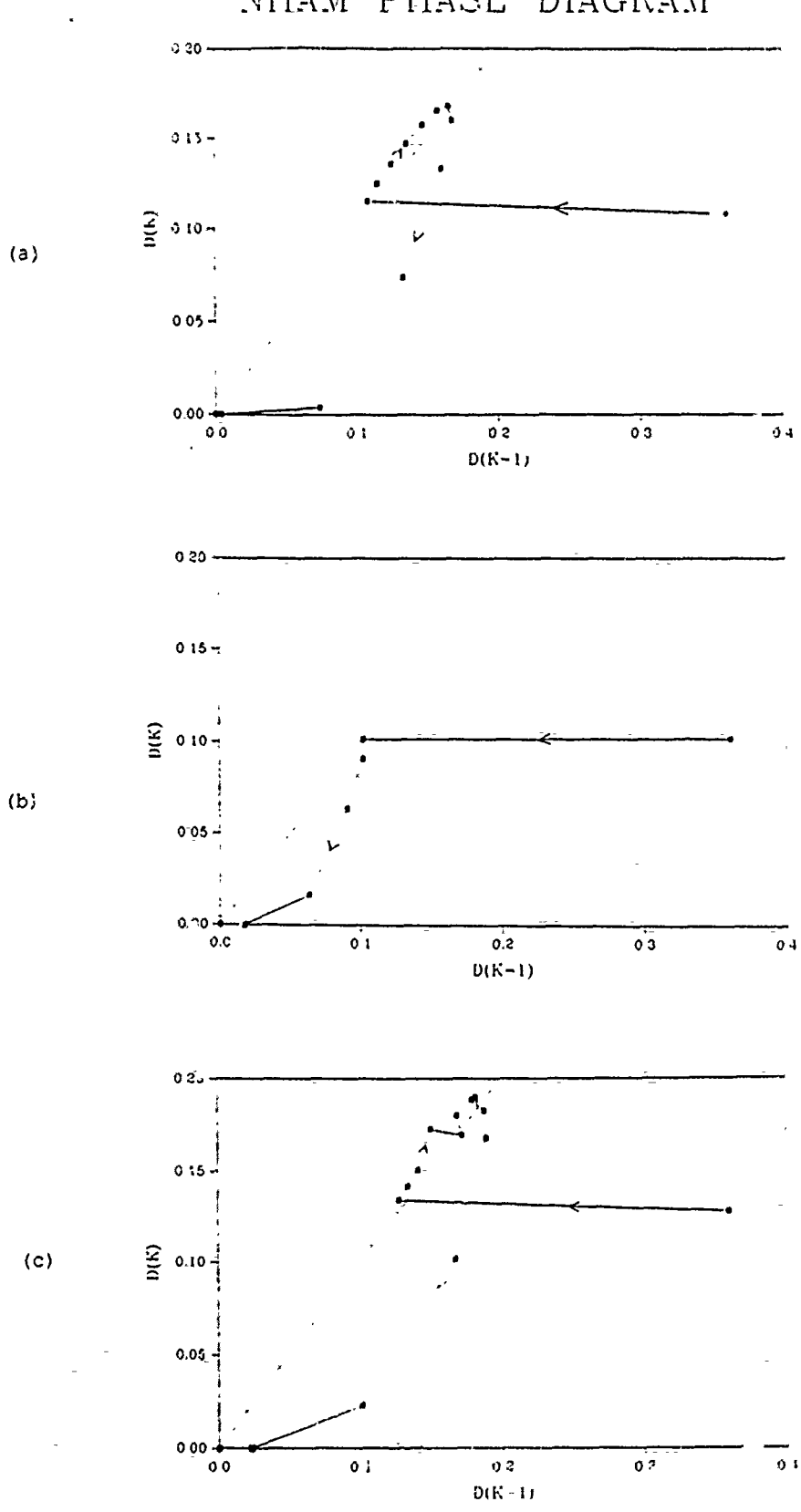

Figure C-3. Phase diagrams of NHAM convergence for different object domain nonlinearities (a and b) and with added noise (c)

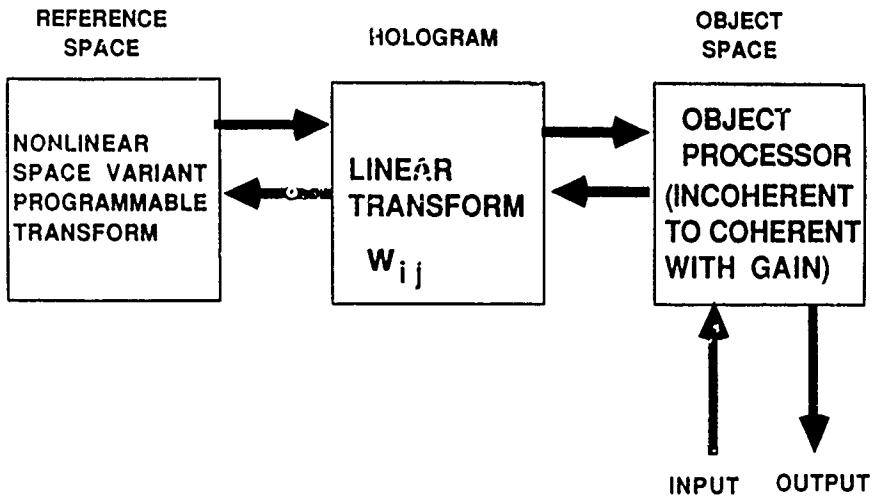

Figure C-4. Block diagram of optoelectronic associative memory

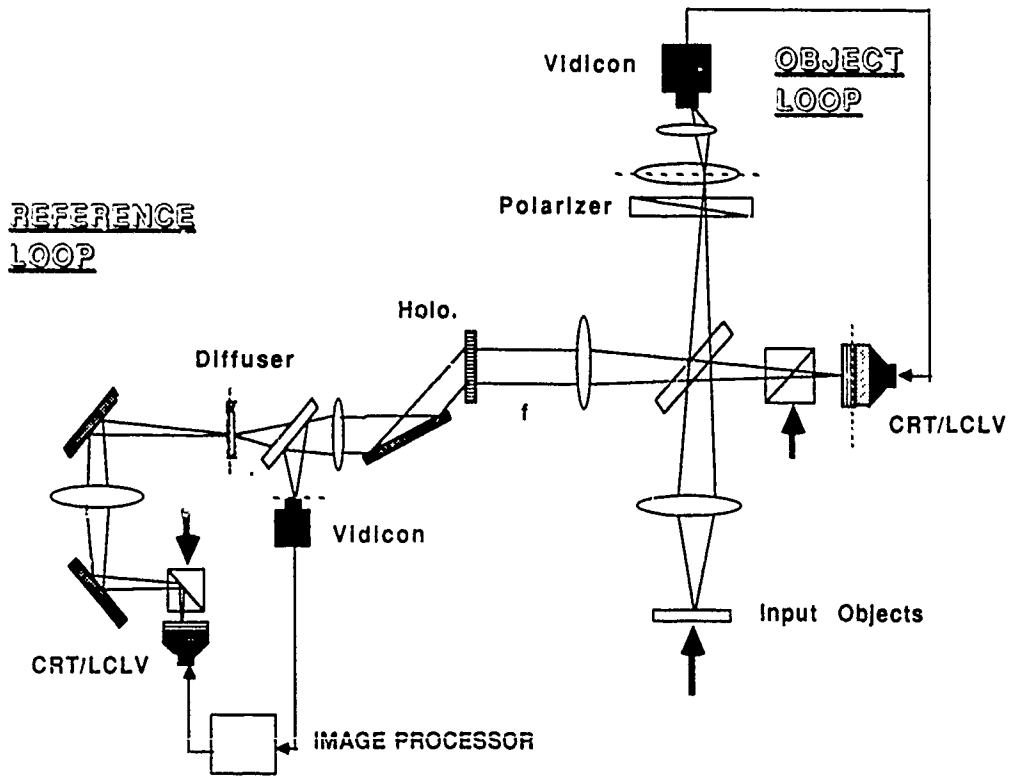

Figure C-5. Experimental setup for optoelectronic NHAM

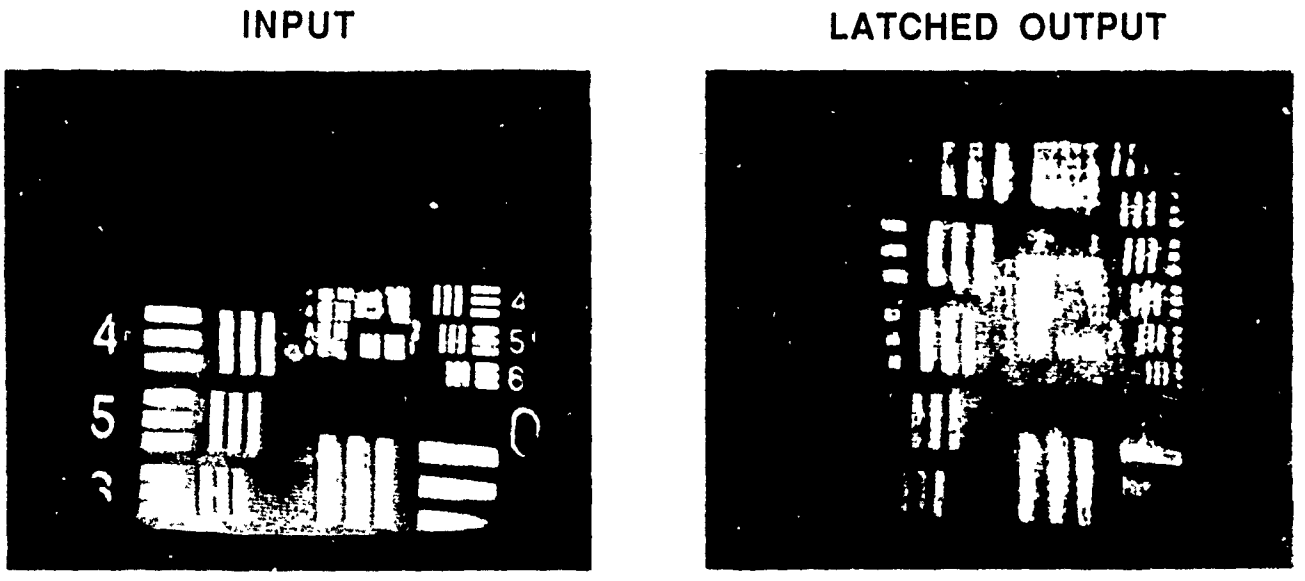

Figure C-6. Experimental association

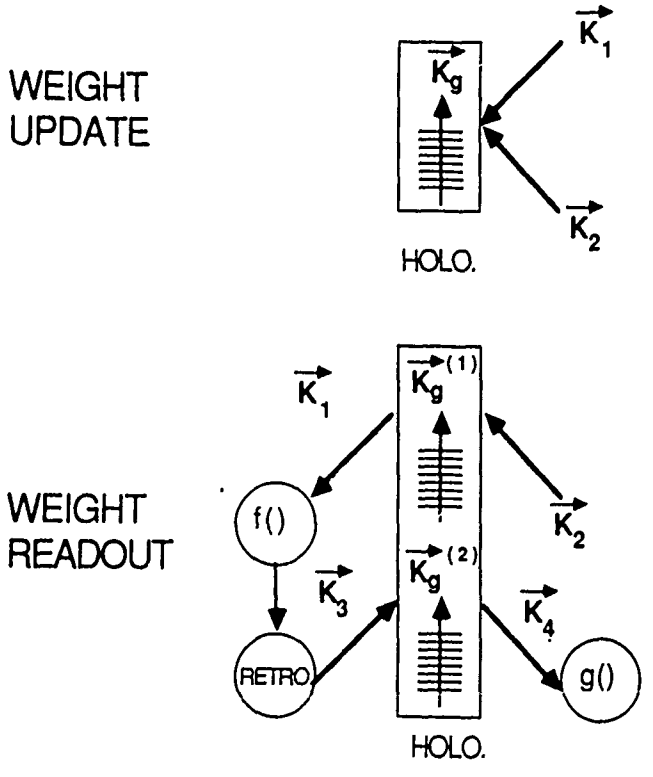

Figure C-7. Weight adaptation and readout in NHAM-based neural network

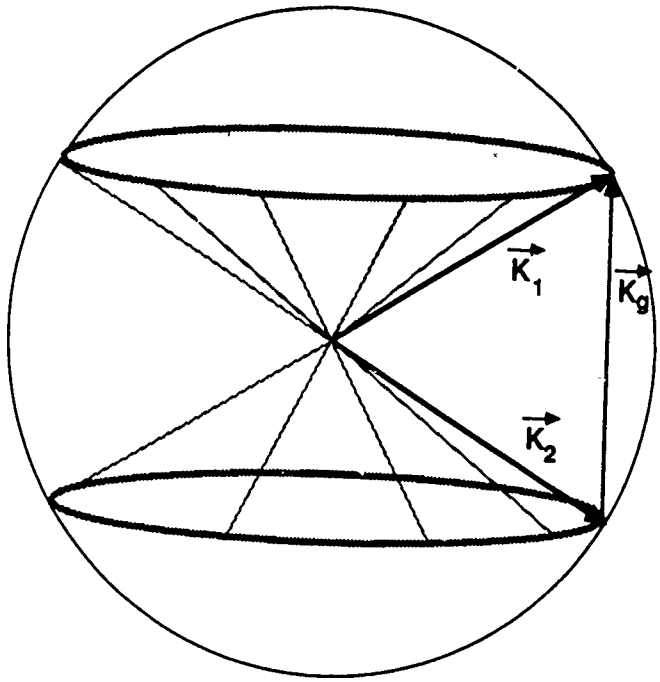

Figure C-8. K_g readout ambiguity

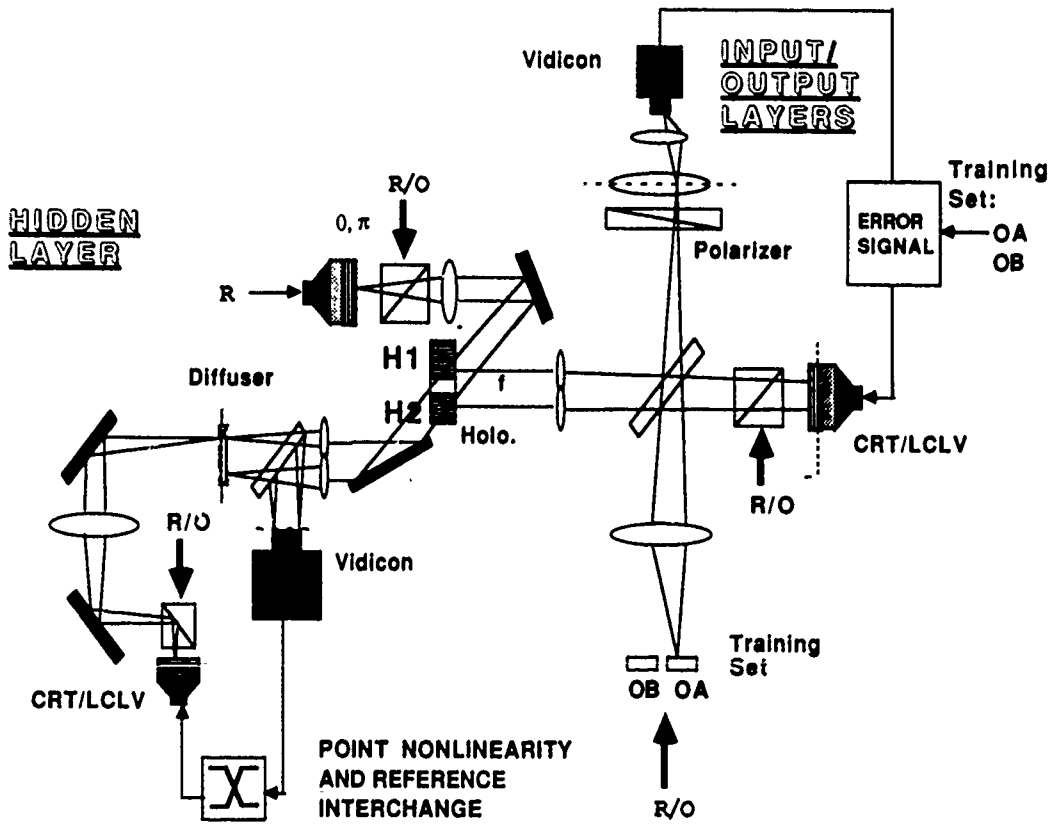

Figure C-9. Schematic of optoelectronic two-layer neural network

REPRINT

APPENDIX D

Critical Reviews
of Optical Science
and Technology

CRITICAL REVIEWS

Reprinted from

Spatial Light Modulators and Applications III

SPIE Volume 1150

7-8 August 1989
San Diego, California

Holographic Associative Memories

Yuri Owechko

Hughes Research Laboratories
Malibu, California

Abstract

A Lyapunov or "energy" function based on Kosko's BAM model of associative memory is derived for optical associative memories based on thin holograms in a nonlinear cavity. The dynamic behavior is illustrated using computer simulations.

1. Introduction

Neural network implementations of associative memory have a wide range of potential applications including content-addressable memories with error correction, pattern recognition, and adaptive sensory-motor mappings for robotic control, among others. A large body of theoretical work on associative neural networks performed over the past twenty years is now beginning to be exploited for such engineering applications. It is commonly felt that conventional serial computers are not suitable for future neural network applications involving large numbers of neurons because of the rapid scaling of connectivity and weight update rates with problem size. Practical systems employing neural network algorithms will require special purpose parallel computers onto which neural network models can be directly mapped.

As an alternative to conventional computers which lack the fine-grained parallelism and connectivity required by neural network models, much work has recently been done on optical and hybrid optical/electronic neural networks. The very high storage capacity, connectivity, and parallelism of optics makes such systems attractive for this application. In particular, nonlinear holographic associative memories (NHAM) have enjoyed a high degree of interest and activity in recent years. These systems improve the associative properties of ghost image holography pioneered by Gabor [1], Van Heerden [2], and Collier and Pennington [3] by placing the hologram in an optical feedback cavity with nonlinear gain. The images stored in the hologram then become the eigenmodes of the cavity and form stable limit points of the system.

In this paper I will interpret the dynamics of thin hologram NHAMs in terms of a neural network model, specifically the Bidirectional Associative Memory (BAM) model of Kosko. I will show that although NHAM systems are direct optical implementations of the BAM model,

the limit points are not in general the intended stored memories unless the memory patterns in one neural layer assume a particular form. This restriction is removed if volume holograms are used together with some precautions to avoid crosstalk, although the natural shift invariance of the thin hologram NHAM is then sacrificed. I will use computer simulations to illustrate NHAM dynamic behavior.

2. NHAM architecture

The basic principle behind the associative properties of holograms is illustrated in Fig. 1 which depicts a highly idealized hologram formation process. During recording, two coherent optical wavefronts, spatially modulated by transmittances a and b, are Fourier transformed and interfere in a photosensitive medium, forming a fringe pattern $|A+B|^2$ where A and B are the Fourier transforms of a and b, respectively. (Nonlinearities in the photoresponse of the medium are ignored.) If after development the hologram is addressed with object α and the output is Fourier transformed with a lens, then the output amplitude is given by

$$output = b^*(a \otimes \alpha) \tag{1}$$

where $\otimes$ and * signify correlation and convolution, respectively. This result holds for a thin hologram in which volume diffraction effects can be ignored. (Two other terms are also produced but they are spatially separated and can be ignored.) This result forms the basis for the early work in ghost image holography: if a has the proper image statistics and α is sufficiently similar to a, the correlation $a \otimes \alpha$ will resemble a delta function and the output will closely resemble b, forming an association between a and b. Unfortunately, for many images the autocorrelation is not sufficiently sharp to prevent significant degradation of the output. Moreover, when attempts are made to store multiple objects crosstalk noise further degrades the output quality. Another problem is that such a linear system is incapable of choosing between competing outputs so that superimposed distorted inputs result in superimposed distorted outputs. It is also very difficult to cascade such linear systems because of the buildup of distortions and noise from stage to stage.

In order to circumvent the above problems we [4] and others [5] [6] [7] [8] [9] [10] [11] proposed and demonstrated nonlinear holographic memories (NHAM) in which optical feedback and nonlinear gain are used to choose between the stored memories. The physical form of the retroreflection/nonlinearity mechanism used by various workers varies from all-optical to hybrid

optical/electronic mechanisms. A diagram of one type of NHAM architecture is shown in Fig. 2. Angularly shifted plane wave reference beams are used to record a set of objects a^m. Each b^m is therefore a shifted delta function. When the hologram is addressed by an input α, the output

$$\beta = \sum_{m=1}^{M} b^m * (a^m \otimes \alpha) \tag{2}$$

is passed through a nonlinearity f() and retroreflected back to the hologram, forming an output

$$\alpha = \sum_{m=1}^{M} a^m * (b^m \otimes \beta) \tag{3}$$

which is in turn passed through a separate nonlinearity F() and retroreflected back to the hologram where the cycle repeats, forming an iterative dynamic system which converges to limit points which are the eigenmodes of the optical cavity formed by the retroreflectors and the hologram. It will be shown in Sec. 3 that if the b^m are shifted delta functions (corresponding to angularly shifted plane wave reference beams) the limit points of the dynamic system correspond to the stored a-b associated image pairs.

The architecture of Fig. 2 can be described in flow diagram format as a closed loop consisting of a forward linear transformation, point nonlinearity, backward linear transformation, and another point nonlinearity (Fig. 3). If we assume the stored memories are one-dimensional vectors, the forward and backward linear transformations H_{ab} and H_{ba} can be described by matrix representations of the linear operations listed in Eqs. (2) and (3), respectively. (The extension to two-dimensional images is straightforward and does not add to the present discussion.) The form of the matrix $H_{a\text{-}b}$ can be determined from inspection and is illustrated in Fig. 4 for angularly multiplexed plane wave reference beams. It is a band $M(2N-1)xN_1$ matrix where each row in band m consists of a shifted version of a^m and m is an index for the stored associative memory vectors. N is the size of the memory vectors, N_1 is the length of the "window" in which the input vector is imbedded (this allows for translational invariance), and M is the total number of stored vectors. The elements of the forward transformation matrix H_{ab} are given by

$$h_{ij} = \sum_{m=1}^{M} a^m_{j-i-mN_1} \tag{4}$$

The backward transformation matrix H_{ba} is similar in form. If the input vector is padded with zeros to increase its length to N_1=M(2N-1) then both matrices are square and H_{ba} is equal to the matrix transpose of H_{ab}:

$$H_{ba} = H_{ab}^T \tag{5}$$

The above formulation of NHAM dynamics is formally equivalent to the bidirectional associative memory (BAM) model described by Kosko. This interpretation of NHAM dynamics is discussed further in the next section.

3. BAM interpretation of NHAM dynamics

Kosko's BAM model[12] is illustrated in Fig. 5. Two fields of neurons F_A and F_B characterized by sigmoidal or hard thresholding activation functions are connected by a set of weights h_{ij}. Patterns activating field F_A are thresholded, weighted, and transmitted to F_B (bottom-up). Those patterns are then in turn thresholded by F_B and transmitted back down to F_A via the same set of weights (top-down). This sequence then repeats in ping-pong fashion. Kosko has shown that the function

$$E(\alpha,\beta) = -(\beta^T H - \theta_\alpha^T)\alpha - (\alpha^T H^T - \theta_\beta^T)\beta \tag{6}$$

always decreases as the system evolves. In the above expression (α,β) are column vectors representing the patterns in (F_A,F_B) and (θ_a^T,θ_b^T) are threshold levels. Since E is bounded from below it is an "energy" or Lyapunov function and NHAM can be modeled as a nonlinear dissipative system. The minima of E correspond to stable limit points. The only necessary condition on the connection matrix is that H (top-down) is the transpose of H (bottom-up). This corresponds to bidirectional weights, e.g. the same weight connects neurons i and j in both directions. Kosko showed that the limit points correspond to stored associative memory pairs a^m and b^m if the connection weights are given by a sum of outer products:

$$h_{ij} = \sum_{m=1}^{M} a_i^m b_j^m \tag{7}$$

The BAM formalism can be applied directly to analyzing NHAM dynamics since BAM dynamics, as evident from Fig. 3, is identical in form to that of the NHAM framework. The

NHAM Lyapunov function is therefore given by the above expression for E if H is the matrix illustrated in Fig. 4 which describes the linear transformation performed by the hologram. In general, the NHAM limit points are not (a^m,b^m) because H is given by a combination of correlation/convolution operations as opposed to the simple sum of outer products of the BAM. The convolutions superimpose multiple blurred output terms which cannot be deblurred using simple point nonlinearities and feedback. However, for the special case of angularly multiplexed plane wave reference beams, the b vectors are spatially shifted delta functions which separate the various correlation terms, allowing point nonlinearities to favor the strongest correlation peak. This can be more easily seen if E is rewritten in the correlation/convolution format:

$$E(\alpha,\beta) = -\left(\sum_{m=1}^{M} a^m * (b^m \otimes \beta) - \theta_\alpha\right)^T \alpha - \left(\sum_{m=1}^{M} b^m * (a^m \otimes \alpha) - \theta_\beta\right)^T \beta \qquad (8)$$

The above expression is locally minimized if (α,β) equal one of the stored associations and the b^m are delta functions,

$$b^m = \delta(x - x_m)$$
$$\alpha = a^{mo}$$
$$\beta = b^{mo} \qquad (9)$$

since the cross-correlation noise is then separated out in both the α and β domains, converting the above expression for E into a sum of two inner products which is minimized for (α,β)=(a^{mo},b^{mo}). The iterative equation for the evolution of the α pattern can then be written as [13]:

$$\alpha_k = F\left(\sum_{m=1}^{M} a^m * f(a^m \otimes \alpha_{k-1})\right) \qquad (10)$$

where it has been assumed that an aperture in the α domain eliminates extraneous holographic reconstructions. If the nonlinearity f() in the β domain is faster than linear or sigmoidal the correlation peak sidelobes will tend to be reduced on each iteration and α will converge to one of the stored memories, assuming that the initial input was sufficiently similar to that stored memory and the hologram is not overloaded.

The results of a computer simulation of this process are shown in Fig. 6 in which a sigmoidal nonlinearity was used. Figure 6a. is a plot of the β domain for five iterations through the NHAM. The corresponding input or α domain is shown in Fig. 6b. The random stored vectors were 25 pixels long and the input pattern was one of the four stored vectors with the first three pixels reversed in sign. Note the error correction as the system evolves. The norm of the vector difference between α and the stored vector is plotted in Fig. 7a, illustrating the convergence of the NHAM to one of the stored states. The monotonically decreasing Lyapunov function is plotted in Fig. 7b. The radius of attraction of the stored states can be estimated from Fig. 8 which shows the probability of convergence as a function of the Hamming distance of the input vector from the nearest memory vector. The four curves are parameterized by the number of stored vectors. The effects of too many errors in the input vector on NHAM performance are evident in Fig. 9. Here the number of pixels per vector was reduced to eight, three of which were in error in the input vector. In this case the NHAM converged to the "wrong" stored memory as is evident from Fig. 9a. The Lyapunov function, of course, still decreased.

4. Summary

In this paper I have discussed a Lyapunov function for thin hologram NHAMs. Such an NHAM can be considered to be a BAM where patterns in one field (corresponding to the NHAM β domain) are coded to prevent overlapping of the correlation terms. The use of angularly multiplexed plane wave reference beams implements this necessary coding. Nonlinearities can then be used to sharpen the correlation peaks and undo the effects of the blurring convolution operations, allowing the NHAM to converge to one of the stored states. A single-pass feedforward NHAM can also be made equivalent to a Hamming neural network[14] by implementing a winner-take-all competitive network in the β domain using excitatory and inhibitory local interconnections to select the strongest correlation peak. Generalized BAMs can be implemented in the NHAM framework if thick holograms are used, as pointed out by Guest and TeKolste[15], although the natural shift-invariance of the thin hologram NHAM is then lost and special techniques must be used to avoid crosstalk[16] [17]. The large storage capacity of a volume hologram is, however, very attractive for neural network applications.

References

1. D. Gabor, "A New Microscopic Principle," Nature 161, 777 (1948).

2. P. J. van Heerden, "A New Optical Method of Storing and Retrieving Information," Appl. Opt. **2**, 387-392 (1963).

3. R. J. Collier and K. S. Pennington, "Ghost Imaging by Holograms Formed in the Near Field," Appl. Phys. Lett. 8, 44-46 (1966).

4. B. H. Soffer, G. J. Dunning, Y. Owechko, and E. Marom, "Associative Holographic Memory with Feedback Using Phase Conjugate Mirrors," Opt. Lett. **11**, 118-120 (1986).

5. D. Z. Anderson, "Coherent Optical Eigenstate Memory," Opt. Lett. **11**, 56-58 (1986).

6. A. Yariv, S. Kwong, and K. Kyuma, "Demonstration of an All-Optical Associative Holographic Memory," Appl. Phys. Lett. 48, 1114-1116 (1986).

7. E. G. Paek and D. Psaltis, "Optical Associative Memory Using Fourier Transform Hologram," Opt. Eng. **26**, 428-433 (1987).

8. Q. W. Song and T. S. Yu, "Holographic Associative Memory System Using a Thresholding Microchannel Spatial Light Modulator," Opt. Eng. **28**, 533-536 (1989).

9. E. G. Paek and A. Von Lehmen, "Real-Time Holographic Associative Memory for Identifying Words in a Continuous Letter String," Opt. Eng **28**, 519-525 (1989).

10. Y. Owechko, "Nonlinear Holographic Associative Memories," J. Quantum Electronics **25**, 619-634 (1989). (Review paper)

11. H. J. White, N. B. Aldrige, and I. Lindsay, "Digital and Analogue Holographic Associative Memories," Opt. Eng. **27**, 30 (1988).

12. B. Kosko, "Adaptive Bidirectional Associative Memories," Appl. Opt. **26**, 1987, 4947-4960.

13. Y. Owechko, G. J. Dunning, E. Marom, and B. H. Soffer, "Holographic Associative Memory With Nonlinearities in the Correlation Domain," Appl. Opt. **26**, 1987, 1900-1910.

14. R. P. Lippmann, "An Introduction to Computing with Neural Nets," IEEE ASSP Magazine, April 1987, 4-22.

15. G. C. Guest and R. TeKolste, "Designs and Devices For Optical Bidirectional Associative Memories," Appl. Opt. 26, 1987, 5055-5060.

16. D. Psaltis, J. Yu, X. G. Gu, and H. Lee, "Optical Neural Nets Implemented with Volume Holograms," OSA Topical Meeting on Optical Computing, Incline Village, Nevada, 1987, Paper TuA3-1.

17. Y. Owechko, "Self-Pumped Optical Neural Networks," Salt Lake City Topical Meeting on Optical Computing, Feb. 1989.

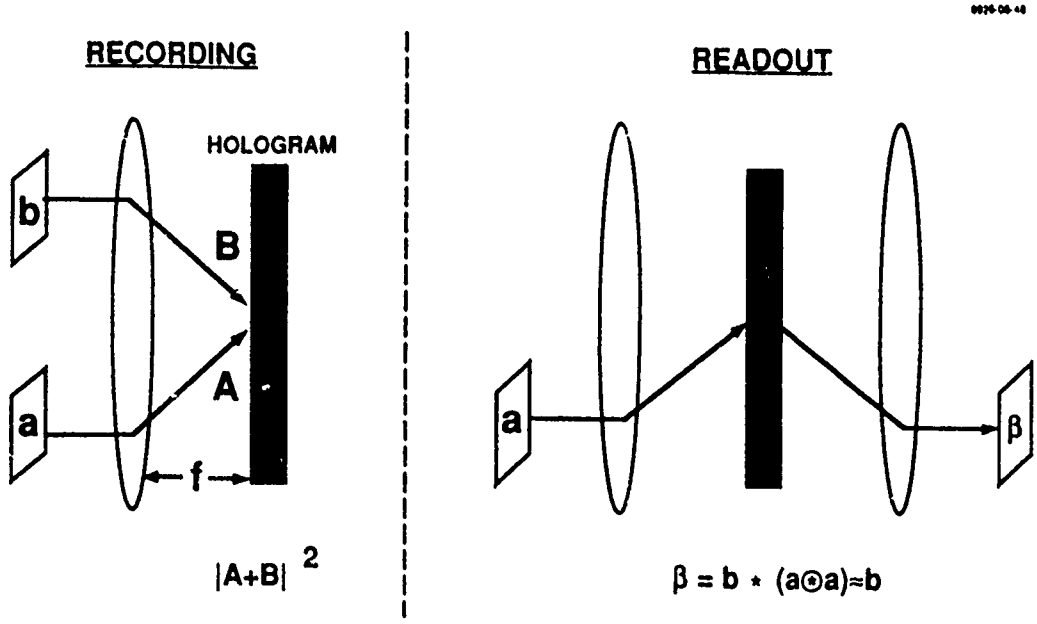

Figure D-1. Schematic of ghost imaging linear holographic associative memory.

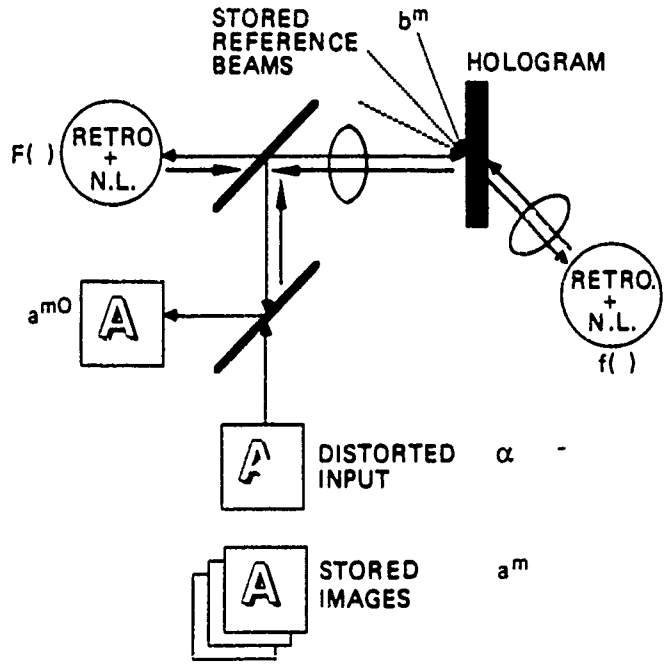

Figure D-2. NHAM architecture.

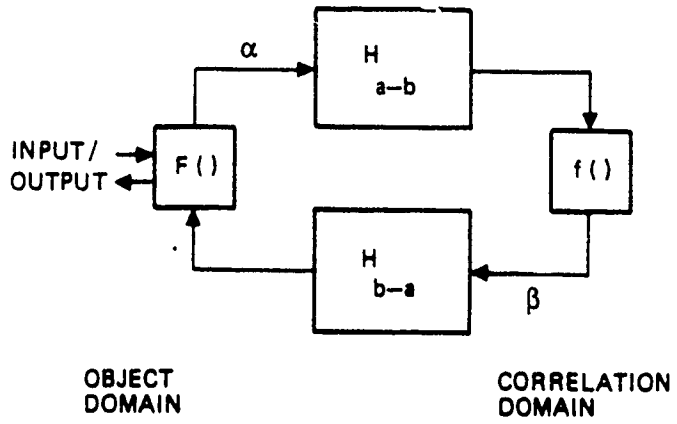

Figure D-3. NHAM flow diagram.

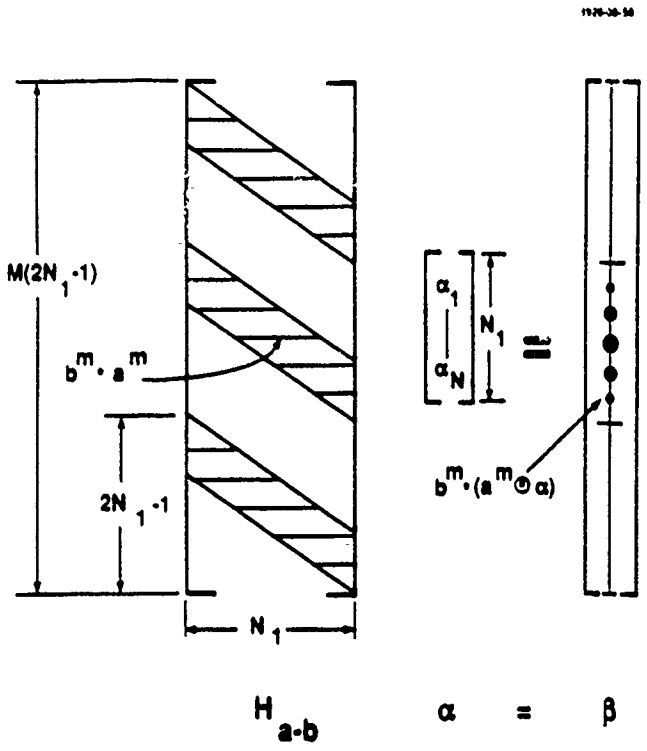

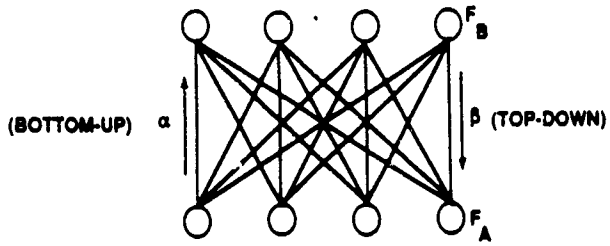

Figure D-5. BAM architecture.

Figure D-4. Matrix description of forward pass through thin hologram.

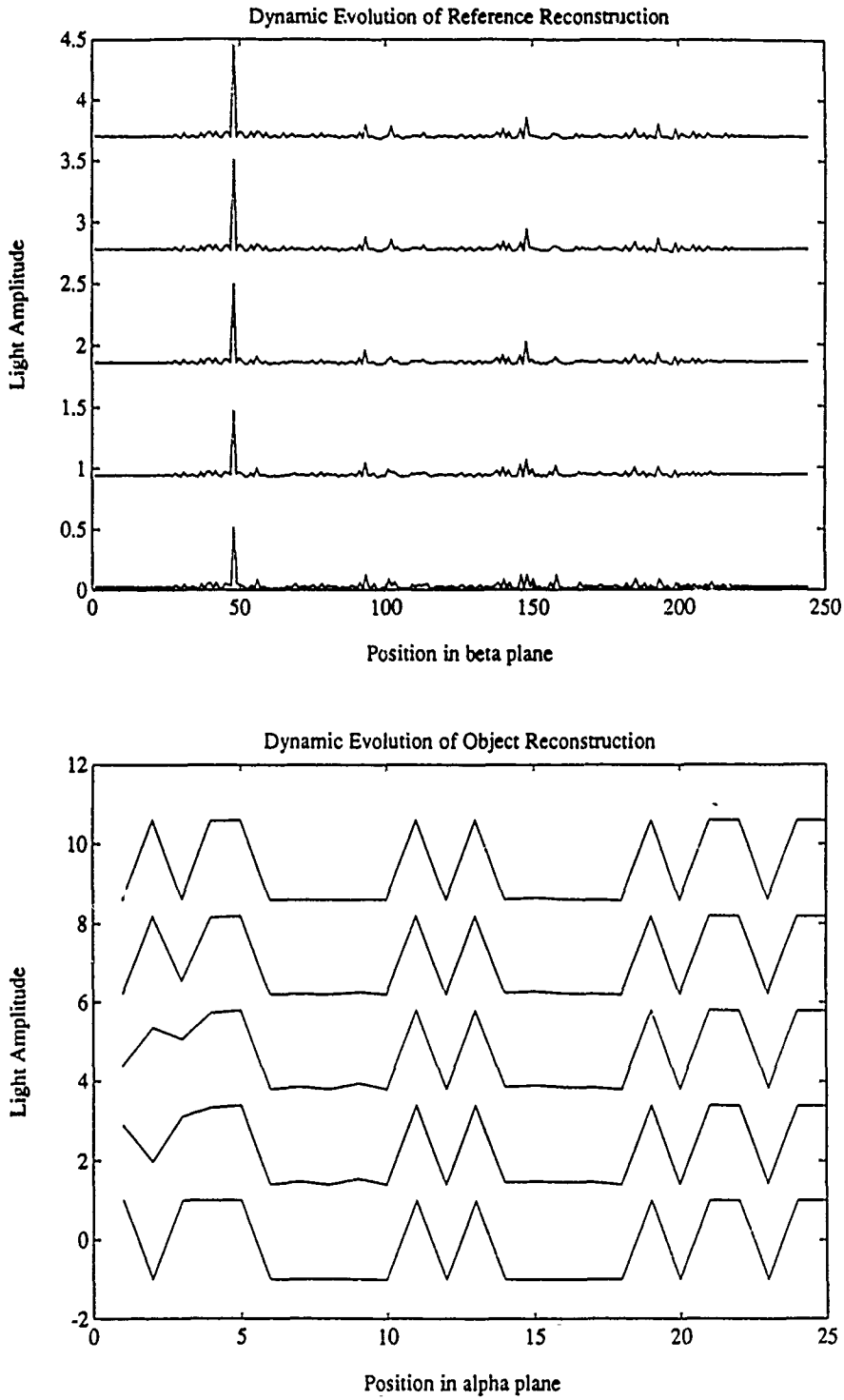

Figure D-6. Results of NHAM computer simulation. a. Evolution of β domain over five iterations showing convergence to a stored state.
b. Corresponding evolution of α domain.

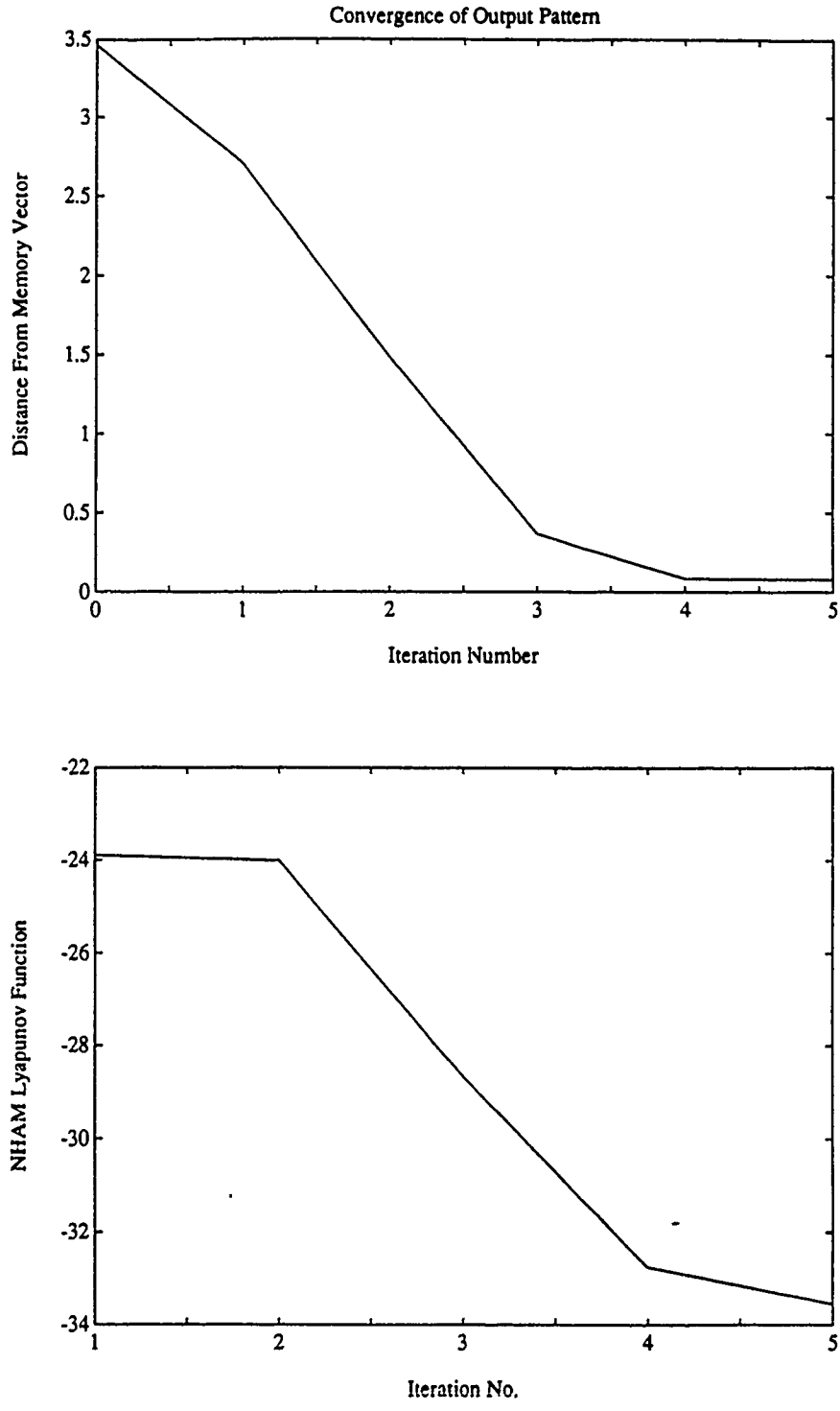

Figure D-7. a. Vector distance of α from nearest stored memory over five iterations showing convergence to that memory. b. Corresponding decrease of Lyapunov function.

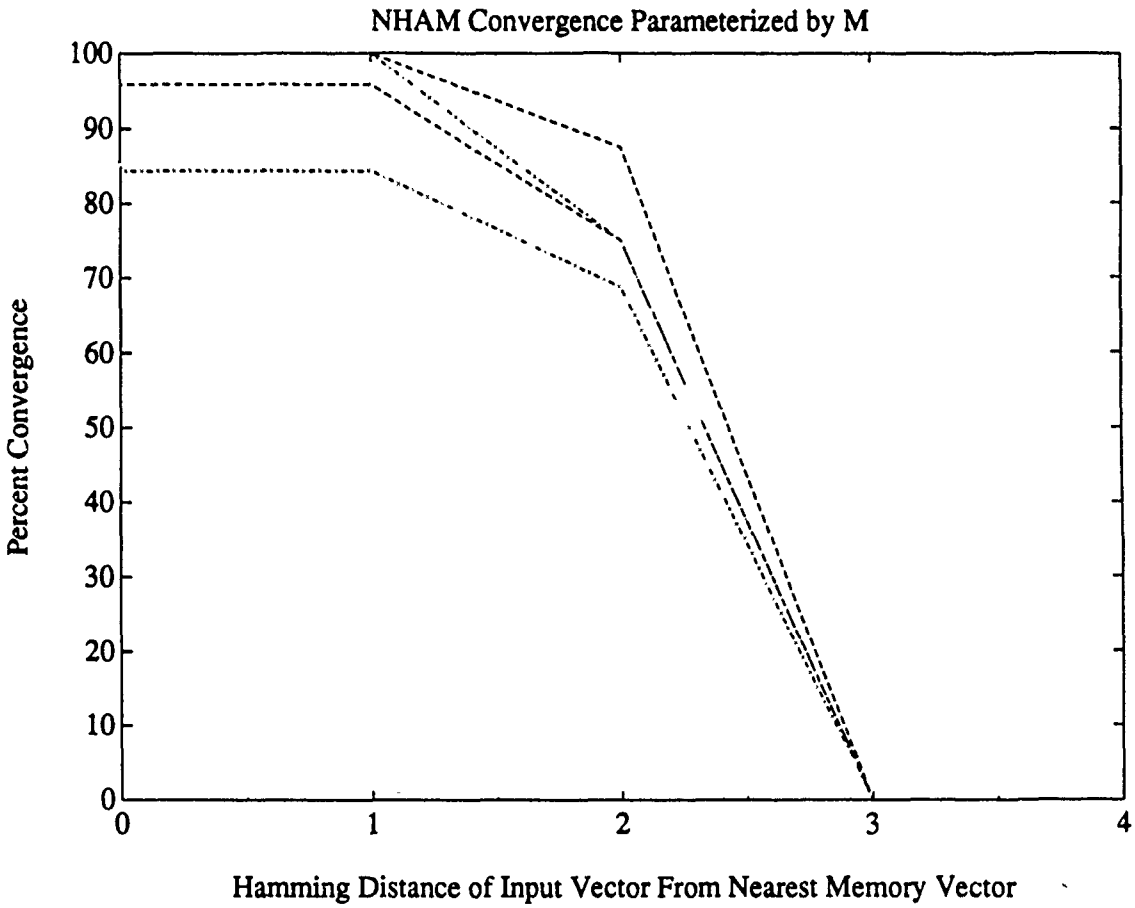

Figure D-8. Probability of NHAM convergence as function of initial errors. The four curves correspond to number of stored memories equal to 2, 4, 6, and 8. The length of the memories was 25.

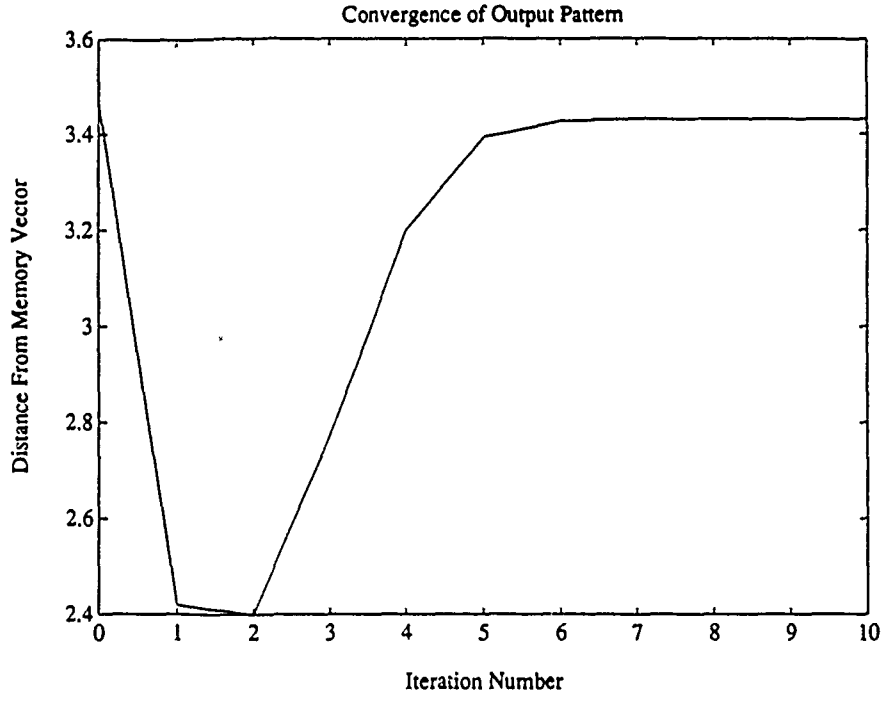

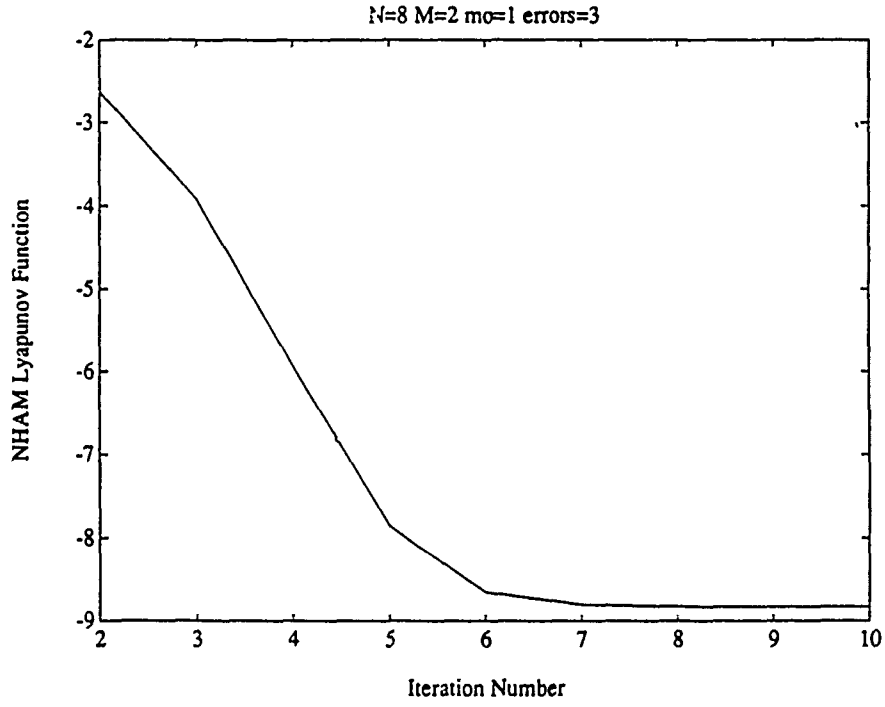

Figure D-9. a. Vector distance of α from nearest stored memory over five iterations for case in which the number of initial errors was too great for convergence to the nearest memory vector. b. The Lyapunov function strictly decreased for this case, as it should for all cases.

APPENDIX E

Self-Pumped Optical Neural Networks

Yuri Owechko

Hughes Research Laboratories

Malibu, California 90265

Optical neural network architectures are described which store each connection weight in a continuum of spatially distributed photorefractive gratings. This approach reduces cross-talk and fully utilizes the spatial light modulator.

Self-Pumped Optical Neural Networks

Yuri Owechko
Hughes Research Laboratories
Malibu, California 90265

Neural network models for artificial intelligence offer an approach fundamentally different from conventional symbolic approaches, but the merits of the two paradigms cannot be fairly compared until neural network models with large numbers of "neurons" are implemented. Despite the attractiveness of neural networks for computing applications which involve adaptation and learning, most of the published demonstrations of neural network technology have involved relatively small numbers of "neurons". One reason for this is the poor match between conventional electronic serial or coarse-grained multiple-processor computers and the massive parallelism and communication requirements of neural network models. The self-pumped optical neural network (SPONN) described here is a fine-grained optical architecture which features massive parallelism and a much greater degree of interconnectivity than bus-oriented or hypercube electronic architectures. SPONN is potentially capable of implementing neural networks consisting of 10^5-10^6 neurons with 10^9-10^{10} interconnections. The mapping of neural network models onto the architecture occurs naturally without the need for multiplexing neurons or dealing with contention, routing, and communication bottleneck problems. This simplifies the programming involved compared to electronic implementations.

Previous optical holographic implementations of neural network models used a single grating in a photorefractive crystal to store a connection weight between two neurons (each pixel in the input/output planes corresponds to a single neuron). This approach relies on the Bragg condition for angularly selective diffraction from a grating to avoid cross-talk between neurons. However, because of the angular degeneracy of the Bragg condition, the neurons must be arranged in special patterns in the input/output planes to fully eliminate cross-talk. This results in sub-sampling of the spatial light modulators (SLMs) and incomplete utilization of the SLMs if the single grating per weight approach is used. Specifically, assuming the SLMs are capable of displaying $N \times N$ pixels, the single grating per weight method can store only $N^{3/2}$ neurons and N^3 interconnections.[1] I describe here an approach in which the Bragg degeneracy is broken by distributing each interconnection weight among a continuum of angularly and spatially distributed gratings. This eliminates cross-talk between neurons, making sub-sampling of the input/output planes unnecessary and allowing full utilization of the SLM space-bandwidth product. In other words, N^2 neurons can be fully interconnected provided the interconnection medium has sufficient degrees of freedom or space-bandwidth product to store the N^4 interconnection weights. By forcing signal beams to match the Bragg condition at many spatially distributed gratings, the signal-to-noise ratio should also be improved.

The continuum of gratings is generated by using a self-pumped phase conjugate mirror (SP-PCM) in conjunction with a SLM, CCD detector, frame grabber, and host computer. Several theories have been published for self-pumped phase conjugation in $BaTiO_3$ crystals, including internal resonators based on four-

wave mixing aided by Fresnel reflections and stimulated photorefractive backscattering. A common feature of these theories is that each pixel in the input plane writes gratings with and pumps all other pixels to form the phase conjugate wavefront. This results in a physical system which is massively interconnected and parallel, and which is a natural medium for implementation of neural network models. The distributed gratings in the crystal serve as the interconnection mechanism while the frame grabber in conjunction with the host computer implements programmable neuron activation functions. By spatially segregating the input/output plane, multiple layer neural network models can be implemented. This hybrid system combines the parallelism and interconnectivity of optics with the programmability of electronics.

A diagram of an experimental system used to demonstrate these concepts is shown in Fig. 1. The "object plane" corresponds to the plane of neurons represented by pixels on an LCLV (liquid crystal light valve). Activation patterns displayed on the LCLV are impressed on a light beam which is focused into the SP-PCM. Connections between the pixels are formed and the phase conjugate return is detected by a video camera. The return is processed on a point by point basis by the frame grabber/image processor before being displayed again on the LCLV. In neural network models such as backpropagation an error signal would be formed electronically and displayed on the LCLV to adjust the weights between neurons. The error signals are formed on a point-by-point basis (local operations) and so are not computational intensive.

An experimental demonstration of optical connectivity using the apparatus of Fig. 1 is shown in Fig. 2. Fig. 2a shows the phase conjugate return for an input consisting of a complete resolution pattern. The input was then switched to the region enclosed by the dashed ellipse in Fig. 2b. The return consisted of the complete resolution pattern, as shown in Fig. 2b, verifying that connection weights were formed globally among all the pixels. Cross-talk suppression is illustrated in Fig. 3. The input to the SP-PCM consisted of an array of dots on a rectangular grid (Fig. 3a). The conjugate return is shown in Fig. 3b. When the input was shifted even a slight amount, the return disappeared (Fig. 3c) which verified that pixels do not have to be arranged in special patterns on the SLM to avoid cross-talk. Finally, in Fig. 4 selective erasure of weights is demonstrated. The central neuron was deactivated in Fig. 4b by shifting the phase of that neuron on the LCLV. This shifts the phase of the gratings written by that neuron and selectively erases connections between it and the other neurons, demonstrating that learning using bipolar error signals is possible.

This work was supported in part by the Air Force Office of Scientific Research.

1. D. Psaltis, J. Yu, X. G. Gu, and H. Lee, "Optical Neural Nets Implemented with Volume Holograms," OSA Topical Meeting on Optical Computing, Incline Village, Nevada, 1987, Paper TuA3-1.

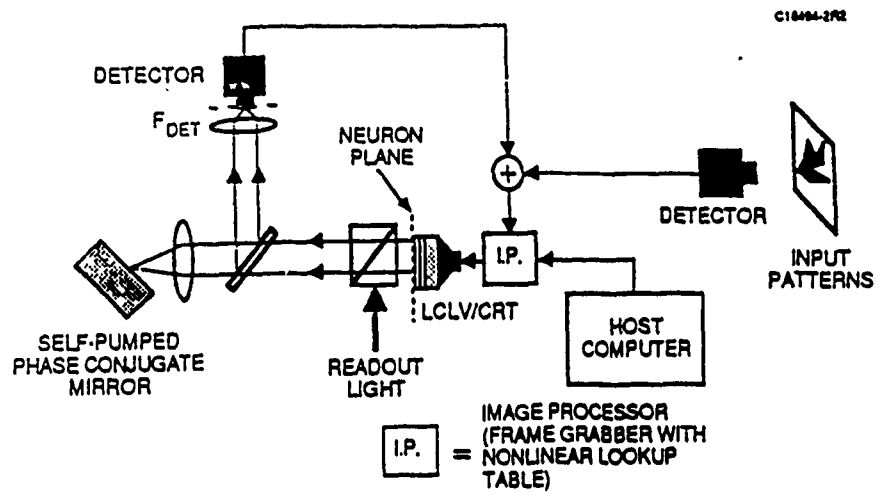

Figure E-1. Schematic of self-pumped optical neural network apparatus.

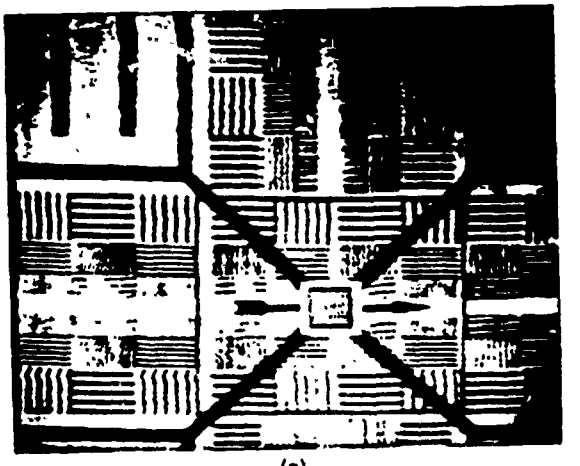

(a)

(b)

Figure E-2 Demonstration of connectivity of self-pumped PCM.

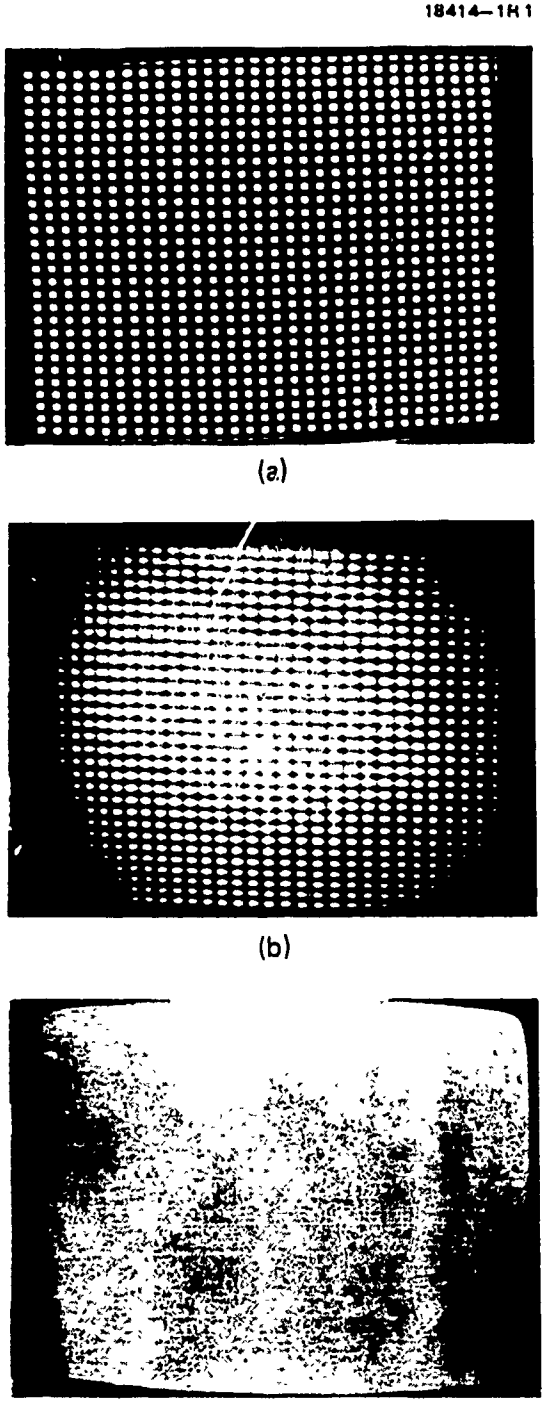

Figure E-3. Demonstration of cross-talk suppression in self-pumped optical neural network.

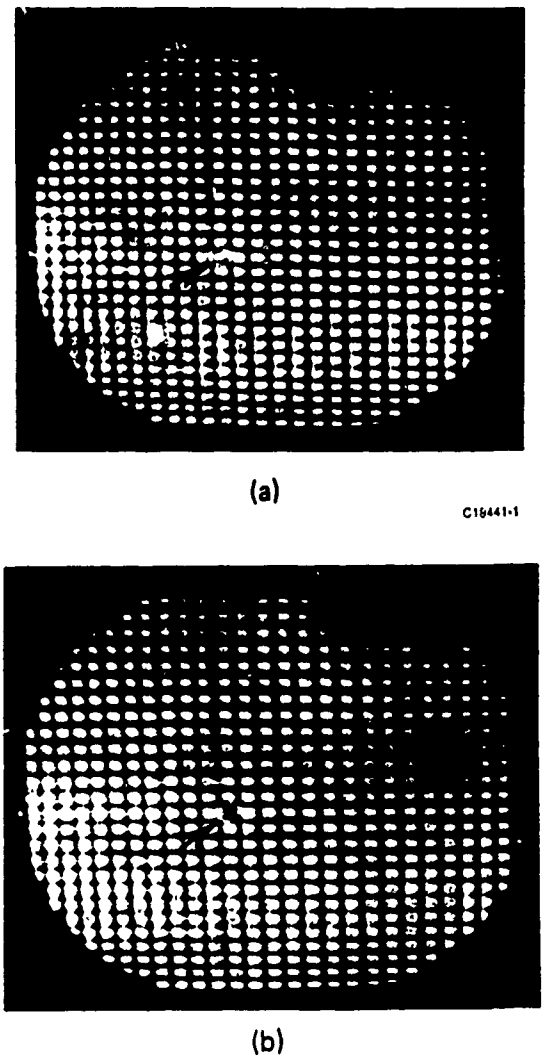

Figure E-4. Demonstration of selective weight erasure.

APPENDIX F

1990 International Topical Meeting on Optical Computing,
Kobe, Japan

Photorefractive Optical Neural Networks

Yuri Owechko
Hughes Research Laboratories
Malibu, California, USA 90265

Neural network models for pattern recognition, clustering, and optimization offer an alternative approach compared to conventional statistical methods, but without a unifying theory the performance of the two paradigms cannot be fairly compared until neural network models with large numbers of "neurons" are implemented in dedicated hardware. Despite the attractiveness of neural networks for computing applications which involve adaptation and learning, most of the published demonstrations of neural network technology have involved relatively small numbers of "neurons". One reason for this is the poor match between conventional electronic serial or coarse-grained multiple-processor computers and the massive parallelism and fine-grain communication requirements of neural network models. Approaches currently being pursued for dedicated hardware implementations include special purpose digital and analog integrated circuits as well as hybrid optical/electronic architectures.

In my talk I will discuss holographic neural network architectures in which the connection weights between neurons are implemented as gratings in a photorefractive crystal. In particular I will discuss the self-pumped optical neural network (SPONN), which is a fine-grained optical architecture which features massive parallelism and a much greater degree of interconnectivity than bus-oriented or hypercube electronic architectures. Connections between neurons are implemented as sets of angularly and spatially multiplexed volume phase gratings. SPONN is potentially capable of implementing neural networks consisting of 10^5-10^6 neurons with 10^9-10^{10} interconnections. The mapping of neural network models onto the architecture occurs naturally without the need for multiplexing neurons or dealing with the contention, routing, and communication bottleneck problems of electronic parallel computers. This simplifies the programming of the optical system.

An alternative approach to optical holographic implementations of neural network models utilizes a single grating in a photorefractive crystal to store each connection weight between two neurons (each pixel in the input/output planes corresponds to a single neuron).[1] This approach relies on the Bragg condition for angularly selective diffraction from a single grating to avoid cross-talk between neurons. However, because of the angular degeneracy of the Bragg condition, the neurons must be arranged in special patterns in the input/output planes to fully eliminate cross-talk. This results in sub-sampling of the spatial light modulators (SLMs) and incomplete utilization of the SLMs if the single grating per weight approach is used. Specifically, assuming the SLMs are capable of displaying N^2 pixels, the single grating per weight method can store only $N^{3/2}$ neurons and N^3 interconnections. In my talk I will describe the SPONN approach in which the Bragg degeneracy is broken by distributing each interconnection weight among a continuum of angularly and spatially distributed gratings. This eliminates cross-talk between neurons, making sub-sampling of the input/output planes unnecessary

and allowing full utilization of the SLM space-bandwidth product. In other words, N^2 neurons can be fully interconnected provided the interconnection medium has sufficient degrees of freedom or space-bandwidth product to store the N^4 interconnection weights. By forcing signal beams to match the Bragg condition at many spatially distributed gratings. the signal-to-noise ratio should also be improved.

The continuum of gratings is generated by using a self-pumped phase conjugate mirror (SP-PCM) in conjunction with a SLM, CCD detector, frame grabber, and host computer. Several theories have been published for self-pumped phase conjugation in $BaTiO_3$ crystals, including internal resonators based on four-wave mixing aided by Fresnel reflections and stimulated photorefractive backscattering. A common feature of these theories is that each pixel in the input plane writes gratings with and pumps all other pixels to form the phase conjugate wavefront. This results in a physical system which is massively interconnected and parallel, and which is a natural medium for implementation of neural network models. The distributed gratings in the crystal serve as the interconnection mechanism while the frame grabber in conjunction with the host computer implements programmable neuron activation functions. By spatially segregating the input/output plane, multiple layer neural network models can be implemented. This hybrid system combines the parallelism and interconnectivity of optics with the programmability of electronics.

A diagram of an experimental system used to demonstrate these concepts is shown in Fig. 1. The "neuron plane" is an optical representation of the neuron activity levels on a spatial light modulator, in our case a LCLV (liquid crystal light valve). Activation patterns displayed on the LCLV are impressed on a light beam which is focused into the SP-PCM. Connections between the pixels are formed and the phase conjugate return is detected by a video camera. The return is processed on a point by point basis by the frame grabber/image processor before being displayed again on the LCLV. In neural network models such as backpropagation an error signal would be formed electronically and displayed on the LCLV to adjust the weights between neurons. The error signals are formed on a point-by-point basis (local operations) and so are not computational intensive.

An experimental demonstration of optical connectivity using the apparatus of Fig. 1 is shown in Fig. 2. Fig. 2a shows the phase conjugate return for an input consisting of a complete resolution pattern. The input was then switched to the region enclosed by the dashed ellipse in Fig. 2b. The return consisted of the complete resolution pattern, as shown in Fig. 2b, verifying that connection weights were formed globally among all the pixels. Cross-talk suppression is experimentally demonstrated in Fig. 3. The input to the SP-PCM consisted of an array of dots on a rectangular grid (Fig. 3a). The conjugate return is shown in Fig. 3b. When the input was shifted by half of the grid period, the return disappeared (Fig. 3c) which verified that pixels do not have to be arranged in special patterns on the SLM to avoid cross-talk in the SPONN approach. Finally, in Fig. 4 selective coherent erasure of weights is demonstrated. The central neuron was deactivated in Fig. 4b by shifting the phase of that neuron on the LCLV. This shifts the phase of the gratings written by that neuron and selectively erases connections between it and the other neurons, demonstrating that learning using bipolar error signals is possible.

Issues which need to be addressed in the SPONN approach include the partial erasure of old recordings by new ones and the volatility of the gratings (gratings are partially erased by the readout process). Partial erasure can be compensated by using an exposure schedule in which early recordings are made with larger exposures than later ones.[2] Grating volatility may be possibly eliminated by "fixing" the gratings using switching of ferroelectric domains in such a way as to transfer the charge pattern in the crystal to the domain pattern, which is permanent at room temperature.[3]

This work was supported in part by the Air Force Office of Scientific Research.

1. D. Psaltis, J. Yu, X. G. Gu, and H. Lee. "Optical Neural Nets Implemented with Volume Holograms," OSA Topical Meeting on Optical Computing, Incline Village, Nevada, 1987, Paper TuA3-1.

2. K. Blotekjaer, "Limitations on Holographic Storage Capacity of Photochromic and Photorefractive Media," Appl. Opt. 18, 57-67 (1979).

3. F. Micheron and G. Bismuth, "Electrical Control of Fixation and Erasure of Holographic Patterns in Ferroelectric Materials," Appl. Phys. Lett. 20, 79-81 (1972).

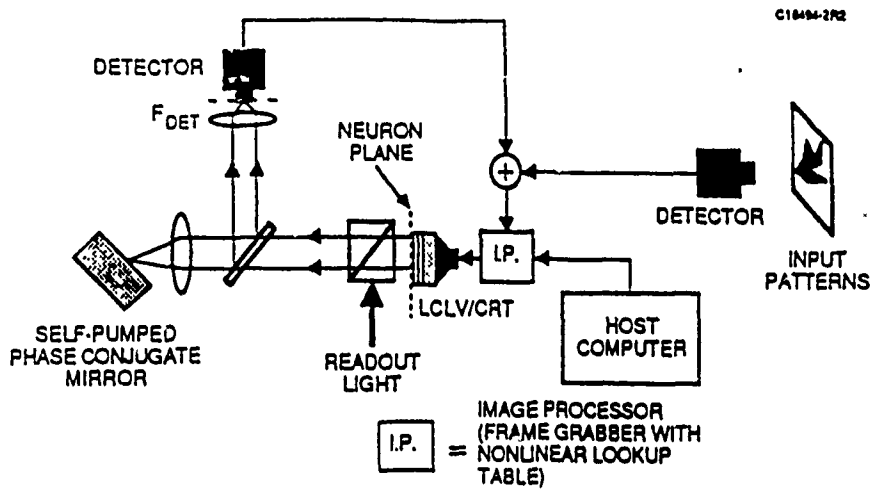

Figure F-1. Schematic of self-pumped optical neural network apparatus.

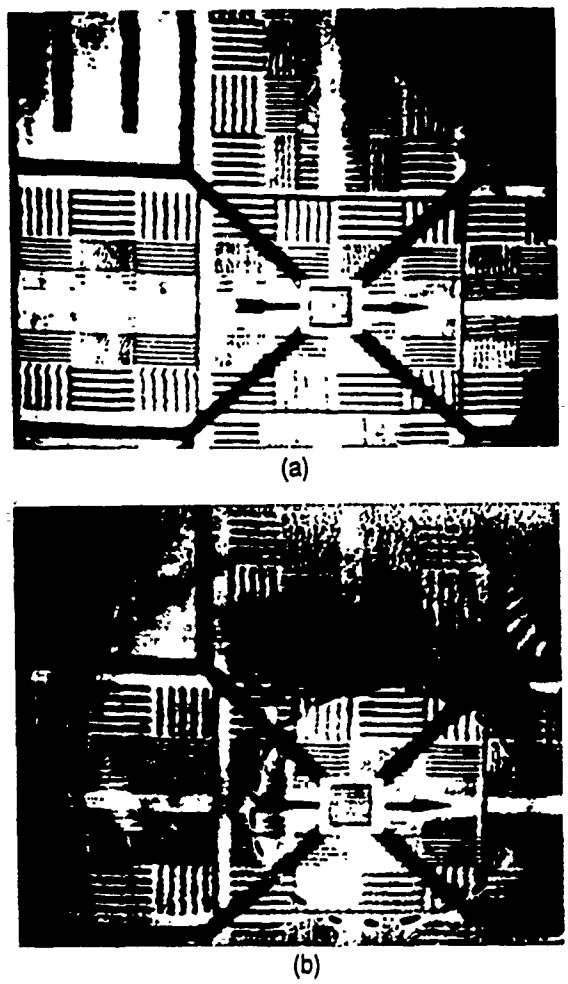

Figure F-2 Demonstration of connectivity of self-pumped PCM.

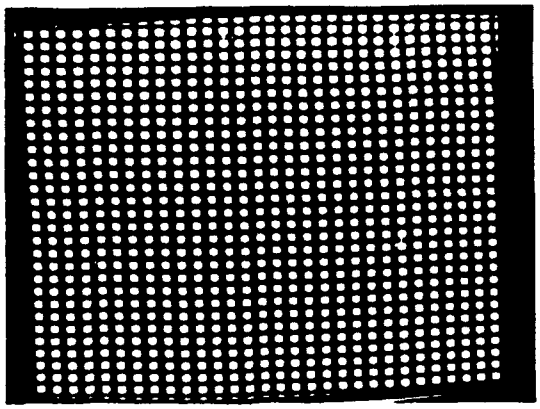

(a)

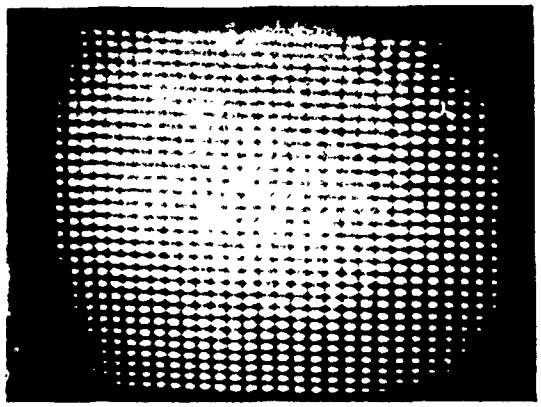

(b)

(c)

Figure F-3. Demonstration of cross-talk suppression in self-pumped optical neural network.

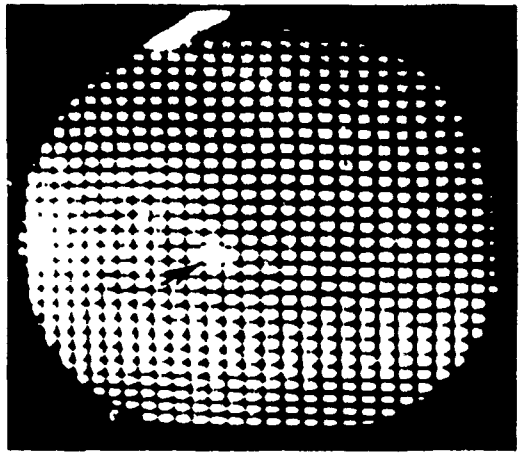

(a)

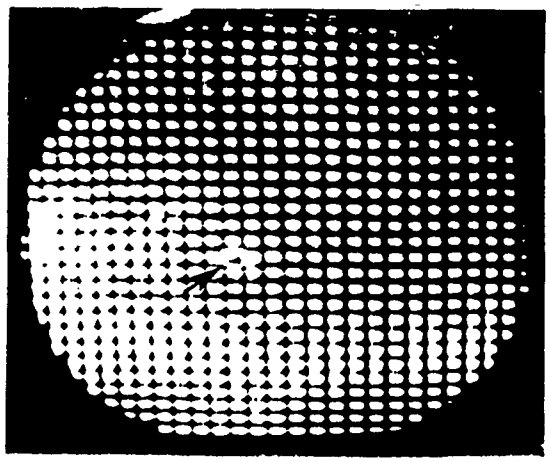

(b)

Figure F-4. Demonstration of selective weight erasure.